

The spatial investigation of temperature across the thalamus

D I S S E R T A T I O N

zur Erlangung des akademischen Grades

Doctor rerum naturalium
(Dr. rer. nat.)

eingereicht an der
Lebenswissenschaftlichen Fakultät der Humboldt-Universität zu Berlin
von
Tobias Marc Leva

Präsidentin der Humboldt-Universität zu Berlin

Prof. Dr. Julia von Blumenthal

Dekanin/Dekan der Lebenswissenschaftlichen Fakultät
der Humboldt-Universität zu Berlin

Prof. Dr. Christian Ulrichs

Gutachter:

1. Michael Brecht
2. James Poulet
3. Brice Bathellier

Tag der mündlichen Prüfung:

22.02.2024

May 2017 – January 2023

Neural Circuits and Behavior, Group Leader Prof. Dr. James Poulet

Max Delbrück Center for Molecular Medicine (MDC)

Haus 89 / Max Rubner House

Robert-Rössle-Str. 10

13125 Berlin

Acknowledgement

I would like to express my gratitude to those who have played a significant role in my journey towards completing this Ph.D. thesis. This achievement would not have been possible without the unwavering support, guidance, and inspiration of numerous individuals and entities.

First and foremost, I want to thank my supervisor, James Poulet. He not only provided me with the invaluable opportunity to pursue this research but also furnished me with the infrastructure, resources, and encouragement necessary to successfully finish this project.

I want to extend my sincere appreciation to my collaborator Clarissa Whitmire, who navigated with me through the intricate aspects of this work, offering insights, expertise, and support.

I am deeply grateful to the entire Poulet lab community for their constant support, intellectual exchange, and camaraderie. The lab provided a nurturing environment and I received valuable supervision, feedback, and encouragement from my peers and mentors. The countless discussions, debates, and, of course, the fun times we shared have left an indelible mark on my academic journey.

My heartfelt thanks also extend to my family, friends and especially Yana Felicia who have been a continuous source of encouragement, understanding, and support. Your belief in me has been a driving force behind my persistence and determination.

A spatial investigation of temperature across the thalamus

Abstract

The capability to create an internal representation of the external world is a fundamental aspect that unites all living higher-order organisms and ensures their survival. In this process, the thalamus encodes sensory information, which it receives from the sensory periphery and relays to cortical centers for subsequent processing. This knowledge is built upon the investigation of the processing of most sensory modalities. However, the physiological thalamic function in processing innocuous temperature and its perceptual relevance remains elusive due to a focus on the homeostatic regulation of body temperature as well as the processing of painful temperatures of already published work. In addition, these studies usually focused on identifying a central thalamic processing hub and failed to recognize that temperature is processed in a parallel manner by various thalamic nuclei. This study will attempt to overcome these limitations by undertaking a detailed and large-scale exploration of thermal processing, connectivity to cortical areas, and the influence on the behavior of three somatosensory-associated thalamic nuclei. This unprecedented study of thermal processing in the thalamus has uncovered a multi-faceted thermal representation with location-specific differences in temperature encoding and connectivity with temperature-sensitive cortical regions. Moreover, it is demonstrated that the thalamus is essential for temperature perception, which emphasizes the relevant roles of multiple thalamic nuclei in the physiological processing of temperature and perception.

Zusammenfassung

Die Fähigkeit, eine interne Repräsentation der Außenwelt zu schaffen, ist ein grundlegender Aspekt, der alle lebenden Organismen höherer Ordnung verbindet und ihr Überleben sichert. Bei diesem Prozess kodiert der Thalamus sensorische Informationen, die er von der sensorischen Peripherie erhält, und leitet sie zur weiteren Verarbeitung an kortikale Zentren weiter. Dieses Wissen beruht auf der Untersuchung der Verarbeitung der meisten Sinnesmodalitäten. Die physiologische Funktion des Thalamus bei der Verarbeitung nicht schmerzhafter Temperaturen und dessen Wahrnehmungsrelevanz sind jedoch nach wie vor wenig untersucht, da der Schwerpunkt bereits veröffentlichter Arbeiten oft auf der homöostatischen Regulierung der Körpertemperatur und der Verarbeitung schmerzhafter Temperaturen lag. Darüber hinaus konzentrierten sich diese Studien in der Regel auf die Identifizierung eines zentralen thalamischen Verarbeitungszentrums und ließen außer Acht, dass Temperatur parallel von verschiedenen thalamischen Kernen verarbeitet wird. Die vorliegende Studie versucht, diese Einschränkungen zu überwinden, indem sie eine detaillierte und groß angelegte Untersuchung der Thalamus spezifischen thermischen Verarbeitung, der Konnektivität zu kortikalen Bereichen und des Einflusses auf das Verhalten der drei somatosensorisch assoziierten Thalamuskerne vornimmt. Diese beispiellose Untersuchung der Temperaturverarbeitung im Thalamus hat eine vielschichtige thermische Darstellung mit ortsspezifischen Unterschieden in der Temperaturkodierung und der Konnektivität mit temperaturempfindlichen kortikalen Regionen aufgedeckt. Darüber hinaus konnte gezeigt werden, dass der Thalamus für die Temperaturwahrnehmung von wesentlicher Bedeutung ist, was die Relevanz des Thalamus bei der Verarbeitung von Temperatur unterstreicht.

Table of Contents

1. Introduction.....	12
1.1 The peripheral somatosensory system	12
1.1.1 Thermosensitive receptors detect temperature changes on the skin.....	13
1.1.2 Primary sensory afferents send sensory information to distinct lamina of the spinal cord	15
1.1.2.1 The encoding of thermal stimuli in primary sensory afferents.....	16
1.2 The spinal cord	17
1.2.1 The Spinothalamic tract.....	19
1.2.2 The Dorsal Column-Medial Lemniscal pathway.....	19
1.2.3 The Spinoparabrachial tract	20
1.2.4 Encoding of temperature in the spinal cord	20
1.3 The Thalamus	21
1.3.1 The Ventral posterolateral nucleus - VPL.....	23
1.3.1.1 Encoding of somatosensory signals in VPL	23
1.3.2 The Posterior triangular nucleus - PoT	25
1.3.2.1 The encoding of somatosensory signals in PoT	26
1.3.3 The Posterior complex of the thalamus - PO	27
1.3.3.1 The encoding of somatosensory signals in PO.....	27
1.4 The Cortex	28
1.4.1 The primary somatosensory cortex – S1	28
1.4.2 The posterior insular cortex - pIC	28
1.5 The lateral parabrachial nucleus and hypothalamus.....	29
1.6 State of the art and aims of the current study	30
1.6.1 Anatomical characteristics of the thalamocortical temperature circuits.....	30
1.6.2 Testing the perceptual relevance of the thalamus in a temperature detection task.....	31
1.6.3 Investigation of thermal encoding principles across the thalamus	33
2. Material and Methods.....	35
2.1 Animals	35
2.2 Surgery	35
2.2.1 Stereotactic alignment of the skull for electrophysiological recordings.....	35
2.2.2 Implantation of head post for electrophysiological recordings	36
2.2.3 Post-operative care	36

2.2.4 Surgery for anatomical tracing experiments	37
2.3 Sensory stimulation	37
2.3.1 Thermal stimulation	37
2.3.2 Vibrotactile stimulation	38
2.3.3 Acoustic stimulation	38
2.4 Extracellular Electrophysiology	38
2.4.1 Signal chains for sensory stimulation and data acquisition	38
2.4.2 Grounding and Referencing	39
2.4.3 Probe Alignment and Insertion.....	40
2.4.4 Data Acquisition and Synchronization	40
2.4.5 Labeling of Probes with lipophilic dyes	41
2.4.6 Measurement of paw movement.....	41
2.5 Habituation	43
2.6 Behavioral experiments	44
2.6.1 Water restriction	44
2.6.2 Pairing and association to sensory stimuli.....	44
2.6.3 Behavioral training and pharmacological manipulation of thalamic activity	44
2.7. Ex-vivo tissue preparation	46
2.8 Data processing	46
2.8.1 Data pre-processing.....	47
2.8.2 Spike Sporting.....	47
2.8.3 Eliminating potential double-counted spikes	48
2.8.4 Eliminating units with non-physiological waveforms	48
2.8.5 Single Unit quality control	48
2.9 Reconstruction anatomical locations.....	53
2.9.1 Alignment of brain slices to Allen Institute Common Coordinate Framework	53
2.9.2 Visualization of Probe Trajectories in 3-D Model.....	55
2.10 Data Analysis	55
2.10.1 Responsive Cells	55
2.10.2 Tuning Index	56
2.10.3 Spatial maps of responsive cells	56
2.10.4 Response Latency	57
2.10.5 Peak Response Time.....	57
2.10.6 Response Duration	57
2.10.7 Duration Index.....	57

2.10.8 Sharpness Index.....	58
2.10.9 Single unit PSTH.....	58
2.10.10 Population PSTH	58
2.10.11 Criteria for exclusion of experiments and single units in dataset.....	58
2.11 Anatomical tracing of brain-wide thermal circuitry.....	59
2.11.1 identification of injection site in S1 and pIC	59
2.11.2 Tracer and Virus injections	59
2.11.3 Histology.....	60
2.11.4 Histological image processing.....	61
2.11.4.1 Atlas registration.....	61
2.11.4.2 Signal detection	61
2.11.4.3 Visualization.....	62
2.11.4.4 Data exclusion.....	63
3. Results.....	64
3.1 Anatomical tracing of thalamocortical projections	64
3.1.1 Functionally targeted dual injections in S1 and pIC.....	64
3.1.2 S1 and pIC receive thalamocortical projections from spatially distinct regions	66
3.1.3 S1 and pIC send corticothalamic projections to multiple thalamic nuclei.....	68
3.2 Behavioral testing of thermal perception	70
3.2.1 Thalamic inactivation during thermal detection task	71
3.2.2 Relationship of injection site with task performance	74
3.3 Innocuous temperature is robustly encoded across mouse somatosensory thalamus.....	76
3.3.1 High-density extracellular recordings across thalamus in awake mice.....	77
3.3.2 Thermally responsive neurons elicit distinct response profiles across the thalamus.....	79
3.3.3 Cooling and warming evoked sensory responses show distinct spatial distributions	83
3.3.4 Anterior and posterior subregions in thalamic nuclei show different thermal representation.....	86
3.3.5 Thermal stimulation evokes diverse response profiles.....	89
3.3.6 The thalamic representation of touch	92
3.4 Encoding of cooling and warming stimulus intensities across thalamic nuclei.....	96
3.4.1 Thalamic temperature encoding is driven by stimulus intensity in the innocuous temperature range	96
3.4.2 Various encoding profiles with anatomical specialization drive thermal encoding in the thalamus.	98
3.4.3 Sensory response-types and anatomical location serve as an indicator of response saturation	102
3.4.4 Sensitivity of thalamic nuclei to cooling and warming stimulation	106
3.5 Investigation of temporal response dynamics of thalamic nuclei.....	109

3.5.1 Cooling and warming elicit sensory responses with distinct temporal dynamics	109
3.5.2 Temporal response profiles vary across thalamic nuclei	113
3.5.3 Three temporal profiles govern the sensory response to cooling and warming	117
3.5.4 The sharpening of the sensory response from anterior to posterior thalamic regions.....	121
3.5.5 Temporal dynamics of tactile evoked sensory response vary across thalamus	123
3.5.6 Tactile response is governed by three temporal response-profiles.....	126
4. Discussion.....	129
4.1 Anatomical tracing of thermal circuits.....	129
4.1.1 Thalamocortical projections to S1 and pIC.....	129
4.1.2 Corticothalamic projections from S1 and pIC.....	131
4.2 Thalamic inactivation during thermal detection task.....	131
4.2.1 Comparison with previous studies of thalamic inactivation in thermal detection tasks	132
4.2.2 Influence of inactivated region on strength and stimulus-specificity in thermal detection behavior	134
4.2.3 Conclusion and future direction	135
4.3 Thermal tuning of thalamic nuclei.....	136
4.3.1 Overrepresentation of cooling compared to warming	136
4.3.2 Low proportion of “Warm” cells and its functional implication	139
4.4 Spatial representation of somatosensory stimuli.....	141
4.4.1 The spatial representation of warming	142
4.4.2 The spatial representation of cooling and touch	143
4.5 The encoding of temperature amplitudes	145
4.5.1 Low proportion of “Specificity” neurons	145
4.5.2 Encoding profile of “Cold-Warm” neurons in comparison to “Cold” neurons.....	146
4.5.3 Increased sensitivity of PoT to low amplitude warming stimuli	147
4.6 Temporal dynamics	149
4.6.1 Temporal dynamics of cooling and warming encoding	149
4.6.2 Anatomical specification of temporal response properties.....	150
5. Conclusion and future direction	151
5.1 Conclusion	151
5.2 Future direction	152
6. Bibliography	154

7. Appendix	170
 7.1 Publications	170
 7.2 Declaration of independence	170
 7.3 Statement of contribution.....	170
 7.4 Abbreviations	172
 7.5 Index of figures.....	174

1. Introduction

The perception of temperature is a fundamental aspect of daily life. It has implications that range from mundane tasks such as adjusting shower water to a comfortable temperature to critical functions like safeguarding the organism from potentially hazardous thermal conditions and identifying metabolically energy-efficient thermal environments. Nevertheless, our current understanding of how central neural structures encode and represent thermal information and the perceptual significance of these neural representations remains limited.

The present study aims to investigate the neural representation of temperature in the rodent thalamus and to test the behavioral relevance of the thalamus for detecting thermal stimuli applied to the forepaw. The sensation of temperature, as of touch, is first received by skin-embedded receptors and carried through multiple ascending pathways to the thalamus and non-thalamic structures before being transmitted to cortical processing nodes.

In Chapter I, I will introduce this network of receptors, pathways, and processing nodes, emphasizing the thalamic representation of temperature (1.3). Additionally, I will outline thermal receptors and the primary afferents (1.1) and ascending spinal pathways (1.2), which deliver the input to the thalamus and non-thalamic structures. Finally, the thermal representations in thalamic downstream processing nodes, i.e., the cortex (1.4) and the lateral parabrachial nucleus (1.5), are presented.

1.1 The peripheral somatosensory system

Somatosensory information is initially transduced by receptors that are embedded in the skin in a cluster-like fashion. Field (Blix 1882) converts physical stimuli like touch and temperature into processable electrical signals. From there, the sensory information is conveyed to the spinal cord via distinct and specialized primary sensory afferents. The following chapter introduces the temperature-specific receptors (1.1.1) and the primary sensory afferents (1.1.2) that act as the first stage of the thermal system.

1.1.1 Thermosensitive receptors detect temperature changes on the skin

The most extensively studied temperature-activated proteins belong to the membrane-embedded Transient Receptor Potential (TRP) ion channel family, but also other receptors have been identified to be thermally responsive, like slowly adapting mechanoreceptors (Burton, Terashima, and Clark 1972) as well as TWIK-related potassium (TREK) channels (Lamas, Rueda-Ruzafa, and Herrera-Pérez 2019). TRP channels are localized at the peripheral terminations of primary sensory afferents in the skin (Kobayashi 2015) in a combinatorial fashion, with multiple, distinct thermal receptors co-localizing in a single fiber (Vandewauw et al. 2018). The TRP family comprises several subgroups. For temperature sensing, the most relevant TRP subgroups are TRPA (ankyrin), TRPM (melastatin) and TRPV (vanilloid). The thermal receptors are characterized by distinct activation temperatures and sensitivity to specific chemical agonists (Figure 1.1.1-1). Interestingly, while TRPM8 has been identified as the essential receptor for innocuous cold sensing, the receptor for innocuous warm sensing has not been identified so far.

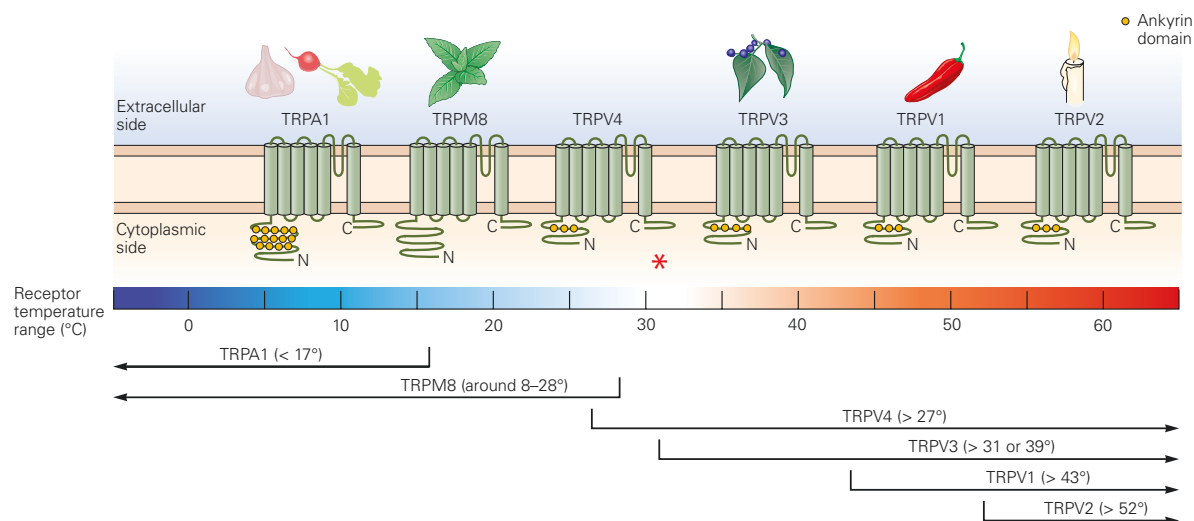


Figure 1.1.1-1 TRP receptor family with activation temperature (bottom) and agonists (top)

TRP channels are comprised of integral membrane proteins characterized by the presence of six transmembrane α -helices. A pore is generated between the fifth (S5) and sixth (S6) helices, derived from the assembly of four subunits. The N-terminal domains of most of these receptors contain ankyrin repeats, and they share a common 25-amino acid motif located adjacent to S6 within the C-terminal domain. Individual TRP channels are composed of four identical TRP protein subunits. Temperature and various chemical ligands serve as gating agents for all TRP channels. Edited from Kandel et al. 2021

TRPA1 (thermal activation range: < 17 °C, agonists: allium-expressing plants, garlic, radish): TRPA1 is located in somatosensory neurons, and its activation is driven by intense cold or cooling agents, potentially mediating painful or unpleasant cold sensations (Karashima et al. 2009; Vandewauw et al. 2018). The role of TRPA1 in cold sensation remains elusive, as some studies found limited cold-sensitive phenotypes in mice lacking TRPA1 (Bautista et al. 2006; Knowlton et al. 2010).

TRPM8 (8 – 28 °C, Menthol) is the main receptor for sensing mild cooling. When studied *in vitro*, cells containing TRPM8 demonstrate an influx of calcium ions (Ca^{2+}) when exposed to cooler temperatures or the presence of menthol (De La Peña et al. 2005; McKemy, Neuhausser, and Julius 2002; Peier et al. 2002). The predominant location for TRPM8 is within sensory fibers that respond to mild cooling, conveying this information to the dorsal region of the spinal cord (Dhaka et al. 2008). The activation point for TRPM8 in response to cooling is around 25 °C (Bautista et al. 2007; Brauchi, Orio, and Latorre 2004). In several studies, mice that don't possess TRPM8 displayed impaired cooling sensations (Paricio-Montesinos et al. 2020; Dhaka et al. 2007; Knowlton et al. 2013; Milenkovic et al. 2014).

TRPV4 (> 27 °C, no natural agonist): TRPV4 is activated by warmth and has been implicated in both non-noxious warmth and noxious heat perception (Güler et al. 2002; Suzuki et al. 2003). However, TRPV4 knockout mice exhibit limited deficits in thermosensation (Phan et al., 2015; Staaf et al., 2010).

TRPV3 (> 31 or 39 °C, camphor): TRPV3 is activated by warm and heat stimuli but may not play a key role in thermosensation, as some studies suggest it is unnecessary for both warming and painful heat perception (Moqrich et al. 2005).

TRPV1 (> 43 °C, capsaicin): TRPV1 is the first identified heat sensor, activated by high temperatures and capsaicin (M. J. Caterina et al. 1997). Its role in heat sensation is debated, as some studies suggest it plays a partial role, while others report no significant defects in heat perception in mice lacking TRPV1 (Woodbury et al. 2004; J. B. Davis et al. 2000; Marics et al. 2014). TRPV1 may also contribute to the non-noxious warmth perception (Yarmolinsky et al. 2016a).

TRPV2 (>53 °C, Cannabidiol, not shown in Figure 1.1.1-1): TRPV2 is a non-selective ion channel activated at very high temperatures. However, TRPV2 knockout mice do not show significant deficits in painful heat perception (Katanosaka et al. 2018; Park et al. 2011).

TRPM2 (40 - 50 °C): TRPM2 is expressed in DRGs of sensory afferents; it exhibits activation *in vitro* when exposed to temperatures exceeding 35 °C (Togashi et al. 2006) and has been implicated in facilitating responses to elevated temperatures, specifically those exceeding 40 °C (Tan and McNaughton 2016). Crucially, the genetic ablation of TRPM2 has been observed to suppress thermal preference behaviors in mice within the temperature range of 33 - 38 °C. TRPM2-deficient mice still manifest avoidance responses at near pain threshold (43 °C) and cold temperatures (23 and 28 °C). A recent study has confirmed that TRPM2 plays a specific and selective role in mediating non-noxious warming perception (Paricio-Montesinos et al. 2020). Furthermore, emerging evidence points towards TRPM2 functioning as a thermal sensor, with activation occurring at temperatures exceeding 38 °C within the preoptic area of the hypothalamus. This function appears to be critical for maintaining physiological thermoregulatory control (Song et al., 2016).

1.1.2 Primary sensory afferents send sensory information to distinct lamina of the spinal cord

Primary sensory afferents are pseudo-unipolar neurons. Their cell bodies are located in the dorsal root ganglions. The axons of these neurons have two branches: the peripheral site at which the sensory receptors are located and the central site where these neurons synapse onto spinal cord fibers (Mantyh 1983). Primary sensory afferents serve two functions: encoding sensory stimuli into electrical signals by the sensory receptors, and transferring the electrical signals to the central nervous system. Several classes of primary sensory afferents exist, including A α -, A β -, A δ -, and C-fibers. The key differences between these fiber types relate to myelination and axon diameter, leading to different conduction velocities of the electrical signals. Myelinated A α -fibres with 20 μ m are the largest in diameter, followed by myelinated A β -fibres of 12 μ m. Myelinated A δ - and non-myelinated C-fibers are considered

small-diameter fibers with 5 and 1 μm axon diameter, respectively. The conduction velocities in A α -fibers were estimated with 120 m/s and in A β -fibers with 72 m/s, which makes them faster than the small-diameter myelinated A δ -fibers (30 m/s). The non-myelinated C-fibers only have one m/s conduction velocity (Necker and Meinecke 1984; Cottrell 1984).

Somatosensory signals like cooling, warming, or touch activate distinct combinations of primary sensory afferents. Touch signals show a widespread activation of all fiber groups introduced above, while cooling-selectively activates A δ -fibers and C-fibers (Abraira and Ginty 2013; Darian-Smith, Johnson, and Dykes 1973). Warming shows a restricted activation profile compared to touch and cooling and only activates C-fibers (Darian-Smith et al. 1979).

1.1.2.1 The encoding of thermal stimuli in primary sensory afferents

Over 100 years ago, Blix discovered that thermal stimulation of spatially distinct regions (cold spots, warm spots) on the skin leads either to cooling or warming sensations in human test subjects (Blix 1882). Interestingly, it was shown that cold spots outnumbered warm spots on the skin and that tactile sensations were evoked by stimulation of different spatial locations on the skin. These observations have been mostly proven and extended to multiple animal models using modern techniques over the last 141 years (Gentle 1989; Darian-Smith et al. 1979; Darian-Smith, Johnson, and Dykes 1973; F. Wang et al. 2018a) and have led to a prominent theory about sensory encoding in primary afferents, the labeled line theory. According to the labeled line theory, distinct sensations like cold, warm, or touch are encoded and transmitted to the brain by parallel fibers that contain exclusively information about the given submodality with no significant information about other modalities (Hensel and Schafer 1984; Yarmolinsky et al. 2016a).

Contrary to the labeled line conception, population coding or pattern theory suggests that sensations emerge from activating diverse sensory afferents, each with distinct sensitivities to various stimulus modalities. (Green 2004; A. D. (Bud) Craig 2003; Prescott, Ma, and De Koninck 2014). Multiple studies have investigated which of the models above provides a more accurate description of sensory encoding in primary afferents, but the results remain inconclusive.

Evidence derived from human and rodent investigations elucidates mechanisms underpinning thermal encoding at the level of sensory afferents. Specifically, distinct fibers have been identified that demonstrate an increase in neuronal firing in response to cooling stimuli and suppression of neural firing in response to warming stimuli, thereby facilitating a straightforward interpretation of the thermal stimulus via the scalable nature of neural firing relative to the applied temperature (Darian-Smith, Johnson, and Dykes 1973; Paricio-Montesinos et al. 2020).

1.2 The spinal cord

The spinal cord is coarsely defined by three functionally distinct segments: the dorsal and ventral horns as well as an intermediate zone that are all further divided into lamina, with lamina I populating the most dorsal part of the spinal cord and lamina X being located at the most ventral part of the spinal cord (Figure 1.2-1 A, B). The functionally distinct segments receive input from different afferent fibers. It has been shown that the largest fibers ($A\alpha$) terminate in the ventral horn, the medium-sized fibers ($A\beta$) terminate in the intermediate zone, and the small diameter fibers ($A\delta$ and C) in the dorsal horn (Kumazawa and Perl 1978; Yates, Thompson, and Mickle 1988; Meyers and Snow 1986) (Figure 1.2-1 C).

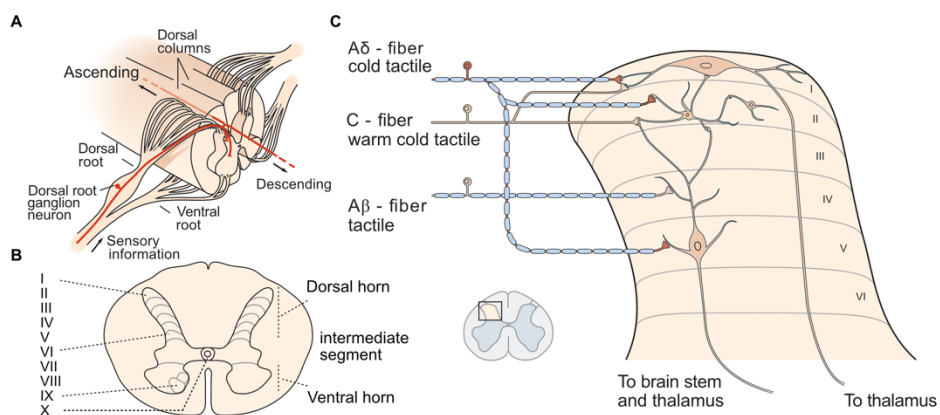


Figure 1.2-1 Input from sensory afferents to the spinal cord

- Overview of a primary sensory afferent with cell body location in the dorsal root ganglion entering the spinal cord through the dorsal root and sending sensory information in an ascending direction via the dorsal column.*
- Coronal section of the spinal cord with labeling of the dorsal horn, intermediate segment, and ventral horn (right) and a schematic of the laminar organization of the spinal cord (left).*

C. Detailed input pattern of 3 types of primary sensory afferents that transmit distinct modalities from the periphery to the spinal cord. The cold and tactile sensitive and myelinated A δ fibers synapse in the dorsal horn of the spinal cord primarily onto the superficial layers (lamina I and lamina II) and deeper lamina V. The multimodal, non-myelinated small diameter C-fibers synapse onto the superficial lamina II of the spinal cord. The tactile responsive myelinated A β fibers primarily target the deeper lamina IV of the spinal cord.

The sensory information is sent from these recipient segments via distinct and modality-specific ascending pathways to the thalamus. The following chapter will present three major pathways that transmit thermal and tactile information to the brain: the Spinothalamic tract, the Dorsal Column-Medial Lemniscal pathway, and the Spinoparabrachial tract (Figure 1.2-2).

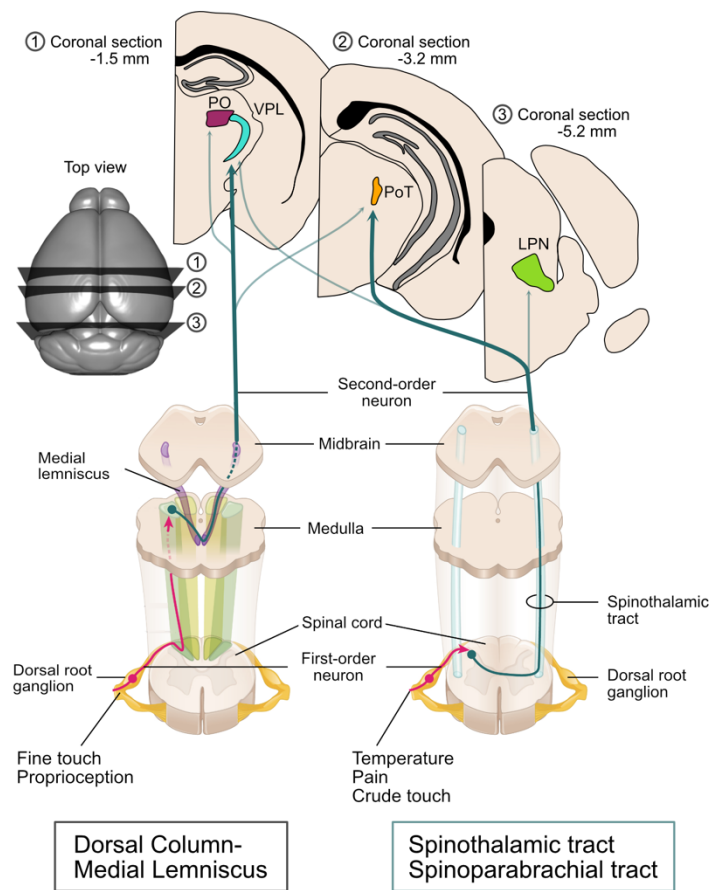


Figure 1.2-2 Overview of ascending spinal cord pathways

Schematic overview of the three major ascending pathways that transmit somatosensory information from the sensory periphery to the thalamus: The Dorsal Column-Medial Lemniscus pathways (left) and the Spinothalamic and Spinoparabrachial tracts (right). Primary sensory afferents (red) with cell bodies in the dorsal root ganglion enter the spinal cord via the dorsal root to the dorsal horn. The sensory afferents that belong to the Dorsal Column-Medial Lemniscus pathway travel the spinal cord in an ascending direction up to the level of the Medulla, where they synapse onto second-order neurons (petrol). From there, the neurons cross the midline, known as the medial lemniscus, and travel via the midbrain to distinct thalamus regions, including the main projection target, VPL (cyan). Projections to PO (bordeaux) and PoT (gold) have also been identified. The sensory afferents that belong to the Spinothalamic tract and Spinoparabrachial tract synapse onto second-order neurons in the dorsal horn and cross the midline of the spinal cord. From there, the spinal cord fibers travel ascending until they reach either the lateral parabrachial nucleus (LPN, green) or the thalamus. The primary thalamic recipient of the Spinothalamic tract is PoT (gold), but projections to VPL (cyan) have also been identified.

1.2.1 The Spinothalamic tract

The Spinothalamic tract is one of the primary ascending pathways for transmitting innocuous thermal and noxious signals within the spinal cord. It comprises the nerve fibers from nociceptive-specific, thermosensitive, and wide-dynamic-range neurons situated in laminae I and V to VII of the dorsal horn (Bokiniec et al. 2018; Davidson, Moser, and Giesler 2014). These nerve fibers cross over the midline of the spinal cord near their point of origin and ascend through the anterolateral white matter before ultimately reaching multiple thalamic nuclei (Kandel et al. 2021). Cells originating from this tract typically possess specific, one-sided receptive fields responsible for our ability to pinpoint the location of painful or thermal stimuli. However, neurons located in lamina VII show larger receptive fields than lamina I neurons (X. Zhang and Giesler 2005; X. Zhang, Davidson, and Giesler 2006a). The thalamic terminations of Spinothalamic tract neurons located in lamina I are located in the posterior part of the Ventral posterolateral nucleus (VPL) (Hodge and Apkarian 1990) as well as in the border region of the Posterior complex (PO) and Posterior triangular nucleus (PoT) (Al-Khater, Kerr, and Todd 2008).

In the domain of thermo-sensory perception, evidence indicates that the selective inactivation of lamina I spinal cord fibers, pivotal for the transmission of thermal information to the cerebral cortex via the Spinothalamic tract, substantially influences thermal perceptual capabilities (Norrsell and Craig 1999).

1.2.2 The Dorsal Column-Medial Lemniscal pathway

The primary sensory afferents of A α - and A β - fibers send their axons through the two dorsal columns to the medulla (Giuffrida and Rustioni 1992). Their axons cross the midline at the level of the medulla to form the medial lemniscus. This prominent fiber tract transmits tactile and proprioceptive information from the contralateral side of the body through the pons and midbrain to multiple thalamic nuclei (Kandel et al. 2021). Although the Ventrobasal complex (VB) that consists of VPL and the Ventral posteromedial nucleus (VPM) was identified as the primary recipient structure of medial lemniscal projections, projections to other nuclei of the

Posterior group (PO, PoT) and subthalamic structures (Zona incerta) were also identified (Feldman and Kruger 1980).

1.2.3 The Spinoparabrachial tract

The Spinoparabrachial tract comprises axons originating from projection neurons located within laminae I and V of the spinal cord. It is implicated in transmitting information that contributes to the affective or emotional aspect of somatosensory signals (Light and Perl 1979; Saper 1995). This neural pathway extends through the anterolateral quadrant of the spinal cord. It sends branching axons to the lateral parabrachial nucleus situated at the level of the pons that terminate at the level of the thalamus (Hylden, Anton, and Nahin 1989). Notably, this tract has numerous collateral connections with the mesencephalic reticular formation and the periaqueductal gray matter. (Browne et al. 2021)

1.2.4 Encoding of temperature in the spinal cord

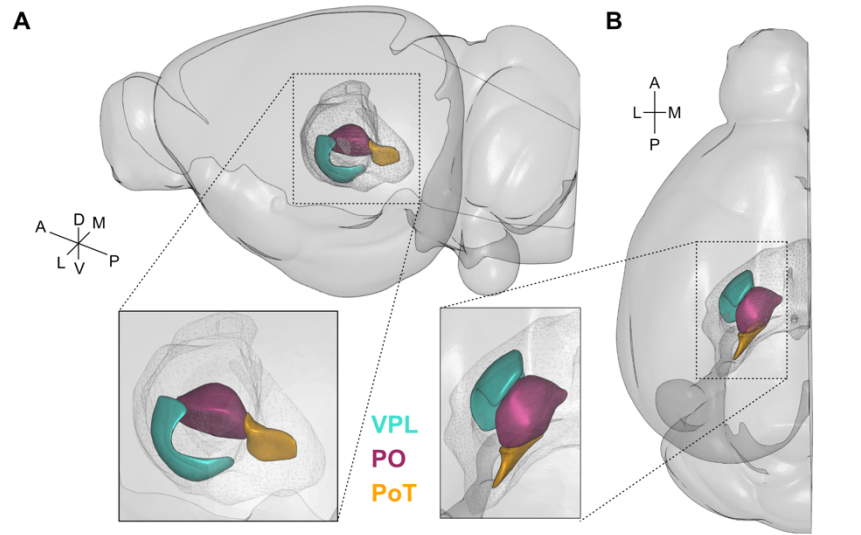
Anatomical investigations have found that primary afferents project predominantly to the superficial layers of the dorsal horn in the spinal cord. However, within the spinal cord, the understanding of temperature encoding remains elusive. Analogous to primary sensory afferents, temperature changes on the skin (approximately 30-32 °C) have been observed to increase neural firing (A. D. Craig and Dostrovsky 2001). Moreover, thermal stimuli with increased intensity tend to activate more spinal neurons than thermal stimuli with mild or low-intensity (Ran, Hoon, and Chen 2016a). Notably, despite the presence of thermosensitive spinal neurons that exhibit specificity towards either heat or cold, a significant proportion of spinal cord neurons showed excitatory responses to both cooling and warming (Ran, Hoon, and Chen 2016a). Using calcium imaging, it was demonstrated that 7 % of lamina I spinal cells responded to innocuous cooling (29 °C) and warming (37 °C), while 44 % of neurons were activated by cold (5 °C) and heat (50 °C). The same study also explored the encoding mechanisms of cooling and warming besides thermal tuning characteristics and demonstrated

that cooling and warming employ intrinsically different encoding schemes. While cooling-responsive neurons in the spinal cord signal the difference between the adaption temperature and the stimulus temperature (relative encoding), warming-responsive neurons instead function as thermostats by signaling the absolute stimulus temperature (absolute encoding) (Ran, Hoon, and Chen 2016a).

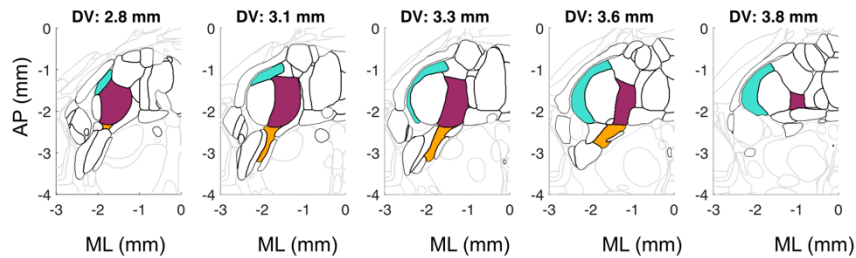
1.3 The Thalamus

The thalamus, a pivotal component of the mammalian brain situated within the dorsal aspect of the diencephalon, represents a complex assembly comprised of approximately 50 nuclei, classified based on cytoarchitectural criteria (S. M. Sherman and Guillery 2001; E. G. Jones 1981). The thalamus is involved in diverse functions such as sensory processing, motor coordination, regulation of arousal, and cognitive processes (Halassa 2023). Considering the thalamus's well-described role in the sensory processing of diverse modalities, it's surprising to note that our understanding of the thermal thalamus remains limited. The behavioral relevance of the thalamus for thermal perception and the basic properties of thermal encoding are still unclear, warranting further investigation.

The subsequent section will provide an introductory overview of thalamic sensory processing, with a particular emphasis on the processing of somatosensory signals within three discrete thalamic nuclei (VPL, PO, and PoT) that are the primary recipients of the Dorsal Column Medial Lemniscus and the Spinothalamic tract, both of which are traditionally related to somatosensory processing (Figure 1.3-1).



C Horizontal Projections



D Coronal Projections

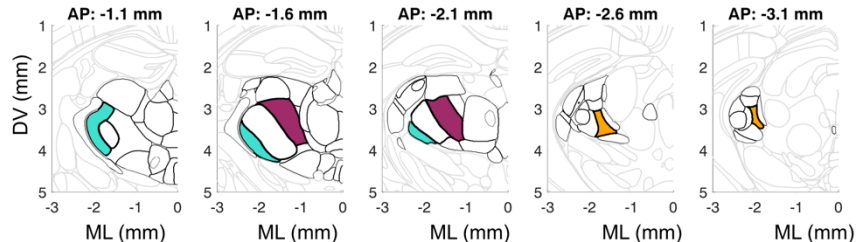


Figure 1.3-1 Anatomical location of VPL, PO, and PoT

- Three-dimensional rendering of mouse brain surface with Thalamus contour (wireframe) and the three thalamic nuclei VPL (cyan), PO (bordeaux), and PoT (gold).
- Same as A from a top-view perspective.
- Horizontal projections of the Thalamus at five distinct dorsoventral sections. Same color code as A.
- Coronal Projections from Thalamus at five distinct anteroposterior sections. Same color code as A.

1.3.1 The Ventral posterolateral nucleus - VPL

The thalamic nucleus VPL forms, together with its medial-located neighboring nucleus VPM, the Ventrobasal Complex (VB), which belongs to the dorsal tier ventral group (Edward G. Jones 1985; Schröder, Moser, and Huggenberger 2020). Its shell-like shape characterizes VPL, composed of densely packed, large, and excitatory cells arranged in a cluster-like fashion (McAllister and Wells 1981).

VPL is one of the primary thalamic recipients of the Dorsal Column-Medial Lemniscal pathway but also receives additional input from the Spinothalamic tract. These pathways transmit somatosensory information like temperature, touch, and pain from the entire body surface, excluding the face and mouth, to VPL. Sensory information coming from facial regions is channeled through VPM, the neighboring thalamic nucleus of VPL (Kandel et al. 2021). The neural representation of the body within VPL has a somatotopic map (Francis, Xu, and Chapin 2008a). The somatosensory signals from the thalamus are relayed to distinct cortical areas tuned to the processing of the respective sensory signal. Well-described thalamocortical projection targets from VPL are primary somatosensory cortex (S1) (Yamawaki et al. 2021) and secondary somatosensory cortex (S2) (Liao and Yen 2008). Further, cortical projections were also identified in the posterior insular cortex (pIC), which, however, show decreased projection strength relative to S1 and S2 (Z.-H. Zhang and Oppenheimer 2000; Gehrlach et al. 2020; Bokiniec et al. 2023).

1.3.1.1 Encoding of somatosensory signals in VPL

It has been shown that VPL encodes the full spectrum of somatosensory stimuli, including touch (Baker 1971; Francis, Xu, and Chapin 2008a; S. E. Sherman, Luo, and Dostrovsky 1997; Emanuel et al. 2021), temperature (Günter Schingnitz and Werner 1980b; Burton, Forbes, and Benjamin 1970a; Sakata, Morimoto, and Murakami 1989; Kanosue et al. 1985; Hellon and Misra 1973), proprioception (Francis, Xu, and Chapin 2008a) and pain (Apkarian and Shi 1994; Kenneth L. Casey and Morrow 1983; Chung et al. 1986; Kenshalo et al. 1980). In particular, the work on tactile and proprioceptive processing in VPL has provided valuable insights into VPL

neurons' functional architecture and encoding properties. For example, Francis and co-workers have demonstrated that VPL is divided into three functional segments along the anterior–posterior axis, each with distinctive tuning and receptive field properties. Receptive fields in the anterior section of VPL covered large parts of a single limb, and the preferred tuning was to joint movements. The middle portion of VPL showed preferred tuning to tactile stimuli with small receptive fields covering single digits of the paw. VPL's posterior segment was tuned mainly to tactile stimulation. However, the receptive fields were large and extended over the entire paw or broad regions of the body surfaces like the trunk or back. Even though functional segmentation of VPL has been shown, it needs to be mentioned that short-latency transient sensory responses across the entire anterior-posterior axis of VPL upon innocuous tactile stimulation of a single paw can be found (Francis, Xu, and Chapin 2008a).

Multiple studies have examined the neural representation of temperature in the thalamus in anesthetized preparations and found diverse results in terms of the representation of temperature, especially concerning the representation of innocuous cooling and warming. Key factors that defined the neural response were the stimulation site (e.g., limb, scrotum), the model organism (e.g., rat, cat, monkey), and the tested temperature range (e.g., innocuous, noxious). The body part that was thermally stimulated had a strong impact on the neural representation of temperature in the rats' VB in an anesthetized preparation. Interestingly, while stimulation of the scrotum evoked cooling and warming responses, limb stimulation completely lacked a warming representation (Günter Schingnitz and Werner 1980b; Sakata, Morimoto, and Murakami 1989; Kanosue et al. 1985; Hellon and Misra 1973; Hellon and Taylor 1982; Jahns 1975) indicating that thermally responsive neurons within VPL are also characterized by receptive fields and exhibit preferred thermal tuning. However, no information about the spatial arrangement of these differentially tuned neurons was provided. Furthermore, the thermal representation in anesthetized animals might be fundamentally different compared to awake animals, as anesthesia has been shown to affect multiple nodes of the thermal system, including thalamic function itself at the primary sensory afferent as well as thermoregulation (Raithel et al. 2018; Huh and Cho 2013).

In addition to the constrained spatial precision associated with the characterization of thermal encoding and the lack of investigation into thermal encoding under awake conditions, the temporal dynamics of thermal stimuli in the aforementioned research studies constrain the insights regarding the encoding characteristics of neurons within VPL. Historically,

temperature stimulations were implemented over a duration of minutes, and subsequent analysis was performed on adapted firing rates of neurons over a time scale of minutes. However, similar to humans, rodents exhibit the capacity to perceive alterations in temperature on a sub-second temporal scale when interacting with either cold or warm objects or discerning the ambient temperature of their surroundings (Paricio-Montesinos et al. 2020; Milenkovic et al. 2014). These dynamic attributes of the thermal sensory system elude exploration when subjected to a slow temperature stimulation paradigm. Consequently, this dynamic feature of thermal encoding remains elusive.

1.3.2 The Posterior triangular nucleus - PoT

In rodents, the PoT nucleus is anatomically the posterior extension of PO. On its lateral side, it is surrounded by the medial geniculate nucleus (MG), the posterior intralaminar nucleus in a ventrolateral direction, and prectothalamic lamina in a medial direction. The cellular composition of PoT is characterized by relatively small and scattered neurons (Márquez-Legorreta et al. 2016; Gauriau and Bernard 2004a). The terminology of PoT has been a matter of scientific debate, and PoT is differently labeled in monkeys (posterior part of the ventral medial nucleus, VMpo) (A. D. Craig et al. 1994; A. D. Craig, Zhang, and Blomqvist 1999) and cats (basal part of the ventral medial nucleus, VMb) (A. D. Craig and Dostrovsky 2001). The definition of PoT is mainly influenced by its input/ output connectivity, independent of the model organism. PoT, or its homologous nuclei in monkeys and cats, receives strong input from the superficial lamina I of the spinal cord, which is mainly utilized by the Spinothalamic tract and transmits thermal and noxious somatosensory information to the thalamus. (Gauriau and Bernard 2004b; 2004b; A. D. Craig and Dostrovsky 2001; Davidson, Truong, and Giesler 2010; William D Willis et al. 2002). From there, the sensory information is transmitted via thalamocortical projections to the main target pIC and also to S2 (A. D. (Bud) Craig 2014; Clasca, Llamas, and Reinoso-Suarez 1997; Bokiniec et al. 2023; Gehrlach et al. 2020).

1.3.2.1 The encoding of somatosensory signals in PoT

The encoding of somatosensory information in PoT has been mainly investigated in the context of pain processing due to its prominent reception of Spinothalamic tract fibers. Only a very limited number of studies have investigated the neural representation of innocuous tactile or thermal stimuli in that structure.

Noxious tactile as well as noxious thermal stimuli have been shown to strongly activate PoT neurons as well as the application of chemicals that induce painful sensations like capsaicin (A. D. Craig et al. 1994; Lipshetz et al. 2018; Gauriau and Bernard 2004a). Interestingly, PoT has a full body representation, including the face. Neurons within PoT showed preferred tuning to distinct body parts and also to different modalities, even though multimodal neurons could be found (Lipshetz et al. 2018). Furthermore, it was shown that neurons within PoT have receptive fields of varying sizes. Nociceptive neurons had, on average, the largest receptive fields, covering the entire trunk and large parts of certain body parts (Gauriau and Bernard 2004a) in comparison to the neurons that were selectively tuned to innocuous stimuli (A. D. Craig et al. 1994; Gauriau and Bernard 2004a). Gauriau and colleagues reported the existence of PoT neurons with receptive fields covering only a single digit and preferred tuning to innocuous tactile stimulation, while others found innocuous thermally tuned neurons with receptive fields covering small parts of the contralateral tongue (Gauriau and Bernard 2004a). The thermally tuned neurons were cold-selective and showed a suppressed response to warming stimuli, resembling the response profiles seen in primary sensory afferents in higher-order model organisms (A. D. Craig et al. 1994; Gauriau and Bernard 2004a).

In summary, PoT has been shown to encode painful as well as non-painful somatosensory stimuli in a stimulus-specific manner, but insights into the encoding of innocuous thermal or tactile stimuli are limited and need further investigation.

1.3.3 The Posterior complex of the thalamus - PO

The PO of the rodent's thalamus is part of the intermediate tier and spans over multiple millimeters in anterior-posterior direction in the thalamus. It is located in dorso-medial direction of VB. The neuroanatomy of this thalamic structure is a matter of scientific debate and is most likely composed of multiple functional and anatomically distinct segments (Edward G. Jones 1985; Schröder, Moser, and Huguenberger 2020). The most extensively described subregion within PO is the medial segment (POm), which is part of the whisker system in rodents. This part of PO receives dominant input from cortical regions and not the sensory periphery like the VB or PoT (S. M. Sherman 2005). However, a recent study has shown that a thalamocortical pathway through POm to S1 exists in which sensory information could reach the cortex (El-Boustani et al. 2020).

1.3.3.1 The encoding of somatosensory signals in PO

The encoding of somatosensory signals applied to the skin has received little attention, which has led to a limited understanding of cellular encoding properties in PO. However, functional magnetic resonance imaging (fMRI) has revealed that PO shows increased activity upon tactile stimulation of the paw (Sanganahalli et al. 2022), indicating that PO might be involved in the processing of somatosensory information. A further indication of the functional involvement of PO in sensory processing comes from a study that recorded nociceptive neurons in spinal cord lamina I that send thalamic projections to the border region of posterior PO and PoT (X. Zhang and Giesler 2005).

The sensory encoding in the medial part of PO, labeled as Pom, has received more attention in the whisker field, where cellular encoding was investigated. Under anesthesia, POm neurons exhibit variable and extended response latencies along with a moderate increase in spike rates after passive whisker stimulation (Diamond, Armstrong-James, and Ebner 1992a). Typically, POm neurons possess receptive fields encompassing more than one whisker, suggesting a weakly somatotopically organized input. Taken together, the sensory encoding

properties of PO remain an active area of research, and only very limited data on somatosensory encoding is available.

1.4 The Cortex

1.4.1 The primary somatosensory cortex – S1

Substantial empirical support exists for the representation of cool thermal information within S1 of mammals. In both rodents and felines, exposure to cooling temperatures has been demonstrated to elicit activation of contralateral S1 neurons (Hellon and Misra 1973; Milenkovic et al. 2014; Vestergaard et al. 2023). Additionally, investigations involving human subjects have revealed that the human S1 is responsive to innocuous cooling and warming stimuli, as discerned through functional imaging and electroencephalography (Egan et al. 2005; Guest et al. 2007). Electrical stimulation of S1 in human subjects drove a cooling sensation (Penfield and Boldrey 1937), and the impairment of thermal stimulus perception has been observed after lesioning S1 (Ploner, Freund, and Schnitzler 1999). Significantly, the pharmacological inactivation of the S1 region has been found to disrupt cooling perception in mice, and a comparable reduction in S1 responsiveness to cooling occurs when the afferent input is deactivated (Milenkovic et al., 2014). Taken together, it is evident that the S1 cortex plays a pivotal role in the thermal perception and encoding of cooling information in mammals.

1.4.2 The posterior insular cortex - pIC

In addition to S1, it has been demonstrated that temperature induces activation in pIC. In the context of human studies, the perception of painful heat has been positively correlated with neural activity in pIC, as evidenced by prior research (K. L. Casey et al. 1996; K. D. Davis et al. 1998). Interestingly, deviations in temperature and pain sensitivities have been documented in humans with lesions in the parietal and insular regions (Starr et al. 2009; Veldhuijzen et al. 2010). These clinical observations align with experimental findings in rodents, where noxious

and innocuous thermal stimulation induces activations in S1 and pIC (Reimann et al. 2016). Moreover, a recent study has shown that pIC shows a robust and specific thermal representation, a somatotopic thermal map of the body, and that pIC activity is necessary for thermal detection (cooling and warming) behavioral experiment (Vestergaard et al. 2023).

1.5 The lateral parabrachial nucleus and hypothalamus

Concomitant with the spinothalamic pathway responsible for transmitting temperature information to the cortex, a subset of axons originating from spinal cord fibers that send projections to the thalamus also project to the lateral parabrachial nucleus (LPN), situated at the intersection of the midbrain and pons (Schröder, Moser, and Huggenberger 2020). Subsequently, the LPN projects to the hypothalamus. While it is widely posited that thalamic and neocortical neurons are instrumental in the mediation of thermal stimulus perception, it is theorized that parabrachial and hypothalamic neurons take a pivotal role in the regulation of homeostasis, specifically in maintaining the body within an optimal thermal range (Nakamura and Morrison 2010; 2008).

Empirical investigations have demonstrated that clusters of parabrachial neurons exhibit activation in response to both cooler and warmer temperatures (Xue et al. 2016). These neurons send projections to the preoptic area (POA) of the hypothalamus (Nakamura and Morrison 2008). When confronted with elevated temperatures, LPN neurons activated by warmth instigate the suppression of thermogenesis and the augmentation of peripheral vasodilation to facilitate increased cutaneous heat dissipation (Yang et al. 2020). Significantly, it has been ascertained that neurons within LPN possess the capacity to influence behavioral thermal preference independently of the thermal thalamus (Yahiro et al. 2017). This supports the claim of different neural pathways for thermal perception and thermal preference i.e. the Spinothalamic tract and Spinoparabrachial tract, respectively. The hypothalamus contains a collection of thermosensitive neurons, which are responsible for detecting internal temperature and thereby acting as a thermostat for the brain. Hypothalamic neurons activated by warmth within the POA are responsible for the regulation of body temperature (Song et al. 2016). Additionally, cool-sensitive neurons have been identified within the

dorsomedial hypothalamus (DMH), which exerts supplementary control over body core temperature. Remarkably, it has been discerned that neurons originating from the POA modulate the activity of neurons within the DMH (Zhao et al. 2017).

In summary, the transmission of temperature information unfolds through a sequence of stages, commencing with afferent signaling, followed by traversal through the spinal cord, the thalamus, and the cortex (specifically, S1, S2, and IC). In parallel, signals journey from the spinal cord to the LPN and subsequently reach the POA of the hypothalamus, thereby orchestrating thermoregulatory responses at both physiological and behavioral levels. Nevertheless, the precise contributions of each of these stages in thermal processing, such as intensity, localization, and valence, remain presently unresolved.

1.6 State of the art and aims of the current study

The following chapter aims to present the state of the research concerning temperature processing and formulate the goals of the present study.

1.6.1 Anatomical characteristics of the thalamocortical temperature circuits

Somatosensory information, including temperature, is transmitted through the Dorsal Column-Medial Lemniscus and the Spinothalamic tract to thalamic nuclei, including VPL, PO, and PoT. These nuclei relay the information to thermally tuned cortical regions, such as S1 and pIC, establishing thermally responsive thalamocortical circuits. The anatomical configuration of these circuits, however, is enigmatic; whether these thalamocortical circuits are structured as anatomically distinct and parallel or exhibit overlapping and potentially redundant pathways remains elusive (Figure 1.6.1-1). Additionally, current knowledge lacks intranuclear spatial specificity regarding the origins of S1- and pIC-specific projections.

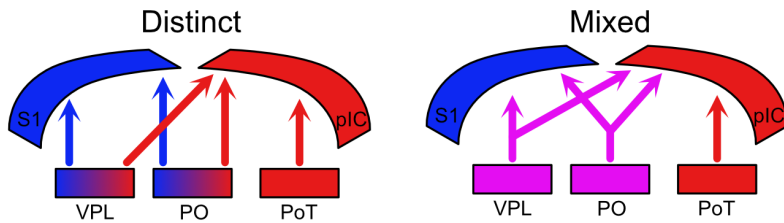


Figure 1.6.1-1 Schematics of potential thalamocortical connectivity motifs. In the 'Distinct' model (left), subregions within the VPL, PO, or PoT would send specific projections to either of the two cortical temperature-sensitive regions S1 and pIC. These projections would arise from distinct cell populations, leading to very few cells projecting to both S1 and pIC. In contrast, the 'Mixed' model shows that S1 and pIC receive projections from the overlapping thalamic subregions, leading to a large number of cells projecting to both S1 and pIC.

Addressing these questions, the present study employs a dual anatomical tracing approach from functionally defined S1- and pIC-specific thermal representations within the same animal. This approach offers a meticulous exploration of the thalamic cell population that interfaces with thermally responsive cortical regions, attempting to discern whether these projections originate from overlapping or distinct cellular populations. Moreover, utilizing a dual injection method, a nucleus-specific projection profile for the thalamic nuclei will be established, thereby enhancing our anatomical understanding of the thalamus.

In adopting a scientifically rigorous yet innovative methodology, this study aims not only to bridge a notable knowledge gap but also to provide substantive, novel insights into the anatomical configuration of thermally responsive neural circuits, augmenting our understanding of thalamocortical interplay and thalamic organization principles.

1.6.2 Testing the perceptual relevance of the thalamus in a temperature detection task

Unveiling the causal relationships between neural activity in brain structures and sensory perception is a fundamental aspect of sensory neuroscience.

The field has used various neural inactivation methods in perceptual tasks to identify specific neural ensembles and structures that are important for the animal perception of external stimuli. This has led to the hypothesis that the thalamus carries perceptual relevant information. Nonetheless, the role of the thalamus in temperature perception remains

elusive. This ambiguity predominantly arises from a lack of studies performing thorough thalamic inactivation during thermal perceptual tasks, partial inactivation of potential thalamic nuclei, and inconsistent results from inactivation approaches during temperature-related behavioral tasks, often resulting in minimal or absent impairment of thermal perception (Figure 1.6.2-1).

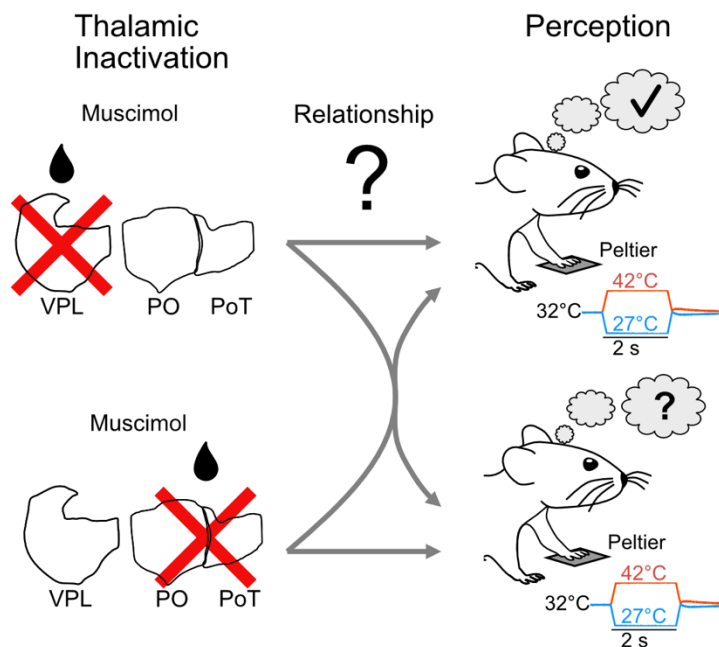


Figure 1.6.2-1 Influence of thalamic inactivation on thermal perception. Schematic of potential relationships between thalamic inactivation and thermal perception. Inactivation of either of the two thalamic regions of interest could result in either an unaffected perception (top right), signifying that the thalamus is irrelevant to thermal perception, or an affected perception (bottom right), meaning that the thalamus is vital to thermal perception.

In the present study, I conducted an investigation regarding the role of the thalamus in a thermal detection task by reversibly blocking neural activity using muscimol, applied via microinjections into multiple thalamic nuclei. These nuclei are connected to cortical temperature representations and relay information from ascending pathways that mediate somatosensory sensibility. This approach is designed to provide insights into the contribution of the thalamus to thermal perception, therefore aiming to bridge the current knowledge gap about thalamic function in thermal perception.

1.6.3 Investigation of thermal encoding principles across the thalamus

Investigations into thermal encoding within the thalamus have revealed that VPL exhibits sensory responses to innocuous temperature stimulation at a single cell level. In contrast, cells responsive to noxious temperatures have been identified in PoT. In the context of PO, only population activity has been observed upon thermal stimulation. This widespread temperature representation has prompted a debate regarding the primary thalamic nucleus responsible for thermal processing (Willis et al., 2002; Craig et al., 1994; Schingnitz & Werner, 1980). The prevailing uncertainty possibly stems from an absence of comparative studies that explore encoding across thalamic nuclei, seeking to elucidate the basic principles of sensory processing in the aforementioned temperature representations. Critical unanswered questions encompass the differentiation between cold and warm representations by single cells, the spatial configuration of thermally responsive cells both within and across nuclei, the amplitude encoding profile of individual neurons concerning response saturation to high amplitude stimuli and sensitivity to low amplitude stimuli, and the temporal profile of single-cell responses (Figure 1.6.3-1). Addressing these topics will provide clarity on the distinct characteristics of thalamic nuclei in thermal encoding.

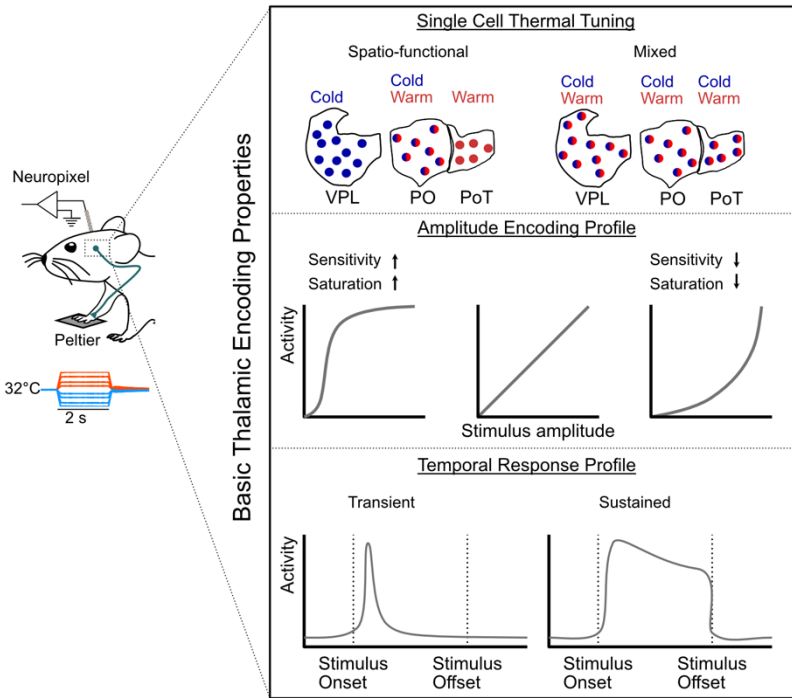


Figure 1.6.3-1 Different models of thermal encoding in the thalamus. Schematics of the basic encoding properties investigated in the present study. Single-cell thermal encoding (top) will test if temperature-responsive cells are arranged in a spatio-functional manner indicated by distinct regions within thalamic nuclei that show specialized tuning to either cold or warm. On the other side of the spectrum lies the ‘Mixed’ model, indicated by very weak thermal tuning and distinct spatial organization of thermally responsive cells. The investigation of the amplitude encoding profile (middle) will test if temperature stimuli of increasing amplitudes are encoded by highly sensitive and saturating neurons, leading to a step-like tuning curve, or by weakly sensitive and non-saturating neurons, leading to an exponential-like tuning curves rendering the physiological function of the thalamic neurons. The temporal response profile (bottom) of thermally responsive neurons provides information on the potentially encoded stimulus feature of a single neuron.

The current study aims to address these constraints by recording activity from several hundred individual neurons across three distinct thalamic nuclei with subsequent analysis of the basic encoding attributes, specifically focusing on the differentiation between cold and warm representations, the amplitude encoding profiles, and a comprehensive examination of the temporal profile of single unit responses. The objective is to discern the physiological disparities in temperature encoding among VPL, PO, and PoT.

2. Material and Methods

2.1 Animals

All experiments were approved by the Berlin Landesamt für Gesundheit und Soziales (LAGeSo), and carried out in accordance with European animal welfare law.

Adult male and female C57BL/6J (wt, n=24) mice from Jackson Laboratories were used for electrophysiological recordings. Mice were housed under 12-hour light/dark cycles and provided with *ad libitum* food and water.

Adult male and female GP4.3 (n=10, C57BL/6J-Tg(Thy1-GCaMP6s)GP4.3Dkim/) mice from Jackson Laboratories (JAX#024275) were used for tracing studies. Mice were housed under 12-hour light/dark cycles and provided with *ad libitum* food and water.

Adult male and female C57BL/6J (wt, n=15) mice from Jackson Laboratories were used for behavior experiments. Mice were housed under 12-hour light/dark cycles and were set on a restricted water regime, receiving 1.75 mL of water per day.

2.2 Surgery

2.2.1 Stereotactic alignment of the skull for electrophysiological recordings

Mice were anesthetized with intraperitoneal injections of ketamine (Ketaminador®, 120 mg/kg, WDT) and xylazine (Rompun® 2 %, 10 mg/kg, Elanco) after receiving preoperative administration of metamizol (200 mg/kg). Mice were placed on a heating pad, eye ointment (Vidisic, Bausch + Lomb) was applied to both eyes, and a rectal probe was inserted to keep the body temperature at 37 °C (DC Temperature Controller, FHC). After 5 to 10 minutes of incubation time with anesthesia, paw-pinch reflexes were controlled. If mice showed no reflexive behavior, ear bars were carefully inserted in the ear canal. The animal was placed into a stereotactic frame (Narishige, SR-9AM). An incision along the midline of the skull was made to expose the parietal bone. Bregma and Lambda suture landmarks were marked with a glass pipette (20-50 µm diameter) that was covered with ballpoint ink. The glass pipette was mounted onto a micro-manipulator system (Luigs & Neumann, Mini 55-XR, SM 7), and the

absolute manipulator position of Bregma was saved and compared with the Lambda position. If the height difference between Bregma and Lambda was more than 100 µm, the tilt of the skull was adjusted. After the correct alignment of the skull, the stereotactic coordinates for thalamic extracellular recordings were marked on the skull using ballpoint ink and a glass pipette.

2.2.2 Implantation of head post for electrophysiological recordings

After the alignment of the skull, the parietal bone was prepared for the implantation of a lightweight metal bar over the right hemisphere of the animal. A scalpel was used to make fine, superficial cuts in the skull. A fine layer of superglue (Loctite 401, Henkel) was applied over both hemispheres. The head post was placed on a holder that was connected to an arm of the stereotactic frame. This ensured the precise placement of the head post. After contact between the head post and skull, dental cement (Super Bond 2020, Sun Medical) was used to cover the head post and sculpt a recording well. The exposed skull was covered with a silicone sealant Kwik-cast (WPI)

2.2.3 Post-operative care

Mice received an injection of warm (37 °C), sterile saline solution after surgery and were placed on a large heating pad (FHC) that was preheated at 40 °C until they woke up from anesthesia. The drinking water was supplemented with metamizol (Novaminsulfon-ratiopharm®, 20 drops in 200 ml, Ratiopharm) for 2-3 days after the surgery, and mice were controlled for stable body weights and symptoms of pain.

2.2.4 Surgery for anatomical tracing experiments

Mice were subjected to anesthesia using isoflurane administered in an oxygen atmosphere (3 %– 4 % for induction and 1 %– 1.5 % for maintenance, CP-Pharma). Subsequently, metamizol was administered via subcutaneous injection for the management of postoperative pain at a dosage of 200 mg/kg. Following anesthesia, eye gel (Vidisic, Bausch + Lomb) was applied to both eyes, and a rectal probe was inserted to keep the body temperature at 37 °C (DC Temperature Controller, FHC).

The left primary somatosensory cortex (S1) was exposed by removing the skin overlaying the parietal bone. The left posterior insular cortex (pIC) was exposed by rotating the head approximately 30 to 40 degrees to the right and displacing the left temporalis muscle from the temporal bone. Anatomical landmarks such as the rhinal vein, middle cerebral artery, and zygomatic bone were used for precise localization of the pIC (Vestergaard et al., 2022). To enhance the image quality of subsequent *in-vivo* imaging, the skull covering S1 and pIC was thinned using a dental drill with a head diameter of 0.5 mm (Komet Dental).

2.3 Sensory stimulation

Awake, head-restrained mice were exposed to thermal, vibrotactile, and acoustic stimuli. The right forepaw was tethered to a Peltier element in order to ensure consistent thermal stimulation throughout the experiment. Vibrotactile stimuli were delivered to the back of the tethered forepaw while it was still in contact with the Peltier element.

2.3.1 Thermal stimulation

For extracellular recordings in thalamic nuclei, thermal stimuli were provided using a gold-plated Peltier element that was controlled by a QST-lab thermal stimulator (QST-lab). The paw was placed in the center of the Peltier element. The forepaw was maintained at a holding temperature of 32 °C and every 20 seconds, thermal stimuli with different amplitudes (22, 26,

28, 30, 31, 25, 28, 40, 41, 42 °C) were provided in a pseudo-randomized order. The duration of thermal stimuli was 2 seconds with onset and offset ramp speeds of 75 °C/s. For behavioral experiments, temperature stimuli were delivered by a ceramic Peltier element that was controlled by a customized feedback-controlled thermal stimulator (ESYS GmbH, Berlin). The Peltier element provided thermal stimuli with a 2-second duration and 20 °C/s onset and offset ramp speed. The holding temperature was 32 °C, and every 20–30 seconds, stimuli with different amplitudes were provided in a pseudo-randomized order.

2.3.2 Vibrotactile stimulation

For extracellular recordings in thalamic nuclei, vibrotactile stimuli (40 Hz) were provided using a force-feedback movement sensor arm (Aurora Scientific, Dual-Mode Lever Arm Systems 300-C) that was held in contact with the back of the forepaw. During vibrotactile stimulation, the paw was kept at 32 °C. The duration of the stimuli was 2 seconds.

2.3.3 Acoustic stimulation

Acoustic stimuli (20kHz) with 2-second durations were delivered using an acoustic buzzer. (PSOT1420, eve GmbH) positioned 15cm above the animal's head. The inter-stimulus interval was 20 seconds.

2.4 Extracellular Electrophysiology

2.4.1 Signal chains for sensory stimulation and data acquisition

Mice were placed in a translucent plastic tube on a recording platform and securely attached to a metal head bar to ensure consistent positioning of the skull across multiple recording sessions. A plastic sheet was positioned above the head to protect the eyes from strong light

exposure. The right forepaw was tethered to a gold-plated Peltier element, which was part of the QST-Lab probe head. The probe head was connected to the QST-Lab TCS control box, which in turn was connected to the National Instruments BNC-2090A breakout box. The breakout box was connected to a National Instruments PCIe-6323 card inside the stimulus computer. This signal chain served to apply thermal stimuli, which were triggered by a custom Python script running on the stimulus computer throughout the experiments, as well as to record the feedback temperature of the Peltier elements, as measured by thermocouples placed on top of the Peltier elements. The feedback temperature was recorded in a trial-by-trial manner, and the data was stored for further analysis.

On the backside of the tethered paw, an Aurora Scientific 300 C-I lever arm was positioned for delivery of vibrotactile stimuli, triggered by the same custom Python script running on the stimulus computer, as well as for movement tracking of the forepaw during recording sessions. The readout from the movement sensor arm was sent via the same signal chain to the stimulus computer. The data for each trial was saved separately and stored for further analysis. Neural recordings were performed using Neuropixel probes (Neuropixel 1.0, IMEC) with 383 active channels. The channels closest to the tip were selected for recordings, spanning 3.84 mm of tissue. Data streams were sent to the IMEC PXIe-1000 Base Station, which was housed in a National Instruments PXIe-1071 chassis and connected to a PCIe-8371 card in the acquisition computer via the National Instruments PXIe-8370 module. Data streams were saved as continuous data files.

2.4.2 Grounding and Referencing

The last grounding pad located on the arm of the Neuropixel Flex Cable arm was soldered to a silver wire that was in electrical contact with the main ground of the experimental setup. A silver wire coated with chloride served as the reference electrode during extracellular recordings when in contact with Ringer's solution. The backside of that silver wire was connected to the Neuropixel probe reference pad.

2.4.3 Probe Alignment and Insertion

Each Neuropixel probe was mounted on a 3-axis micromanipulator (MPM, New Scale), respectively. The aimed target coordinates (AP, ML, DV) were translated into absolute micromanipulator coordinates by the New Scale MPM-VCS system. The probes were placed 10 mm above the desired insertion point in a fully retracted configuration. One by one, probes were manually lowered until the probe tip was in contact with the pia surface. The position of each 3-axis manipulator was saved, and the probes were further lowered until the first spikes appeared on the electrodes closest to the tip. After the visual conformation of spiking, the probes were automatically lowered at a rate of 200 $\mu\text{m}/\text{min}$ until a depth of 2.5 mm was reached. The insertion rate was reduced to 100 $\mu\text{m}/\text{min}$ until the target position was reached. Probes were allowed to settle for 5 minutes until the recording started.

2.4.4 Data Acquisition and Synchronization

Neuropixel data acquisition was done with a 30 kHz sampling rate and 500 x gain for the spike band and with a 2.5 kHz sampling rate and 250 x gain for the LFP band. Open Ephys GUI (<https://open-ephys.org/gui>) was used as acquisition software. Each probe was connected to the Imec HS-1000 head stage, and data was sent to the Imec PXIe-1000 Base Station via the Imec CBL-1000 cable. The base station was housed in a National Instruments PXIe-1071 chassis, which was connected to a National Instruments PCIe-8371 card inside the data acquisition computer via the National Instruments PXIe-8370 module.

Synchronization of simultaneously recorded spike bands and stimulus application was achieved by sending TTL pulses to the Imec PXIe-1000 Base Station at the beginning of each trial and at the timepoint of sensory stimulation, which were registered by both probes, led to the synchronization of both data streams. The same TTL pulse was also used to trigger the QST-Lab TCS box, which led to the synchronization of the neural data with the stimulus application. To compensate for the individual sampling rates of Neuropixel probes, the neural data was aligned to each TTL encoding the trial start.

2.4.5 Labeling of Probes with lipophilic dyes

Neuropixel probes were coated with either Dil, Dil-CM, or DiD (Thermo Fisher Scientific, 1mM in 100 % Ethanol) to localize the recording location during the *ex-vivo* imaging of fixed brain slices. A small volume (20- 50 µl) of the fluorescent solution was pulled with a syringe, and a single drop of liquid on the tip of the syringe was brought into contact with the shank of a Neuropixel probe and moved from the tip to the bottom of the shank for 2-3 times.

2.4.6 Measurement of paw movement

Measurements of paw movement were done using the Aurora Scientific 300 C-I Dual Mode system. An indenter arm was positioned in proximity to the tethered forepaw, and contact between the arm and the paw was ensured. The system was configured to record the applied force on the indenter arm, which was caused by the paw's movement. The following figure (Figure 2.4.6-1) provides an in-depth analysis of the stimulus-evoked paw movement during extracellular recordings, which was used to select neurons that initiated their sensory response prior to the onset of paw movement. This selection was used throughout the extracellular recordings and has shown that the population of thermally responsive cells is contaminated with neurons being activated by paw movement. Interestingly, these neurons tend to be localized in aVPL and aPO with increased proportions compared to the pVPL, pPO, and especially PoT, which only had a very small proportion of movement-responsive cells.

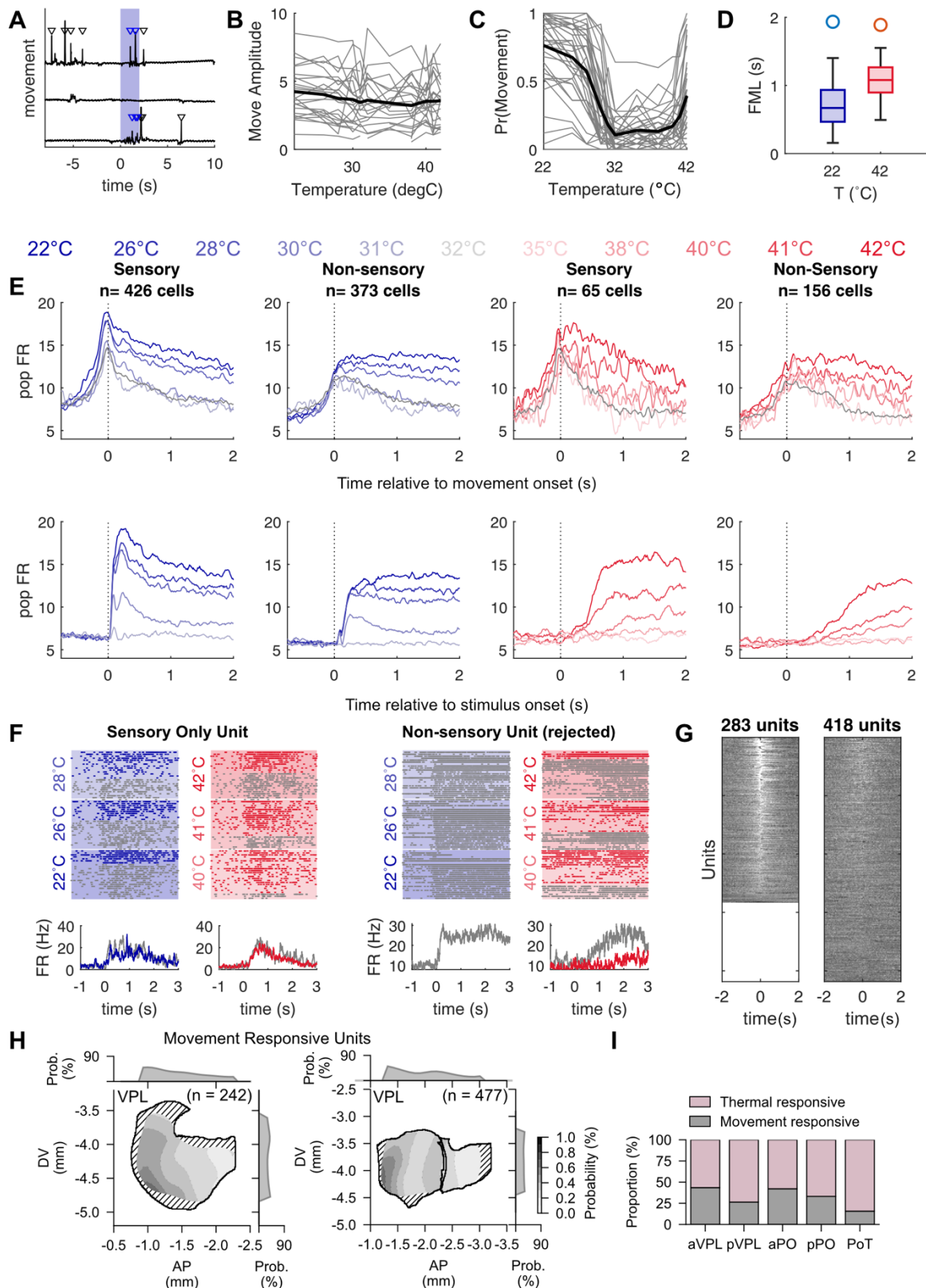


Figure 2.4.6-1: Thermosensation Stimulation-Induced Paw Movements and Their Thalamic Correlates (Analysis by Dr. Clarissa Whitmire and Tobias Leva, Visualization of results by Dr. Clarissa Whitmire and Tobias Leva)

- A. Example movement recording traces for three stimulus presentation trials (black). Thermal stimulus presentation (22°C) is indicated by the shaded blue bar. Detected movement events are indicated by the inverted triangle (blue triangle: movement during stimulus presentation; black triangle: movement outside of stimulus window).

- B. The amplitude of the movement events across stimulus intensities. Each gray line indicates a single session ($n = 39$ sessions; black line indicates mean). No relationship between movement intensity and stimulus amplitude.
- C. The probability of stimulus-evoked movement across stimulus intensities is strongly modulated by stimulus intensity ($n = 39$ sessions).
- D. First movement latency in response to cooling (22 °C; median 0.674 seconds) and warming (42 °C; median 1.110 seconds) stimulation (median +/- IQR).
- E. Population averaged peristimulus time histogram for cooling (blue) and warming (red) stimulation for units classified as sensory or non-sensory. Population PSTH is aligned to movement onset (top) or stimulus onset (bottom). Note the graded response amplitude prior to movement onset for sensory units relative to non-sensory units, indicating they are not purely movement-driven responses.
- F. Example raster and PSTH are split by movement (grey) and non-movement trials (color). Left: Cooling-evoked responses (grey: movement trials, blue: non-movement trials). Right: Warming-evoked responses (grey: movement trials, red: non-movement trials) shown for a unit that has both a thermosensory response (left) and an excluded unit that has only a movement response (right).
- G. Peristimulus time histogram for each thermally responsive unit in response to a spontaneous movement event for units that are (left) and are not (right) driven by movement events.
- H. Spatial density maps for thalamic units responsive to movement in VPL ($n = 242$ movement responsive units) and in the PO complex ($n = 477$ movement responsive units).
- I. Proportion of movement- responsive neurons by thalamic sub-region.

2.5 Habituation

Mice were gradually habituated to head and paw fixation over a period of up to 2 weeks. Within the first 2-3 days, mice were handled by the experimenter and introduced to the head-fixation apparatus. Within the initial time period, mice were head-restrained for less than a minute, several times per day. A reward with sweetened milk (Milchmädchen, Nestlé) was provided to create a positive association with the head-fixation protocol. When mice reached 5 minutes of head fixation (after 2-3 days) mice were introduced to paw fixation. Again, the time of paw fixation was gradually increased, with the first session lasting less than a minute. Medical tape (Leukosilk) was placed on top of the paw and was tethered to a small platform on which the mice were able to rest during the habituation procedure. When mice were comfortable with head and paw fixation for short durations, the time of head fixation as well as paw fixation was increased by 10-15 minutes per day until the mice were comfortable with 2 hours of head and paw fixation.

2.6 Behavioral experiments

Head-fixed and paw-tethered mice were trained to perform in a stimulus detection paradigm. A water reward (2-4 µl) was provided via a lick spout if mice were able to report the sensory stimulus. A correct detection was achieved if mice licked at least once within a 2-second window of opportunity after stimulus presentation.

2.6.1 Water restriction

During behavioral testing, mice were kept under a restricted water regime. 24 hours prior to the pairing session, the water bottle was removed from the home cage, and during the following time period of the behavioral testing, mice received 1.75 mL water each day.

2.6.2 Pairing and association to sensory stimuli

In order to create a positive association between stimulus and reward in water-restricted mice, a pairing session was performed. During these sessions, a water reward was delivered 250 ms after stimulus presentation in all trials. The reward (2- 4 µl water) was delivered via the lickspout, and licks were recorded. The sessions were successful if the mice licked with high reliability in at least 50 trials.

2.6.3 Behavioral training and pharmacological manipulation of thalamic activity

The stimulus detection paradigm was designed to study the ability of mice to detect and report stimuli, such as cooling, warming, or sound. The paradigm consisted of two phases: training and testing. During the training phase, mice were presented with a stimulus for 2

seconds, followed by a 2-second window-of-opportunity to report the stimulus by licking at a lick spout. If the mice licked at least once within this window, a water reward was delivered. The time duration between stimulus presentations was 15- 20 seconds. To estimate the spontaneous licking frequencies of the animals, trials in which a stimulus was presented (stimulus trials) were interleaved with catch trials in which no stimulus was delivered. The number of stimulus trials and catch trials were equal in every experiment and was pseudo-randomized.

If a mouse was able to report the stimulus in a 'stimulus trial', this trial was counted as a 'hit'. If the animal missed reporting the stimulus presentation, the trial was counted as a 'miss'. If the animal licked within the window-of-opportunity in a 'catch trial', this trial was counted as a 'false-alarm'. To assess the animal's performance, the Hit-rate and FA-rate were calculated. The Hit-rate was defined as the number of hits divided by the total number of stimulus trials, and the FA-rate was defined as the number of false alarms divided by the total number of catch trials. If an animal had Hit-rates above 70 % on two consecutive days, as well as FA-rates below 30 % on two consecutive days, the training phase was finished, and the animal entered the testing phase.

During the testing phase, pharmacological inactivation of thalamic activity was done by precise injections of Muscimol (5 mM, 100 nL, Thermo Fisher Scientific) into two distinct thalamic regions, the posterior part of VPL and PoT. On the first day of the testing phase, a single craniotomy was performed to access the target region with an injection pipette. Mice were allowed to recover for at least 2 hours in their home cage after the procedure. The experiments were started if the mice showed no signs of pain. Mice were head fixed, and 50 nL of Ringer's solution was loaded into a glass pipette with a 20 µm diameter, which was connected to a manual oil injector. The loaded pipette was positioned above the exposed pia surface and manually lowered until it reached a depth of 3.5- 4.0 mm relative to the pia surface. The Ringer's solution was ejected with a flow rate of approximately 100 nL/min. The pipette was left in place for 5 minutes and slowly retracted afterwards. The craniotomy was sealed, and the mice were allowed to recover for 30 minutes in their home cage before the stimulus-detection experiment was started.

On the second day of the experiment, the animal received a micro-injection of 100 nL Muscimol at the same site as the day before. The glass pipette was covered with Dil-CM for post-hoc *ex-vivo* imaging to reconstruct the injection site. After the injection, the animal was

placed in their home cage for 30- 45 minutes. After the recovery time, the animal was placed in their experimental setup, and the paradigm was started. On the third day, the animal received an injection of 100 nL Ringer's solution mixed with CTB in a 1:1 (volume/ volume) ratio using a DiD-covered glass pipette. After the experiment, animals were perfused, and the brain was dissected for *ex vivo* imaging.

2.7. Ex-vivo tissue preparation

The animals underwent deep anesthesia through an intraperitoneal injection of a ketamine/xylazine mixture and were then positioned in a perfusion chamber. Cold phosphate-buffered saline (PBS, 0.1 M, pH 7.4) was used to perform transcardial perfusion on the mice, followed by a fixation with paraformaldehyde (PFA, 2 % in 0.1 M PBS). The solution flow rate was maintained at 15 µl/min. Subsequently, the brain was extracted and immersed in 2 % PFA for 12 hours. After a PBS rinse, the brain was sectioned at 100 µm using a Leica VT1000s Vibratome. These sections were then placed on glass slides using a DAPI mounting solution (DAPI Fluoromount-G, SouthernBiotech). Image capture was carried out using a Zeiss AX10 microscope with a 5x magnifying objective.

2.8 Data processing

The following chapter includes multiple data processing steps specific to Neuropixel recording. An open-source package including all functions and sub-packages were provided by the Allen Institute for Brain Science and was used in the course of this project (https://github.com/AllenInstitute/ecephys_spike_sorting/tree/master)

2.8.1 Data pre-processing

The raw data was saved on disk, with each sample being encoded as a 16-bit integer and adjusted according to the gain levels of every channel. Distinct data files were made for both the LFP band and spike band, as well as additional files to log synchronization event timings. Before the spike sorting process, the spike-band data underwent four pre-processing stages: offset elimination, median subtraction, filtering, and whitening. The median of each channel was first deducted to centralize the signals around zero. Following that, the median across all channels was deducted to remove universal noise. The original dataset is then replaced by the median-subtracted version. For any necessary future reconstruction of the original data, the median value for each 16-channel block is stored separately. This median-subtracted data file is forwarded to Kilosort2, which uses a 150 Hz high-pass filter and conducts whitening in 32-channel blocks. A distinct file is created to store the filtered, whitened data for the spike-sorting phase.

2.8.2 Spike Sporting

Kilosort2 was used to pinpoint spike timings and allocate them to distinct units. Contrary to conventional spike sorting techniques that take sections of the initial signal and group them after the projection into a simpler feature space, Kilosort2 takes the whole dataset as an amalgamation of spike templates. The form and positions of these templates are progressively fine-tuned until the data can be faithfully reconstructed using N templates at M spike times, with each template scaled by a pre-defined amplitude. One of the notable capabilities of Kilosort2 is its adaptability in allowing the templates to morph over time, capturing the relative motion of neurons to the probe throughout the study. Over the course of a 2-hour experiment, a gradual shift in the probe is noticeable. Kilosort2 proficiently tracks units as they move along the probe's axis, negating the necessity for hands-on merging as was essential with the initial Kilosort version.

2.8.3 Eliminating potential double-counted spikes

Kilosort2 might occasionally assign a waveform template to the leftover residue after another template has been subtracted from the raw data, causing spikes to be counted twice. This can lead to an exaggerated count of ISI violations for a unit or an inflated synchrony between adjacent units at zero-time lag. To prevent this faux synchrony from impacting the data assessment, the results from Kilosort2 undergo post-processing. This involves the removal of spikes that have peak timings within a span of 5 samples (0.16 ms) and peak waveforms within a range of 5 channels (approximately 50 µm).

2.8.4 Eliminating units with non-physiological waveforms

Kilosort2 creates templates with a consistent duration (2 ms) corresponding to the timeline of a spike waveform. Yet, the template's form isn't bound by any constraints, leading to scenarios where the algorithm adapts templates to voltage variations that don't feasibly align with the current dynamics of an action potential. These templates, tied to such units, are deemed as 'noise'. They are systematically screened out utilizing three determinants: spread (single channel or more than 25 channels), shape (lack of peak and trough, as determined by wavelet decomposition), or multiple spatial peaks (waveforms are not localized along the probe axis).

2.8.5 Single Unit quality control

To prepare for potential further analysis, units that are not considered noise are organized into Neo-package files (<https://neuralensemble.org/neo/>).

Given that various analyses might necessitate distinct criteria for the inclusion of putative single units, several metrics are devised to aid in the unit filtering process (Figure 2.8.5-1). These metrics evaluate both the innate attributes of the units' waveforms and their distinction in relation to other units within the same recording.

Firing rate (Threshold (Thr.) = 0.1): The firing rate is represented as n_{spikes}/T , where n_{spikes} is the number of spikes and T is the total duration of the recording in seconds. Units with firing rates smaller than 0.1 Hz are excluded from further analysis.

Presence ratio (Thr. = 0.9) The presence ratio is a measure of how frequently a particular unit generates spikes during a recording session. The session is split into 100 equal-sized segments, and the presence ratio is calculated as the number of segments that contain at least one spike from the unit divided by the total number of blocks. A low presence ratio may indicate that the unit has drifted out of the recording range or was not properly followed by Kilosort2 for the duration of the recording. Units with a Presence ratio below 0.9 were not considered for further analysis.

Maximum Drift (Thr. = 80): To calculate the Maximum Drift for a single unit, the peak channel is determined by analyzing the top principal components of each spike. The peak channel values are then grouped into 51-second intervals, and the median value is calculated for all spikes within each interval (if there are at least 10 spikes per interval). The Maximum Drift is defined as the difference between the highest and lowest peak channel values across all intervals. Sessions with a high level of probe movement relative to the brain can be identified by analyzing the average Maximum Drift across all units. Units with Maximum Drift values above 80 μm were not considered for further analysis.

Waveform amplitude: The amplitude (in μV) of the waveform on a single channel, calculated as the difference between the peak and trough.

Waveform spread: The spatial spread (in μm) of channels where the amplitude of the waveform is more than 12 % of the highest amplitude.

Waveform duration (Thr. = 1ms): The temporal difference (in ms) between the peak and trough of the waveform on the channel with the highest amplitude. Units with waveform durations larger than 1ms are not considered for further analysis.

ISI violations (Thr. = 0.5): The ISI violations metric is used to identify instances where multiple neurons are firing simultaneously within a single unit. It does this by measuring the relative frequency of "violations" of the refractory period, which is a period of time immediately following a spike during which another spike cannot occur. The metric is calculated by dividing the number of violations (spikes that occur within 1.5 ms of each other) by the total amount of time during which violations could occur and then normalizing by the overall spike rate. The resulting value is always positive, but there is no maximum value it can take. Units with ISI-violation rates larger than 0.5 are not considered for further analysis.

Signal-to-noise ratio: The signal-to-noise ratio (SNR) was determined by subtracting the mean waveform from 1,000 individual spike waveforms of the peak amplitude channel and then taking the ratio of the waveform amplitude and twice the standard deviation of the residual waveforms. However, this method for calculating SNR can be inaccurate due to changes in the unit's waveform caused by probe movement and only takes into account the peak channel, not the overall isolation quality of the unit.

Isolation distance (Thr. = 10): The squared Mahalanobis distance is used to find the same number of "other" spikes as the total number of spikes for a unit in principal component space. Like SNR, isolation distance is sensitive to electrode drift and changes in waveform shape over time, which can reduce the isolation distance calculated for the entire session. Units with an Isolation distance smaller than 10 are not considered for further analysis.

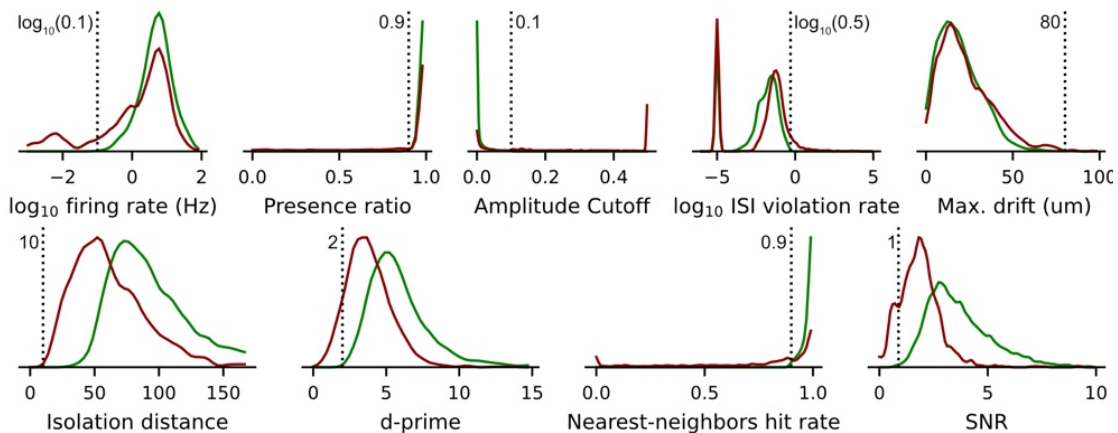
d' (Thr. = 2): Linear discriminant analysis (LDA) is a technique used to identify the line that best separates different groups in a dataset by projecting the data into principal component space. The metric d' is used to measure the separability of a unit of interest from all other units. However, d' is sensitive to changes in the waveform shape over time, and electrode drift can reduce its overall value as calculated throughout a session. Units with d' values less than 2 are not considered for further analysis.

Amplitude cutoff (Thr. = 0.1): The false negative rate (FNR) of a unit is approximated using a metric that involves creating a histogram of spike amplitudes and identifying the minimum amplitude. The proportion of spikes above the equivalent amplitude on the opposite side of

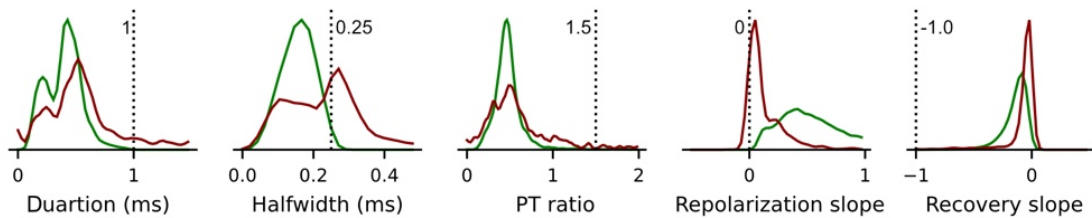
the histogram peak is calculated as the FNR. If the minimum amplitude is equal to the histogram peak, the amplitude cutoff is set to 0.5, which suggests that a high proportion of spikes are likely to be missing. However, it is important to note that this metric is based on the assumption of a symmetrical distribution of amplitudes and no drift and, therefore, may not accurately reflect the true FNR. Units with amplitude cutoffs larger than 0.1 are not considered for further analysis.

Nearest neighbors hit rate (Thr. =0.9): This metric evaluates the isolation quality of a unit by identifying the four nearest spikes in principal component space for each spike of the unit of interest and then calculating the fraction of those spikes that belong to the unit of interest. However, it is important to note that electrode drift, which can alter the waveform shape, can negatively impact this metric without necessarily changing the isolation quality of the unit at any given time point. Units with Nearest neighbors hit rate below 0.9 are not considered for further analysis.

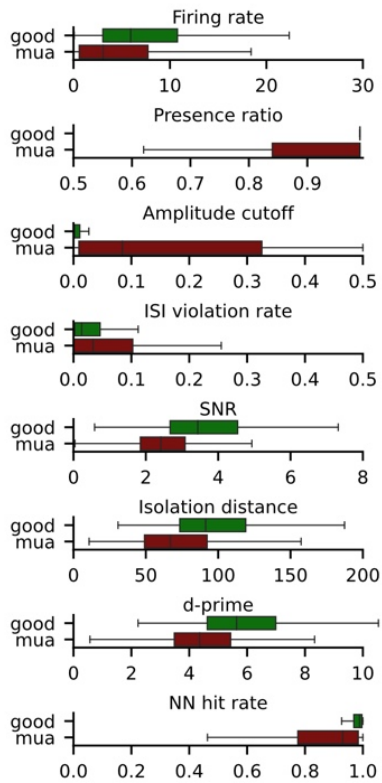
A Quality Measures - Spiking



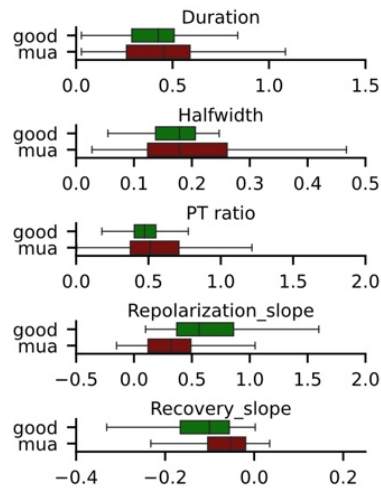
Quality Measures - Waveform



B Quality Measures - Spiking



C Quality Measures - Waveform



D

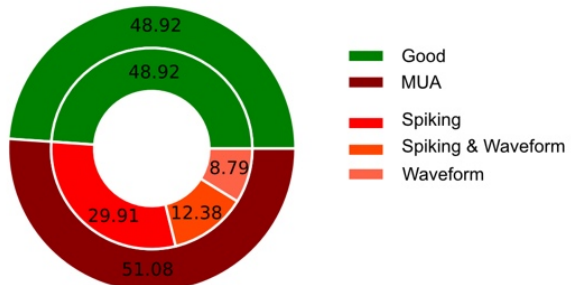


Figure 2.8.5-1 Quality metrics employed in the categorization of units

- A. The distributions of spike quality metrics are presented for all units categorized as either good (green) or multi-unit activity (MUA, red). Vertical dashed lines demarcate the threshold for identifying good units. From left to right and top to bottom, the exhibited metrics encompass unit firing rate, presence ratio, inter-spike-interval violation rate,

signal-to-noise ratio, isolation distance, d-prime value, Nearest neighbors hit rate, waveform duration, waveform half-width, waveform peak-to-trough ratio, repolarization slope, and recovery slope.

- B. *Box-and-whisker plots provide a visual comparison of each spiking quality measure between good units (green) and MUA (dark red).*
- C. *Similar to B, this section presents box-and-whisker plots for the waveform quality measures.*
- D. *The proportion of all recovered units is detailed in relation to their classification as either good units or MUA. The MUA classification is further subdivided based on whether the units fail to meet the threshold for spiking quality measures, waveform quality measures, or both.*

2.9 Reconstruction anatomical locations

2.9.1 Alignment of brain slices to Allen Institute Common Coordinate Framework

The digital images were processed using the MATLAB-based software, SharpTrack (<https://github.com/cortex-lab/allenCCF>). The individual images were first down-sampled and cropped to their final size. Subsequently, each image was registered to the Allen Institute Common Coordinate Framework (CCFv3). Probe points were then manually labeled, allowing the reconstruction of the units in the CCFv3. To account for variations in brain size and changes due to fixation and other procedures affecting the shape of the extracted brain, the precise positions of the units were scaled based on several criteria. These included: 1) the relative LFP power across channels, as a dramatic decrease in LFP power indicates the brain surface as well as the Hippocampus-Thalamus border, 2) anatomical landmarks, such as ventricles or the corpus callosum, where only low unit counts were expected, and 3) the waveform duration of units assigned to inhibitory structures in the thalamus, where the majority of cells have a short duration waveform. The 3-dimensional coordinates of each unit were entered as indices into the CCFv3 reference volume to retrieve its estimated location in the mouse brain (Figure 2.9.1-1).

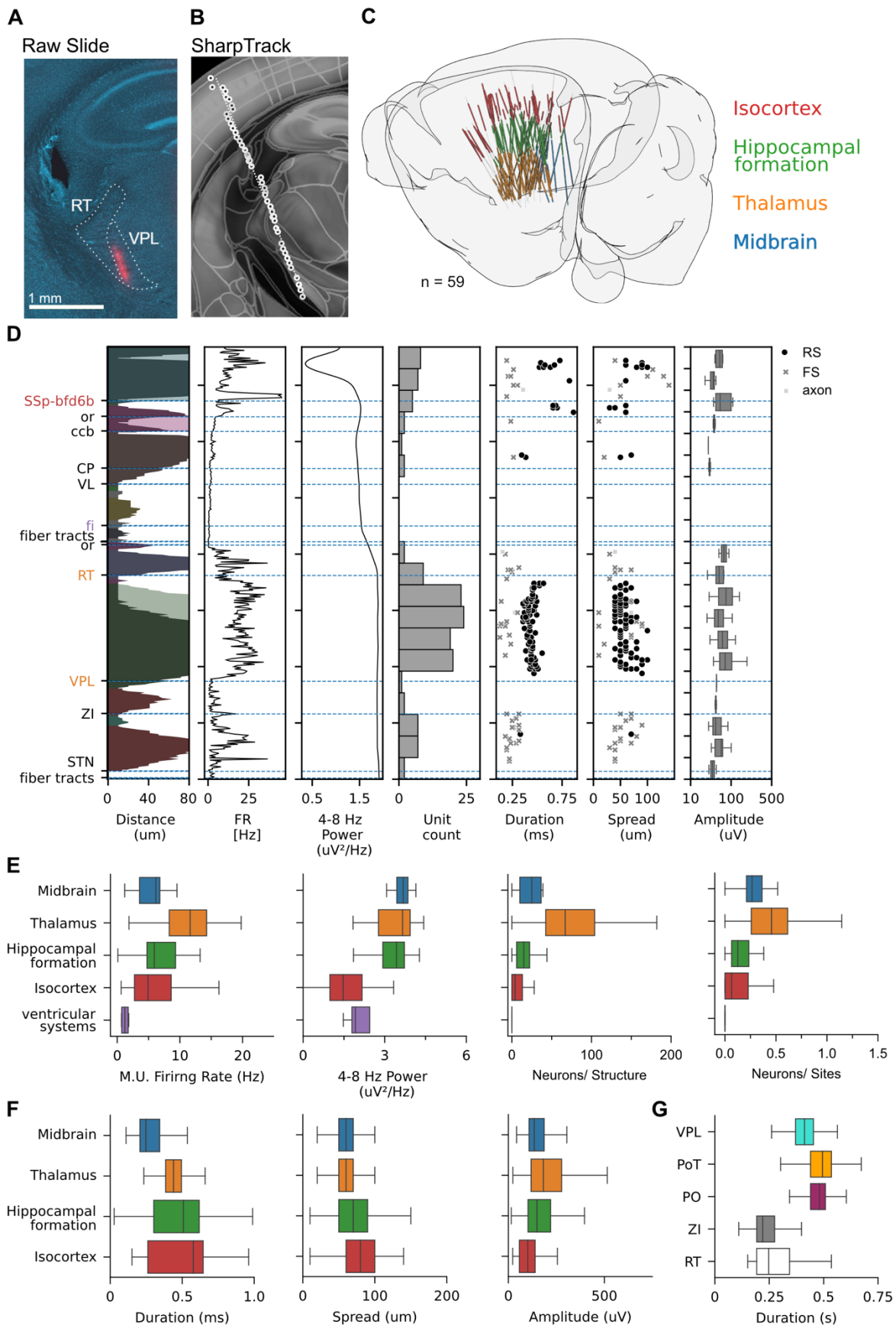


Figure 2.9.1-1 Anatomical reconstruction of Neuropixel probe trajectories

- A. An illustrative coronal brain slice exhibits a probe trajectory traversing through the VPL region, with DAPI staining in blue and Dil labeling in red. The scale bar represents 1 mm.
- B. Utilizing SharpTrack, an example mouse's probe trajectory from Panel A is reconstructed. Dots mark the reconstructed locations, while a dashed line delineates the probe's path.
- C. Depicted here are the reconstructed probe trajectories for all recordings, totaling 59 probes. Probe contacts are color-coded based on their gross anatomical structures.
- D. A parameterization of an example probe reconstruction is presented, encompassing the estimated brain region, firing rate, low-frequency power, number of units, and three waveform parameters of the recovered units: waveform duration, spread across the probe, and waveform amplitude. The data pertains to the example showcased in Panel A.
- E. The distribution of probe reconstruction parameters within each major brain division is visualized across recordings ($n = 59$ recordings). These parameters include multiunit firing rate, low-frequency power, neurons per structure, and neurons per site.
- F. Within each major brain division across the 59 recordings, the distribution of probe reconstruction parameters related to spiking waveforms is presented. This encompasses spike waveform peak-to-trough duration, spike waveform spread, and amplitude of the spike waveform.
- G. A comparative analysis of spike waveform peak-to-trough ratios is conducted for thalamic nuclei housing predominantly excitatory projection neurons (VPL, PoT, PO) and those responsible for thalamic inhibition (ZI, RT).

2.9.2 Visualization of Probe Trajectories in 3-D Model

First, a straight line was fitted through the probe points using a custom Python script. Utilizing the geometry of Neuropixel probes and the known depth of the recording, the position of each channel in the CCFv3 could be estimated. Visualization of probe trajectories was done by rendering spheres with 10 μm diameter at the position of an active channel using BrainRender (<https://github.com/brainglobe/brainrender>).

2.10 Data Analysis

2.10.1 Responsive Cells

For each unit, spike trains were binned in 100-ms bins, and the maximum spike-count bin within a 2-second baseline time window before stimulus onset was compared with spike-count bins within a 2-second time window during stimulus presentation using a Wilcoxon

signed-rank test. A unit was classified as ‘responsive’ if the p-value of the statistical test was smaller than 0.013, respectively. If stimulus-evoked spike counts were larger than the spike count in the baseline window, the unit was classified as ‘excitatory’. Units with smaller spike counts in the stimulus window were classified as ‘suppressed’.

2.10.2 Tuning Index

The Tuning Index (TI) was calculated using the trial-averaged and baseline-corrected peak firing rate during 2 s of stimulus duration at maximum cold and warm temperature amplitudes using the following equation:

$$TI = \frac{Peak\ Fr_{Cold} - Peak\ Fr_{Warm}}{Peak\ Fr_{Cold} + Peak\ Fr_{Warm}}$$

2.10.3 Spatial maps of responsive cells

Kernel Density Estimations (KDE) of coordinate values in the anterior-posterior and dorsal-ventral axes were used to visualize the spatial distribution of significant cooling and warming-responsive cells, respectively. A null distribution of all recorded cells in a particular region was used to normalize the cooling- or warming-responsive spatial distributions, respectively, in order to estimate the probability of a responsive cell in a defined spatial bin. If the number of neurons was insufficient to calculate the proportion of cooling or warming-responsive cells, the spatial bin was excluded from further analysis. Spatial maps showing the proportion of warming and cooling-responsive cells per bin were overlayed with contours of thalamic structure in order to visualize the spatial distribution.

2.10.4 Response Latency

Spike trains were binned in 1 ms bins for each responsive unit and smoothed with a Gaussian kernel with 10 ms bandwidth for cooling-responsive units and 100 ms bandwidth for warming-responsive units. The latency of the response is defined as the peak of the 2nd derivative of the smoothed spike train between stimulus onset and the peak of the 1st derivative.

2.10.5 Peak Response Time

Spike trains were binned in 1 ms bins for each responsive unit and smoothed with a Gaussian kernel with 100 ms bandwidth for warming-responsive and 10 ms bandwidth for cooling-responsive cells. The peak response time was defined as the peak of the smoothed spike train.

2.10.6 Response Duration

The duration of a sensory response was defined as the time from response latency (onset) to the time point when the firing rate equaled the peak firing rate multiplied by a factor of 0.2.

2.10.7 Duration Index

The Duration Index (DI) was calculated using the trial-averaged and baseline-corrected peak firing rate during the initial second and final second of stimulus presentation using the following equation:

$$DI = \frac{Peak Fr_{initial} - Peak Fr_{final}}{Peak Fr_{initial} + Peak Fr_{final}}$$

2.10.8 Sharpness Index

The Sharpness Index (SI) of a responsive neuron was calculated using the trial-averaged and baseline-corrected peak firing rate in a first time window that was temporally defined by the stimulus start and the peak response time. A second time window of the same length as the first time window was defined and started at a timepoint that was defined by the peak response time multiplied by the factor 2.5 using the following equation:

$$SI = \frac{\text{Peak } Fr_{\text{timewindow}I} - \text{Peak } Fr_{\text{timewindow}II}}{\text{Peak } Fr_{\text{timewindow}I} + \text{Peak } Fr_{\text{timewindow}II}}$$

2.10.9 Single unit PSTH

Individual spike trains from units classified as responsive were binned in 1 ms bins, and smoothed with a Gaussian kernel (50 ms bandwidth) and aligned to the start of the stimulus.

2.10.10 Population PSTH

Individual spike trains from units classified as responsive were binned in 5ms bins, and a population spike matrix was created, which was averaged across units and smoothed with a Gaussian kernel (25 ms bandwidth). The resulting population-spiking vectors were aligned to stimulus onset.

2.10.11 Criteria for exclusion of experiments and single units in dataset

In order for an experiment to be included in the dataset, multiple criteria must be met. First, the noise level of the neural recording, estimated by the RMS of the voltage traces, must be smaller than 150 μ V. Second, the quality of the brain slices must be good in order to

reconstruct the anatomical location of the recording electrode. Third, the proportion of fast-spiking single units must be less than 5 % in non-inhibitory thalamic nuclei.

In order to include a single unit in the dataset, the response latency must be smaller than 750 ms as well as earlier than the onset of paw movement. Furthermore, the peak response time must be shorter than 2 seconds.

2.11 Anatomical tracing of brain-wide thermal circuitry

2.11.1 identification of injection site in S1 and pIC

Widefield calcium imaging was employed for the identification of thermal representations in the forelimb S1 and pIC. This methodology utilized an sCMOS camera (Hamamatsu ORCA-Flash4.0 LT) coupled with an epifluorescence stereomicroscope (Leica MZ10 F) that is equipped with a CoolLED pE-300 LED Microscope illuminator. Image acquisition happened at a frame rate of 20 Hz with a 35 ms exposure time. cooling stimuli were administered to the right forepaw using a Peltier element. The cooling stimuli involved a temperature drop of either 10 °C or 14 °C from an adapted temperature of 32 °C and had a duration of 2 seconds with an onset ramp of 20 °C per second. The precise location of pIC was corroborated by identifying the surrounding auditory cortex and, in some instances, the insular auditory field via auditory stimulation with an 8 kHz, approximately 65 dB, 1-second acoustic stimulus delivered through a loudspeaker. Mice underwent a minimum of three stimulation trials to confirm functional responses. Craniotomies of approximately 1 × 1 mm dimensions were subsequently performed over regions responsive to thermal forepaw stimulation.

2.11.2 Tracer and Virus injections

For the injection procedure, custom-written Python code (Python version 3.7, Python Software Foundation) was employed to determine the center point of the widefield response during the imaging session. Glass pipettes with a diameter of approximately 20 µm, containing cholera toxin subunit B (CTB) for input mapping or adeno-associated virus (AAV) for axonal

output mapping, were inserted perpendicularly to the cortical surface into the center of the thermal response. Two injections of 50–75 nL each (injected at a rate of 100 nL/min) were performed, one at a depth of 700 µm and a second at 400 µm from the pial surface, using an oil hydraulic manipulator. The pipettes remained in place for 5– 10 minutes following each injection and were subsequently retracted. Injections into S1 utilized either CTB Alexa Fluor 647 or AAV-smFP-myc, while injections into pIC employed either CTB Alexa Fluor 555 or AAV-smFP-FLAG. AAV cortical injection sites were visualized *in vivo* by mixing AAVs with a low concentration of CTB Alexa Fluor 488.

To confirm the accuracy of the injection site within the center of the functional response, fluorescence tracer imaging was conducted 10 minutes post-injection using either an orange light or a green LED light while maintaining the same angle, orientation, and field-of-view as the original imaging session. A thin layer of bone wax was applied to both craniotomies to prevent tissue damage. Subsequently, the exposed skull was covered with dental cement, and the mice were provided with drinking water supplemented with metamizol for postoperative pain management over a period of 2– 3 days.

2.11.3 Histology

Histological assessment was performed either 7 days after CTB injection or 21 days after AAV injection. Mice were anesthetized with a ketamine/xylazine overdose and transcardially perfused with PBS, followed by 4 % paraformaldehyde (PFA). After post-fixation in PFA at 4 °C overnight, whole brains were sectioned coronally into 50 µm slices using a vibratome. Every fourth section containing CTB was mounted directly onto glass slides with a DAPI Fluoromount-G mounting medium. Sections containing AAV were prepared for immunohistochemical processing, involving PBS washes, blocking, and incubation with primary and secondary antibodies. These sections were also mounted onto glass slides with DAPI Fluoromount-G mounting medium.

Brain sections were visualized using a Zeiss upright microscope (Axio Imager A.2) and ZEN Imaging software. Images were captured with a 10x/0.45NA objective, maintaining consistent exposure times for both AAV and CTB across all mice.

2.11.4 Histological image processing

2.11.4.1 Atlas registration

Image processing began by segregating images based on fluorophore, aligning them sequentially, rotating them to the accurate orientation, and downsampling them by 20 % using ZEN Imaging software. A 1 mm boundary was then masked over the center of the injection sites along the anterior–posterior, medial–lateral, and dorsal–ventral axes and excluded from further analysis. Registration of all slices to the Allen Brain Atlas Common Coordinate Framework v3 was achieved through the QUICKNii (<https://www.nitrc.org/projects/quicknii>) software package. Potential section distortions along various axes were corrected using QUICKNii, followed by contrast adjustments to ensure clear anatomical landmarks matched with the atlas. RGB atlas images corresponding to the registered sections were exported from QUICKNii.

2.11.4.2 Signal detection

Identification of cell somata was facilitated through a modified version of AIDAhisto (<https://www.microlist.org/listing/aidahisto/>) that permitted interaction with the Allen Brain Atlas. Images underwent filtering using the Leung–Malik Filter Bank, aimed at detecting noncircular cells with sizes ranging from 8 to 10 pixels (equivalent to 20–25 μm in the down-sampled image). A universal threshold for cell detection was empirically determined and applied consistently across datasets. To reduce false-positive identifications, XY cell positions were cross-referenced with a binarized DAPI nuclei image using k-nearest neighbor classification within a 1.5-pixel radius. Detected cells were compared to their respective micrographs, and any remaining false-positive cells were excluded. Allen Brain Atlas coordinates were then obtained by matching the new XY cell positions with the transformed atlas images from the Atlas registration step. Subsequently, the number of detected cells within a region was counted.

Axonal projection density analysis was conducted using custom-written software in MATLAB. Initial denoising of images involved a Wiener filter with a 2 \times 2 neighborhood size. Saturated

signal edges due to histological processing were corrected by edge removal based on a binarized DAPI micrograph. Axon detection relied on convolving images with the Maximum Response 8 (MR8) Gaussian filter bank using a width ranging from 3 to 6 pixels (equivalent to axon widths of 1.2 μm to 2.4 μm in the downsampled image). A uniform threshold for axon detection, determined empirically, was applied consistently across all datasets. Images were closely aligned with the original micrographs to validate axon detection and to manually eliminate any residual noise pixels resulting from tissue processing. ABA RGB coordinates were obtained by matching XY pixel positions with the transformed RGB atlas images from the Atlas registration step. The number of detected pixels within a region was then quantified.

2.11.4.3 Visualization

Following atlas registration and signal detection, cell somata (input) and axons (output) were projected onto a 3D reference atlas using Imaris volumetric image software. This process utilized matrix transformations for the Allen Brain

$$\begin{aligned} Overlap_{input} \\ = \frac{\sum S1_{binary,input} AND pIC_{binary,input}}{\sum S1_{binary,input} + \sum pIC_{binary,input} - \sum S1_{binary,input} AND pIC_{binary,input}} \end{aligned}$$

$$\begin{aligned} Overlap_{output} \\ = \frac{\sum S1_{binary,output} AND pIC_{binary,output}}{\sum S1_{binary,output} + \sum pIC_{binary,output} - \sum S1_{binary,output} AND pIC_{binary,output}} \end{aligned}$$

Random datasets, consisting of 50 samples per subdivision, were created under the null hypothesis by randomizing the labeling of each coordinate utilized in the analysis for Monte Carlo hypothesis testing. The calculation of the P-value was based on the ratio of simulated overlap coefficients exceeding the observed overlap coefficient.

For the purpose of visualizing spatial overlap, a 3-dimensional contour plot was generated without binarization. Specifically, an isosurface plot was created using MATLAB at the 30th quantile of the non-zero voxels.

2.11.4.4 Data exclusion

Data were subject to exclusion under the following conditions: if the injection site did not align with the cortical functional response, if post hoc analysis indicated a misplacement of the injection site, or if the retrograde injection extended into the underlying white matter tract, such as the corpus callosum.

3. Results

3.1 Anatomical tracing of thalamocortical projections

The following chapter presents data that has been published in a collaborative effort by Phillip Wisinski-Bokiniec, Clarissa Whitmire, James Poulet, and Tobias Leva (doi:10.1093/cercor/bhac 386). The work investigated the anatomical connectivity of both thermally responsive cortical regions, S1, and pIC. In particular, the research sought to determine if S1 and pIC are components of distinct or overlapping thermal pathways. Both regions were demonstrated to receive inputs from different neuronal structures, including the thalamus, through functional-specific injections of retrograde tracers and anterograde viruses. This is in line with the parallel pathway hypothesis from subcortical to cortical areas. Outputs from S1 and pIC showed widespread projections to multiple target regions across the brain, including the thalamus. Even though outputs from S1 and pIC showed overlap in their projection targets, the axonal projections were separable, confirming that S1 and pIC are anatomical nodes of separate thermal pathways. Within this chapter, the thalamus-specific key findings of the study are presented.

3.1.1 Functionally targeted dual injections in S1 and pIC

In this study, we utilized wide-field calcium imaging in anesthetized GP 4.3 mice to target the thermosensitive regions of S1 and pIC (Fig. 3.1.1-1 A). To evoke sensory responses, a cooling stimulus ranging from 32 to 22 °C was applied to the right forepaw, and the resulting responses were recorded and visualized in real-time (Fig. 3.1.1-1 B and D, left). The position of the sensory representation in pIC was confirmed by the functional identification of the adjacent auditory cortex (Fig. 3.1.1-1 D and E, left). Tracers or viruses (CTB or AAV) were centrally injected into the identified area (Fig. 3.1.1-1 A), and the spatial overlap between the functional response and injection site was confirmed through *in-vivo* imaging (Fig. 3.1.1-1 C and E, left).

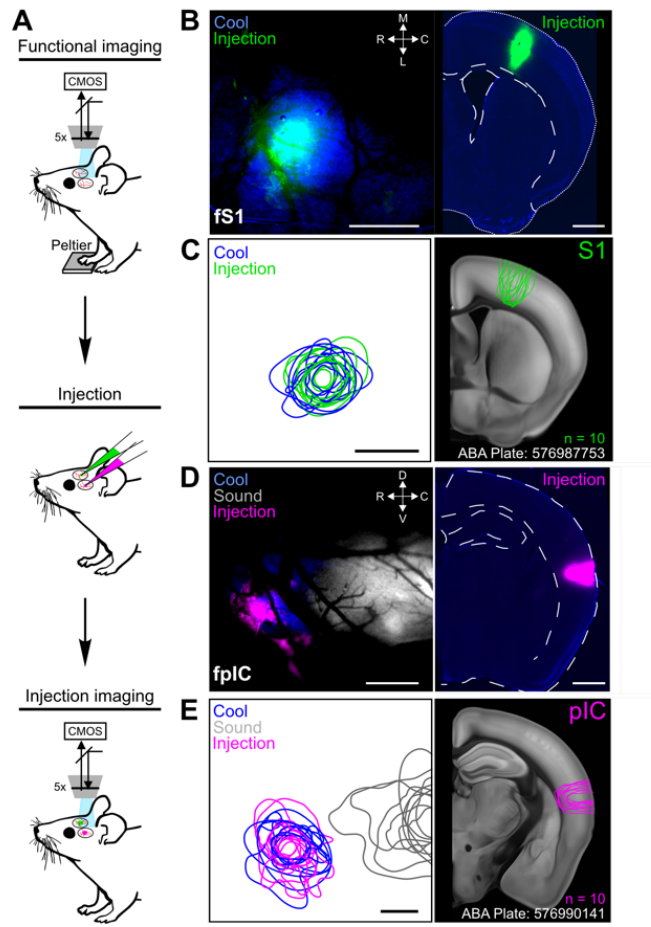


Figure 3.1.1-1 Dual Injections in functionally targeted thermal representations of S1 and pIC

- A. Schematic representation of the experimental procedure. It includes widefield calcium imaging for the functional identification of thermal cortical regions (top), the injection of different retrograde traveling tracers or anterograde traveling viruses (middle), and confirmation of the spatial overlap of the thermal representation and injection site (bottom).
- B. Representative mouse, showcasing the imaging of S1 alongside its related coronal brain segment. The left section combines the functional response to a temperature stimulus (blue) with the injectant (green). The right section shows a subsequent brain section, highlighting the position of the injection within S1. The scale is set to 500 μm .
- C. Location of injections and S1 functional responses observed in 10 mice. The left section displays the 80 % contour lines of the widefield sensory response (blue) and the fluorescent signal (green). The reconstructions of the injections in a coronal brain section are shown on the right.
- D. Same as B, but for pIC. The left panel displays the functional response to temperature (blue) and sound (grey) and the fluorescent tracer (green). The right panel presents a post hoc brain slice with the injection site in pIC. The scale bar is 500 μm .
- E. Same as C for pIC and includes the response to 8 kHz sound stimulation (grey). The right panel shows the outlines of all injection sites localized on a coronal brain slice from the Allen Brain Atlas. The scale bar for all figures is set to 500 μm .

Following a sufficient incubation time for the tracer or virus, the mice underwent perfusion, and their brains were extracted for histological examination. Inspection of the injection sites

in S1 and pIC indicated a comparable dispersion of the fluorescent signals within the injection region, spanning the full cortical column (medial/lateral pIC: 565 ± 40 μm , S1: 653 ± 77 μm ; dorsal/ventral pIC: 927 ± 46 μm , S1: 986 ± 50 μm ; anterior/posterior pIC: 800 ± 55 μm , S1: 800 ± 43 μm , Fig. 3.1.1-1 C and E). In order to determine the brain-wide input and output schema, images of the whole brain were acquired and subsequently registered to the CCFv3.

Areas extending 1 mm in both anterior/posterior and dorsal/ventral directions relative to the central injection point were omitted from subsequent analysis. This is because the intensity of the fluorescent signal hindered the automated detection of cell structures or the discernment of marked axons. To create comprehensive maps of brain-wide connectivity, we examined coronal slices set 200 μm apart, ranging from +1.4 to -7.0 mm relative to Bregma. The olfactory bulbs, anterior cortical areas, and the cerebellum were excluded from the analysis. Given the variability in the count of detected neurons (S1: 5147 ± 800 , pIC: 7737 ± 330 cells, for 5 mice) and labeled axons (S1: $2,323,883 \pm 245,388$, pIC: $1,862,505 \pm 286,668$ pixels, for 5 mice) among different mice, the values for inputs and outputs were normalized with the total number of input cell bodies or axonal output pixels observed throughout the whole brain.

3.1.2 S1 and pIC receive thalamocortical projections from spatially distinct regions

Utilizing a three-dimensional projection with varying angles, we visualized the inputs to S1 and pIC. This comprehensive mapping revealed dense labeling across numerous cortical and thalamic nuclei (Fig. 3.1.2-1 A). In general, the majority of inputs exhibited similar innervation strengths to both S1 and pIC. However, specific exceptions were notable across thalamic nuclei.

S1 received significantly more innervation from nuclei within VB and the PO group (Fig. 3.1.2-1 B, Ci, and Cii), including the ventral posterolateral (VPL) with 4.1 % innervation to S1 and 0.87 % to pIC ($P = 0.014$, $n = 5$ mice), the ventral anterolateral (VAL) with 0.72 % innervation to S1 and 0.07 % to pIC ($P = 0.039$, $n = 5$ mice), and the PO with 2.6 % innervation to S1 and 0.41 % to pIC ($P = 0.020$, $n = 5$ mice, Fig. 3.1.2-1 B and Cii). Conversely, thalamic innervation of

pIC was more diverse than S1, with significantly more input from the MG with 0.5 % innervation to pIC and 0.03 % to S1 ($P = 0.002$, $n = 5$ mice) and a prominent innervation from PoT (Fig. 3.1.2-1 B and Ciii) with 1.2 % innervation to pIC that was absent in S1.

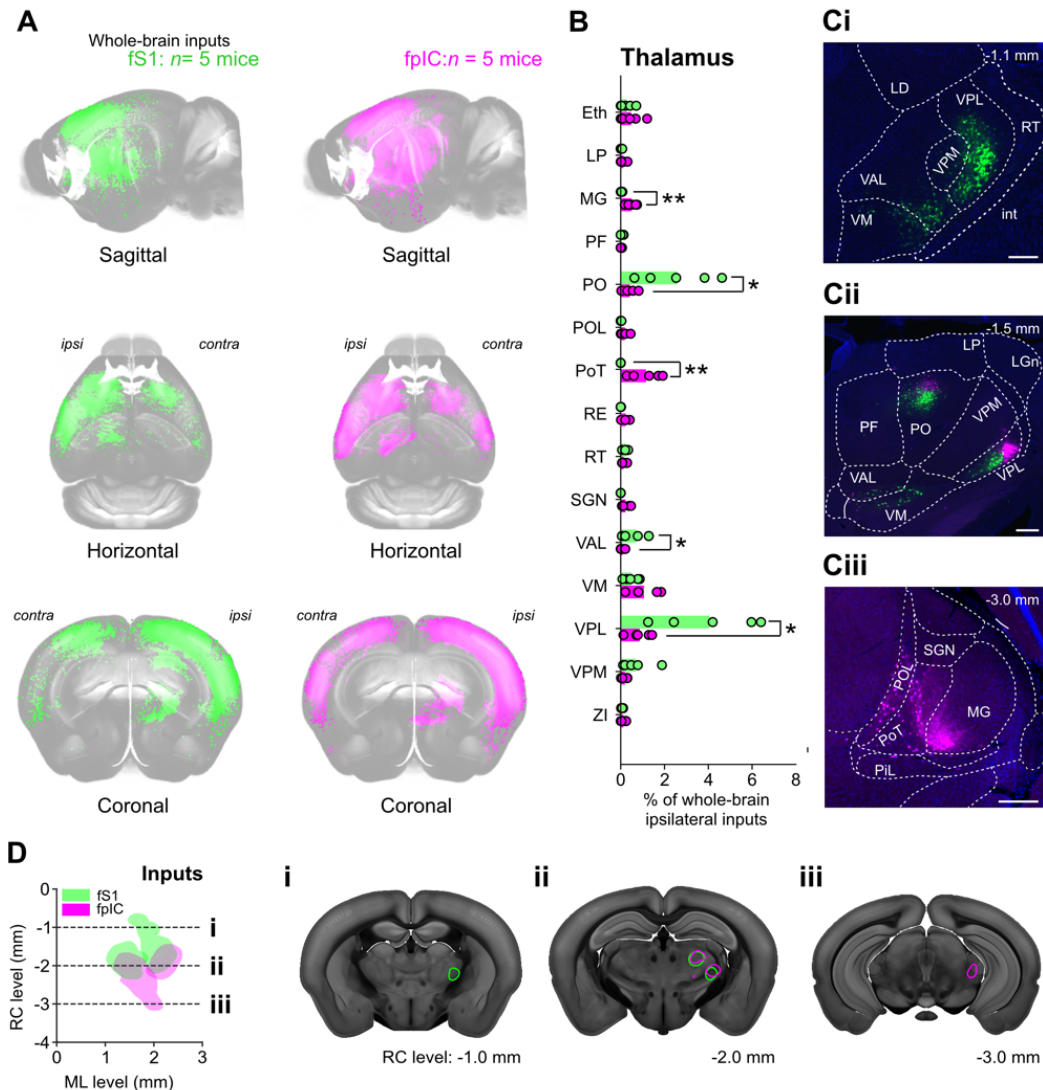


Figure 3.1.2-1 Whole-brain ipsilateral inputs to S1 and pIC

- 3D image of the entire brain featuring labeled cell bodies (CTB-647,green, representing S1 injection; CTB-555,magenta, representing pIC injection) from five mice. Identified cell bodies were registered to the Allen Brain CCFv3.
- Proportions of inputs to S1 (green) and pIC (magenta) from various thalamic subregions are depicted in bar graphs. The means are represented by bars, and individual data points from five mice are shown as circles. Statistical significance is indicated by * for $p < 0.05$ and ** for $p < 0.01$.
- Example brain slices depicting inputs to S1 (green) and pIC (magenta) from selected thalamic nuclei. Scale bars are set to 250 μ m.
- Reconstructed inputs to S1 (green) and pIC (magenta) from VPL, PO, and PoT. The left panel displays a horizontal view (anterioposterior vs. mediolateral), while the right panel shows coronal sections highlighting three regions: (i) an anterior region with input to S1 only, (ii) an intermediate anterioposterior region with input to both S1 and pIC and (iii) a posterior region with inputs to pIC only.

In a horizontal projection encompassing the three thalamic nuclei that have been associated with somatosensory processing (VPL, PO, and PoT), we observed distinct spatial localization patterns of inputs to S1 and pIC (Fig. 3.1.2-1 D). Specifically, S1 inputs were predominantly localized in the anterior region of the thalamus, while pIC inputs were predominantly localized in the posterior regions. Coronal slices at more anterior levels exclusively contained S1 projecting cells (Fig. 3.1.2-1 Di), whereas at posterior coronal slices, only pIC projecting cells were evident (Fig. 3.1.2-1 Diii). Notably, at intermediate anterior-posterior levels, there was some overlap with both S1 and pIC projecting cells co-existing (Fig. 3.1.2-1 Dii). However, intriguingly, the study identified only a very small population (522/84,639) of cells that project to both S1 and pIC, suggesting that while thalamic regions may show overlapping cortical projections, their fine-grained cell-level organization follows a scheme in which a cell either projects to S1 or pIC.

3.1.3 S1 and pIC send corticothalamic projections to multiple thalamic nuclei

Axonal projections originating from the S1 and pIC regions exhibit extensive innervation throughout various regions of the mouse brain, as illustrated in Figure 3.1.3-1 A. Notably, both S1 and pIC demonstrate a higher number of output regions compared to input regions. Further examination of thalamic nuclei reveals significant differences in the strengths of innervation, as depicted in Figure 3.1.3-1 B.

Focusing on specific nuclei, S1 exhibits notably more outputs to VAL (S1 0.7 %, pIC 0.09 %, P = 0.003, n = 5 mice, Fig. 3.1.3-1 Ci), ventral medial nucleus (VM, S1 0.7 %, pIC 0.46 %, P = 0.044, n = 5 mice, Fig. 3.1.3-1 Ci), parafascicular nucleus (PF, S1 0.5 %, pIC 0.18 %, P = 0.025, n = 5 mice, Fig. 3.1.3-1 Cii), and PO (S1 1.5 %, pIC 0.89 %, P = 0.013, n = 5 mice, Fig. 3.1.3-1 Cii). Conversely, pIC exhibits stronger innervation of MG (pIC 0.8 %, S1 0.2 %, P = 0.004, n = 5 mice), the suprageniculate nucleus (SGN, pIC 0.2 %, S1 0.01 %, P = 0.003, n = 5 mice), and the posterior limiting nucleus (POL, pIC 0.4 %, S1 0.08 %, P = 0.002, n = 5 mice). Consistently with the inputs, pIC innervates PoT selectively (0.6 %; Figure 3.1.3-1Ciii) and S1 does not project to this region.

Curiously, we did not find any meaningfully altered output proportions for VPL, the nucleus that was characterized by spatially distinct regions that send thalamocortical projections to either S1 or pIC. This finding was confirmed by Figure 3.1.3-1 D, presenting the labeled axons in VPL, PO, and PoT in a horizontal plane. S1 and pIC outputs are characterized by large overlap and less separability across the three nuclei compared to the inputs. One has to consider that the data shown here includes all labeled axons coming from pIC or S1, which means axons of passage will be included as an input value (Discussion chapter 4.1.2).

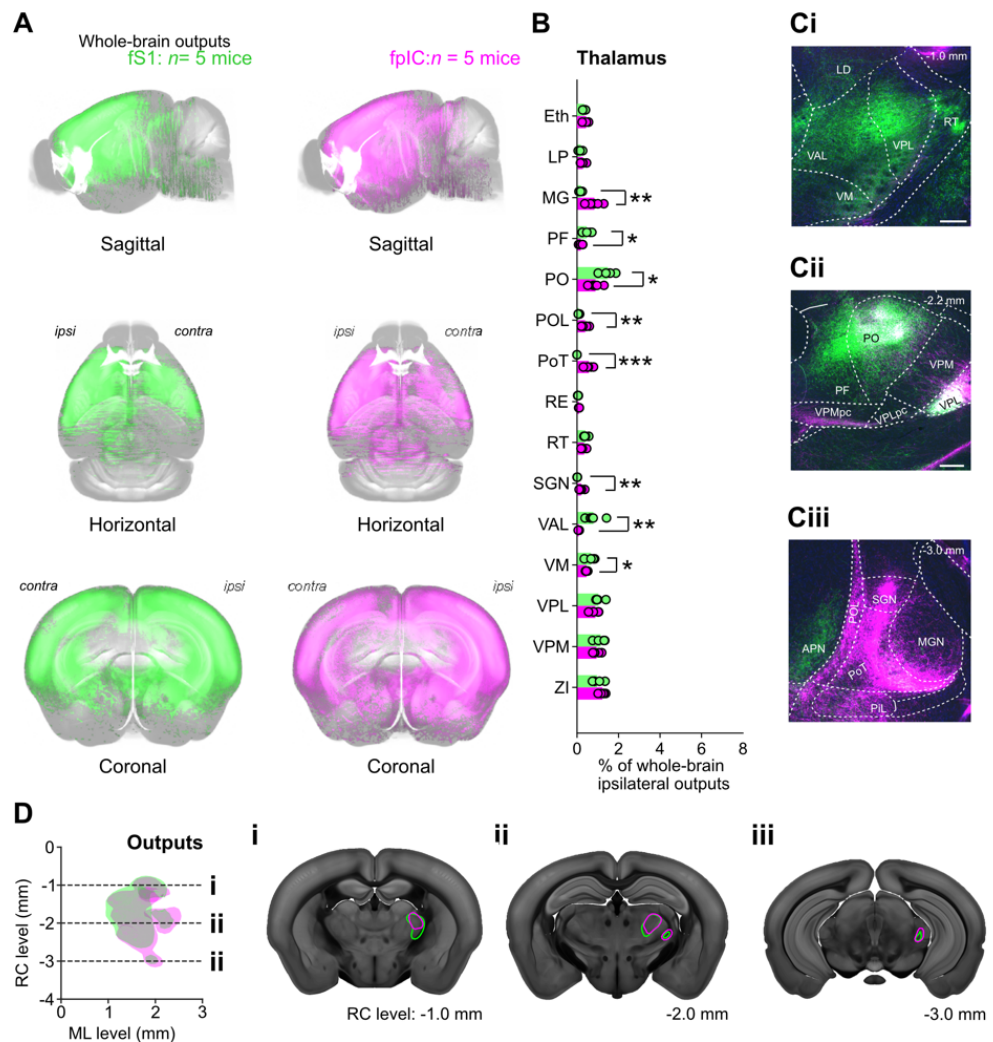


Figure 3.1.3-1: Whole-brain ipsilateral outputs from S1 and pIC

- AAVs were injected into the temperature-responsive areas of S1 (left) and pIC (right) following widefield imaging. Axons projecting from S1 or pIC were then extracted and registered to the Allen CCFv3 in five mice.
- Bar graphs showing the proportions of whole-brain ipsilateral outputs from S1 (green) and pIC (magenta) to thalamic nuclei. The means are represented by bars, and individual data points from five mice are shown as open circles. Statistical significance is indicated by * for $p < 0.05$ and ** for $p < 0.01$.
- Ci-Ciii The figure presents representative brain slices illustrating outputs from S1 (green) and pIC (magenta) targeting different thalamic nuclei. Scale bars are set to 250 μ m.

D. The diagram showcases the reconstructed outputs from S1 (green) and pIC (magenta) to VPL, PO, and PoT in five mice. The left panel displays a horizontal view (anterioposterior vs. mediolateral), while the right panel shows coronal sections highlighting three anterioposterior levels.

3.2 Behavioral testing of thermal perception

The identification of neural structures underlying the perception of external stimuli holds significant importance in the field of sensory neuroscience. In order to establish a causal relationship between neural activity within these structures and perception, researchers often employ selective and temporally precise inactivation approaches during perceptual tasks (Miyashita and Feldman 2013; Talwar, Musial, and Gerstein 2001; Guo et al. 2017; Fitzmaurice et al. 2003; Slonina, Poole, and Bizley 2022; Staiger and Petersen 2021). Within the field of thermo-sensory processing and perception, targeted inactivation of lamina I spinal cord fibers showed a profound effect on thermal perception (Norrsell and Craig 1999). Additionally, when cortical inactivation experiments were performed in S1 and pIC, both structures exhibited significant impairments in the thermal perception (Paricio-Montesinos et al. 2020; Vestergaard et al. 2023; Milenkovic et al. 2014).

However, thalamic inactivation experiments led to inconclusive results in terms of identifying thalamic key structures for thermal perception. This can be explained by: incomplete and off-target lesioning of the somatosensory thalamus (Norrsell and Craig 1999), recovery of thermal detection behavior after lesioning (Cragg and Downer 1967), administration of ineffective neuronal antagonists (Duncan et al. 1993) as well as the investigation of the causal relationship of thalamic nuclei in a task-learning paradigm (Finger and Frommer 1970). In order to overcome these limitations, I aimed to perform reversible thalamic inactivation, specifically targeting the somatosensory thalamus housing VPL, PO, and PoT, which send thalamocortical projections to S1 and pIC. The objective is to examine the effects of thalamic inactivation on thermal perception and further advance our understanding of this area and the relationship between its neural activity and thermal perception.

3.2.1 Thalamic inactivation during thermal detection task

In order to test the role of the somatosensory thalamus in thermal perception, we performed pharmacological inactivation (Muscimol, GABA receptor agonist, 5 mM, 100 nL, Thermo Fisher Scientific) of the somatosensory thalamus in mice that were trained to perform a go/no-go 10 °C warming, 5 °C cooling from 32 °C baseline, or 4 kHz acoustic detection task (Figure 3.2.1-1 A, B). Following the successful training of the mice to detect the stimuli, defined as a Hit-rate greater than 70 % and a FA-rate below 30 %, the animals proceeded to the testing phase, which consisted of three experimental sessions spanning three days. Prior to each behavioral session (30 min), the mice received injections of 100 nL Ringer's solution on day 1, 100 nL Muscimol on day 2, and 100 nL Ringer's solution in the somatosensory thalamus on day 3. It was ensured that the injection site for each mouse was set to a specific position across the three testing days and that the location of the injection site was not changed.

After injecting Ringer's solution into the somatosensory thalamus, the mice accurately reported each stimulus during the behavioral session on day 1 (Figure 3.2.1-1 C, Day 1, mouse 1,2). On day 2, the GABA-agonist Muscimol was injected to selectively deactivate the thalamocortical projection neurons. The injection of Muscimol had a significant impact on the perception of both warming and cooling stimuli, as evidenced by the absence of licking responses to thermal stimuli on day 2 (Figure 3.2.1-1 C, day 2, mouse 1,2). Subsequently, on day 3, following the injection of Ringer's solution, the mice displayed performance levels comparable to those observed on day 1 (Figure 3.2.1-1 C, Day 3, mouse 1, 2). The injection of Ringer's solution on days 1 and 3 confirms that the injection procedure itself does not alter thermal perception. Furthermore, while the Muscimol injections into the thalamus caused a reversible impairment in the thermosensory tasks, they did not impair performance in the auditory task (Figure 3.2.1-1 C, mouse 3). This indicates that thalamic inactivation did not affect the motivation, or in general the ability of the mice to perform the task.

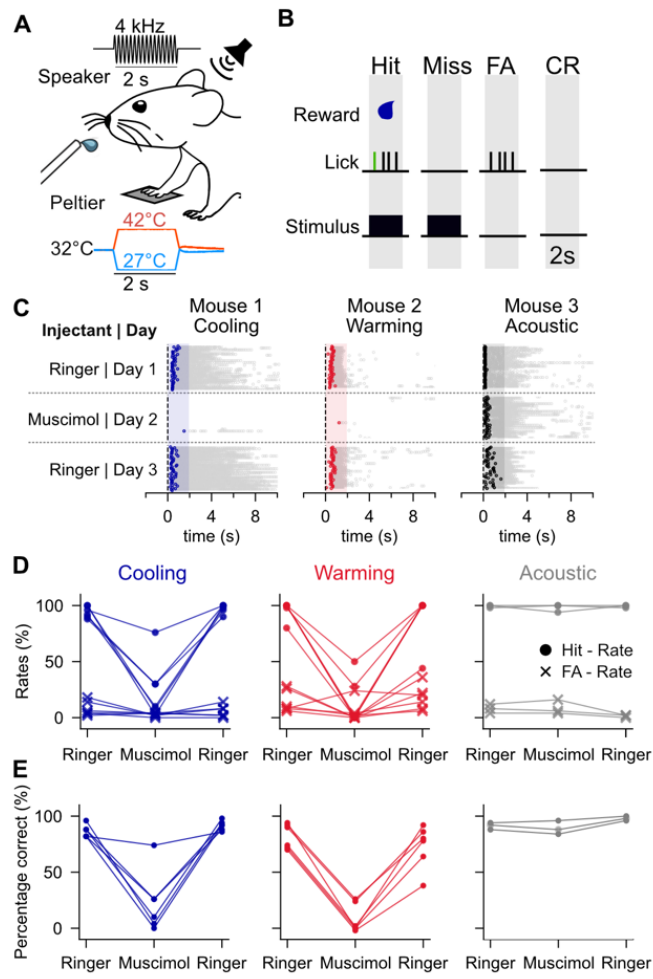


Figure 3.2.1-1 Stimulus detection task and pharmacological inactivation of somatosensory thalamus

- Experimental paradigm, mice were head-fixed and paw-tethered and received either cooling (5°C), warming (10°C) or acoustic (4 kHz) stimuli with a duration of 2. A Lick spout was used for the reporting of stimulus presence and the reward delivery.
- Design of behavioral paradigm and trial categories. If a stimulus was presented and mice reported via licking during the response window (grey shaded region) a water reward was delivered (Hit), if a stimulus was presented but mice failed to report the stimulus, no water reward was delivered (Miss). If mice licked during the response window in the absence of a stimulus (Catch trial) no water reward was delivered (FA). If mice withheld licking in Catch trials no reward was delivered (CR).
- Lick rasters of cooling-trained, warming-trained and acoustic-trained animals over three consecutive testing days. Each dot displays a lick, colored dots show the first lick of a stereotypical licking-bout. Dotted line represents stimulus onset and shaded region displays response window.
- Hit-Rates (%) and FA-rates (%) over 3 consecutive testing days for all mice trained to cooling ($n=6$), warming ($n=6$) or acoustic ($n=3$) detection. Hit-Rates (%) = Number of Hit-trials/ total number of trials; FA-Rates (%) = Number of FA-trials/ total number of trials.
- Percentage correct rates (%) of all animals trained to detect cooling ($n=6$), warming ($n=6$) or acoustic ($n=3$) stimuli. Percentage correct (%) = Hit-rate (%) - FA-rate (%).

In the cohort of mice engaged in the cooling detection task (Figure 3.2.1-1 D, left, $n=6$), muscimol injections resulted in a significant impairment of stimulus detection. Three mice

exhibited a nearly complete loss of their ability to detect cooling stimuli, with Hit-rates below 10 %. Two mice displayed a moderate reduction in performance (Hit-rates < 50 %), while only one animal showed a mild impairment (Hit-rate < 80 %). Interestingly, all tested mice demonstrated a recovery of performance on day 3 following the injection of Ringer's solution, regardless of the strength of inactivation induced by muscimol on day 2. It is noteworthy that the False alarm (FA) rates showed little variability across the three testing days (FA-rates < 30 %).

In the cohort of mice tested for warming detection (Figure 3.2.1-1 D, middle, n=6), four animals exhibited a profound reduction in stimulus detection due to muscimol injections, with Hit-rates below 10 %. Two animals showed moderate impairment, with Hit-rates below 50 %. However, on day 3, five out of six animals demonstrated a strong recovery in performance, achieving Hit-rates close to 100 %. One animal displayed poor recovery, with a Hit-rate of 45 %. There was slightly more variability in the FA-rates among the mice tested for warming detection compared to those tested for cooling detection. Two animals exhibited slightly increased FA-rates at the onset of the testing phase on day 1 (Ringer's). However, following muscimol injection on day 1, 5 out of 6 animals displayed a complete absence of FA trials, with FA-rates close to zero. One animal showed a slightly increased FA-rate. On the recovery day 3 five animals exhibited FA-rates below 30 %, while one animal showed an increase in FA-rate (40 %).

In the cohort of animals that were tested for acoustic stimulus detection (Figure 3.2.1-1 D, right, n=3), stable Hit-rates (> 95 %) were observed during the testing sessions. Muscimol injections showed no behavioral effect, and the FA-rates displayed only slight variations across the testing days (FA-rates < 15 %).

In order to evaluate the performance of animals in the behavioral detection paradigm, we utilized the percentage of correct trials (Hit-rate – FA-rate) as a comprehensive measure, incorporating both the Hit-rate and FA-rate. Across all mice trained for cooling detection (Figure 3.2.1-1 E, left), the percentage of correct trials exceeded 90 % in all animals on day 1. However, the administration of muscimol injections on day 2 resulted in a significant reduction of correct trials in four animals. Two animals showed a moderate reduction and achieved 26 % correct trials. Only one mouse exhibited a minimal decrease in the correct trials measurement following muscimol administration compared to day 1 (74 % correct trials).

Notably, all animals demonstrated similar performance levels on day 3, indicating the reversible nature of thalamic inactivation.

Regarding the mice trained for warming detection (Figure 3.2.1-1, middle), three out of six animals initially performed almost perfectly, achieving 90- 94 % correct trials, while the remaining three mice in the group exhibited good performance values, with 70- 74 % correct trials on day 1. Among the three animals with perfect performance on day 1, one mouse displayed a complete loss of performance, while the other two exhibited a moderate reduction (24- 26 % correct trials). Interestingly, all three animals with good performance on day 1 exhibited a profound reduction in correct trials following muscimol injection. Performance on day 3 resembled that of day 1 for all three animals that initially exhibited perfect performance. However, greater variability in the recovery of performance was observed in the group with good performance on day 1. Two animals displayed lower recovery performance compared to day 1, with one animal only reaching 38 % correct trials.

In the case of the animals trained for acoustic stimulus detection (Figure 3.2.1-1, right), they commenced the experiments with near-perfect performance and showed no signs of performance reduction following muscimol injection on day 2 or Ringer's injection on day 3.

3.2.2 Relationship of injection site with task performance

In the previous chapter, muscimol injections in the somatosensory thalamus were shown to selectively disrupt thermal detection behavior. Differences were present in the degree of impairment seen in the animals trained for either cooling or warming detection. In this section, the effect of the injection site on the deterioration of performance in the task is explored. To determine the anatomical position of the injection site, the injection glass pipette used for muscimol injection on day 2 and the injection pipette used for Ringer's solution injection on day 3 were coated with lipophilic dyes (Dil-CM on day 2, Dil on day 3) (Figure 3.2.2-1 A).

This procedure enabled the post-hoc reconstruction of injection sites for each mouse. To assess the behavioral impairment for each animal, the effect size of an injection was calculated by subtracting the percentage of correct trials on day 2 from the percentage of correct trials

on day 1. Plotting the injection sites in a horizontal plane (Figure 3.2.2-1 B) and sagittal plane (Figure 3.2.2-1 C) revealed that injections predominantly targeted the posterior region in VPL (pVPL) and PoT. pVPL injections spanned from -1.5 mm to -2.5 mm in the medial-lateral direction, -1.5 mm to 2.5 mm in the anterior-posterior direction, and -4.4 mm to -4.8 mm in the dorsal-ventral direction. PoT injections spanned from -1.5 mm to -2.25 mm in the medial-lateral direction, -2.5 mm to -3.2 mm in the anterior-posterior direction, and -3.7 mm to -4.5 mm in the dorsal-ventral direction.

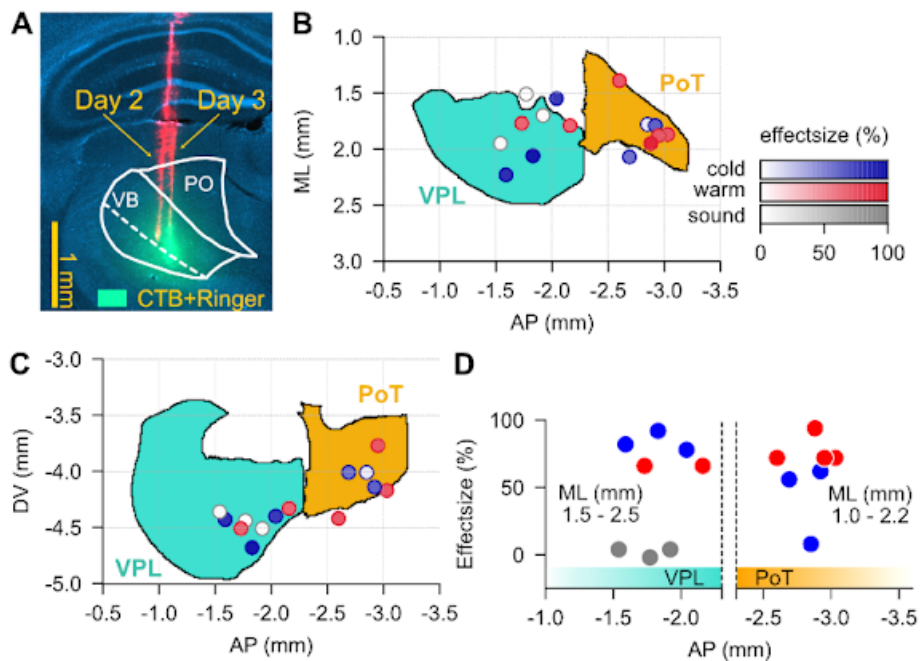


Figure 3.2.2-1 Relationship of inactivation site and strength of behavioral impairment

- Microscopy picture was taken from a coronal slice of a mouse with dual injection marks (Day 2, Day 3, red signal). CTB was mixed in a 1:1 v/v ratio with Ringer's solution on day 3. Thalamic borders are shown in white
- Horizontal projection of VPL and PoT with reconstructed tip locations of injection pipettes. Each dot represents the injection site of an individual mouse. The color-code represents the stimuli mice were trained on, and the opacity of the dots displays the effect size (%) of a muscimol injection. Effect size (%) = percentage correct day 2 (%) - percentage correct day 1 (%)
- Same as B in sagittal plane.
- Effect size of individual muscimol injections as a function of the anterior-posterior position of the injection site. Color-code as in B. Cyan and gold-shaded regions, represent the anterior-posterior spatial extent of VPL and PoT, respectively.

To examine the impact of the anatomical position of the injections on behavioral impairment, Figure 3.2.2-1 D presents the effect size as a function of the anterior-posterior position, as this

axis exhibits the largest variance in the data points. The effect size for cooling detection (blue) is substantial in the anterior region (78, 82, and 92 %) and is decreased in the posterior region (8, 56, and 62 %), with one data point showing a small effect size in PoT. The effect size for warming detection (red) demonstrates relative independence from the anterior-posterior position (66, 66, 72, 72, 72, and 94 %), except for one data point exhibiting a large effect size in the posterior region compared to the other warming-related effect sizes.

The acoustic-trained animals (grey) showed small effect sizes for all three thalamic inactivation procedures (0, 4, and 4 %), and injections were limited to posterior VPL. In summary, his chapter has demonstrated that the somatosensory thalamus, specifically the posterior VPL and the PoT, are important for thermal detection. A moderate relationship between the anterior–posterior position of the thalamic inactivation and the strength of the behavioral impairment was seen. Inactivation of the anterior region had a stronger effect on cooling behavior, while warming was similarly affected by anterior and posterior inactivations.

The assessment of the aforementioned outcomes necessitates the acknowledgment of the constraints imposed by muscimol injections concerning the specificity of the inactivated region (Discussion chapter 4.2.2).

3.3 Innocuous temperature is robustly encoded across mouse somatosensory thalamus

The previous chapters have shown that VPL, PO, and PoT send thalamocortical projections to the cortical thermo-sensitive regions S1 and pIC. Furthermore, it was shown that the somatosensory thalamus in which VPL, PO, and PoT are located plays a crucial role in thermal detection behavior. This chapter will provide insights into the neural representation of temperature. Specifically, the recording technique will be introduced (3.3.1), which was used to investigate the fundamental thalamic representation of cooling and warming (3.3.2). Next, the spatial representation of thermally responsive cells is investigated across and within thalamic nuclei (3.3.3, 3.3.4, and 3.3.5), and finally, the spatial representation of touch is investigated and compared to the thermal representation (3.3.6).

3.3.1 High-density extracellular recordings across thalamus in awake mice

The methodological aim of the present study is the investigation of temperature representation on a single cell level with millisecond temporal resolution in three thalamic nuclei that span multiple millimeters of tissue deep in the brain of awake animals. Deep-tissue structures like the thalamus are difficult to target by conventional optical methods due to the scattering properties of the tissue (Svoboda and Yasuda 2006; Takasaki, Abbasi-Asl, and Waters 2020). New developments in the optical recording field (Yu and Murari 2021; Bocarsly et al. 2015) overcome this optical limitation by implanting lenses deep in tissue to record single-unit activity with larger spatial coverage compared to common electrophysiological methods. However, the temporal resolution of these methods is still limited by the nature of the calcium signal as well as the kinetics of calcium indicators (Y. Zhang et al. 2023), and the method requires the displacement of a large amount of brain tissue to make space for the implanted lens. This led to the exclusion of optical methods when deciding on the recording technique in the initial phase of the study. Electrophysiological methods are able to penetrate deep structures and record single-unit neural activity, but they face the limitations of restricted spatial coverage and small sampling efficiency. However, the latest development of high-density extracellular recording probes (Jun et al. 2017) allows sampling over multiple millimeters along the recording shank, which drastically increases spatial coverage and sampling efficiency. Furthermore, algorithm-based reconstructions of recording locations (Shamash et al. 2018) have also improved recently, providing a possibility to identify the positions of electrode contacts within the mouse brain post-hoc. These developments made high-density extracellular recordings the method of choice for the investigation of widespread thalamic activity due to increased temporal resolution, extended spatial coverage, and large sampling efficiency. In the present study, we sought to investigate the neural representation of various innocuous temperatures at the single-cell level to identify the functional significance of distinct thalamic nuclei during thermal encoding.

Extracellular electrophysiology was performed in awake wild-type mice ($n=59$ recording sessions from 24 mice), and neural activity was recorded in various thalamic nuclei using high-density extracellular electrodes (Neuropixels, IMEC). Mice were head-fixed, and their right forepaw was tethered to a gold-plated Peltier element for fast ($75\text{ }^{\circ}\text{C/s}$) and reliable thermal

stimulation. The thermal stimulation range was exclusively innocuous to prevent any sensitization due to painful temperatures (baseline: 32 °C, range: +/- 10 °C). The dorsal surface of the forepaw was in direct contact with a lever arm that served for the recording of paw movements (Figure 3.3.1-1 A).

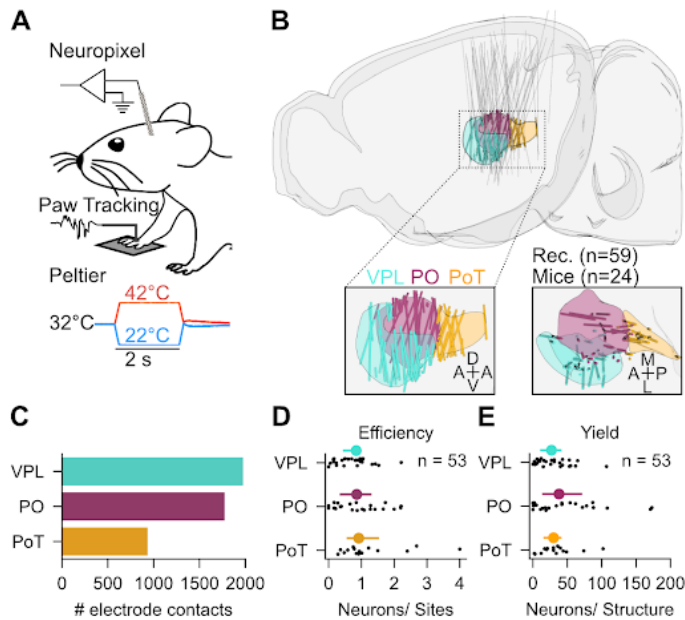


Figure 3.3.1-1 Acute extracellular electrophysiology in awake, head-fixed mice

- A. Schematic representation of the head-fixed mice with their right forepaw tethered to a gold-plated Peltier element for thermal stimulation. Recording of paw movement via lever arm placement on the dorsal surface of forepaw
- B. Reconstruction and spatial assignment of recording sites in the thalamic nuclei.
- C. Distribution of assigned channels in Ventral posterolateral nucleus (VPL), Posterior complex (PO), and Posterior triangular complex (PoT).
- D. Comparison of single unit extraction per channel across the target nuclei. Dots display median, error bars represent 95 % confidence interval.
- E. Comparison of single unit yields across the target nuclei. Dots display median, error bars represent 95 % confidence interval.

The present study focused on three thalamic nuclei in the rodent's thalamus, VPL, PO, and PoT, as the target regions for extracellular recordings since these regions have been shown to send thalamocortical projections to thermosensitive cortical regions S1 and pIC, and VPL as well as PoT have been shown to be necessary for thermal detection behavior. For each probe insertion, the positions of individual electrodes ($n=59$) were reconstructed and mapped onto a virtual three-dimensional reference space using the histological data of labeled probe

trajectories. This mapping allowed the estimation of the position of each recording site along the entire length of a Neuropixel recording shank. Subsequently, the position of a channel associated with the maximum waveform amplitude of a putative single unit was defined as the cell's location. In order to account for any possible deviations in the reconstructions and the range within which the electrode can effectively detect signals, a designated channel was allocated to each specific structure if it fell within a buffer zone of 100 µm from the border of any of the target nuclei (Figure 3.3.1-1 B). Out of the 59 recordings, a total of 53 recordings successfully targeted at least one of the aforementioned nuclei. Across these 53 recordings, a total of 1,976 channels were assigned to VPL, 1,774 channels were assigned to PO, and 934 channels were assigned to PoT (Figure 3.3.1-1 C). On average, an efficiency of 0.84 (95 % confidence interval (ci): 0.64-1.04) single units per recording site was achieved in VPL, 0.85 (95 % ci: 0.55-1.16) in PO, and 0.92 (95 % ci: 0.37-1.47) in PoT (Figure 3.3.1-1 D). These single units were isolated from the raw voltage traces using Kilosort2 (Pachitariu, Sridhar, and Stringer 2023) and met established quality criteria (Siegle et al. 2019) commonly employed in the field. Moreover, these units exhibited a physiological waveform shape. The yield of a recording was defined as the ratio of the number of isolated single units to the total channel count from the respective structure. No apparent differences were observed across the target nuclei, with yields of 30.0 (95 % ci: 15.89-44.21) single units per total channel count of a single experiment assigned to VPL, 27.0 (95 % ci: 17.24-36.76) in PO, and 30.0 (95 % ci: 15.89-44.21) in PoT (Figure 3.3.1-1 E).

3.3.2 Thermally responsive neurons elicit distinct response profiles across the thalamus

Prior investigations into thermal encoding in the thalamus have predominantly focused on a singular thalamic structure (either VB or PoT), utilizing a limited range of thermal stimuli, often examining only the encoding of pain or just cooling or warming (Gottschlich and Werner 1985; Günter Schingnitz and Werner 1980a; G Schingnitz and Werner 1980; 1983; Günter Schingnitz and Werner 1980c; A. D. Craig et al. 1994). However, the previous chapters have indicated that multiple thalamic nuclei exhibit strong potential for being involved in thermal processing due

to their connectivity with thermo-sensory cortical regions (see chapter 3.1) and involvement in thermal detection (see chapter 3.2). In the present study, I aim to overcome the constraints of spatial sampling by investigating the thermal encoding of cooling and warming across three distinct thalamic nuclei. This approach provides an opportunity to investigate how multiple thalamic nuclei represent temperature, a sensation that is tightly interwoven in our daily life experiences. In order to identify the thermally responsive neurons, the statistical significance of sensory responses was evaluated using the Wilcoxon signed-rank test, wherein the distributions of spike counts during sensory stimulation were compared to a baseline distribution. The baseline distribution, sampled from a 2-second time window preceding stimulus onset, matched the length of the stimulus-evoked distribution. Only cells that showed a faster sensory response onset compared to the onset of micro-movement due to stimulation were included in the dataset (Figure 2.4.6-1). Further, the response onset had to be within 750 ms and the peak firing rate time within 2 s after sensory stimulation, independent of whether or not a movement occurred.

Thermally responsive cells were classified based on their response profiles to maximum cooling (22 °C) and warming (42 °C) stimulus amplitudes. "Cold" cells exhibited significant spiking at 22 °C but failed to elicit a significant sensory response at 42 °C. These cells also demonstrated Tuning Index values greater than 0.3 (Figure 3.1.2 A, cells 1&2; B). The Tuning Index was calculated as the ratio of the difference between the peak firing rates at maximum cooling and warming temperatures to the sum of peak firing rates at those temperatures. Individual "Cold" units displayed distinct temporal dynamics and thermal specificity. The response to cooling stimulation evoked temporally precise spiking, as shown by the blue raster plot, while no significant response was observed during warming (red). The response to cooling stimulation primarily involved neurons with a short-duration, "transient"-like sensory response (Figure 3.3.2-1A, cell 1) and neurons with a prolonged, "sustained"-like response (Figure 3.3.2-1A, cell 2). "Cold-Warm" cells displayed significant spiking responses to both 22 °C and 42 °C stimulation, with Tuning Indices ranging between -0.3 and 0.3 (Figure 3.3.2-1 A cell 3; B). In the example "Cold-Warm" unit, the response to cooling stimulation resembled that of the "Cold" unit, characterized by a fast and temporally precise onset (blue). On the other hand, the response to warming (red) started later in time compared to cooling, indicated by the rightward shift in the spiking onset of the raster plot and the response in the peri-stimulus time histogram (PSTH).

"Warm" cells exhibited significant spiking responses at 42 °C but did not show significant spiking at 22 °C stimulation, with Tuning Index values below -0.3 (Figure 3.3.2-1 A cell 4; B). In the example "Warm" unit, the response to warming was still temporally delayed compared to cooling responses, but the unit demonstrated a strong preference for warming stimuli. Across all recorded neurons, the likelihood of eliciting an excitatory response to cooling or warming was greater compared to a suppressed response (cooling: excitatory 26.5 %, suppressed 3.2 %; warming: excitatory 3.9 %, suppressed 1.2 %, Figure 3.3.2-1 C).

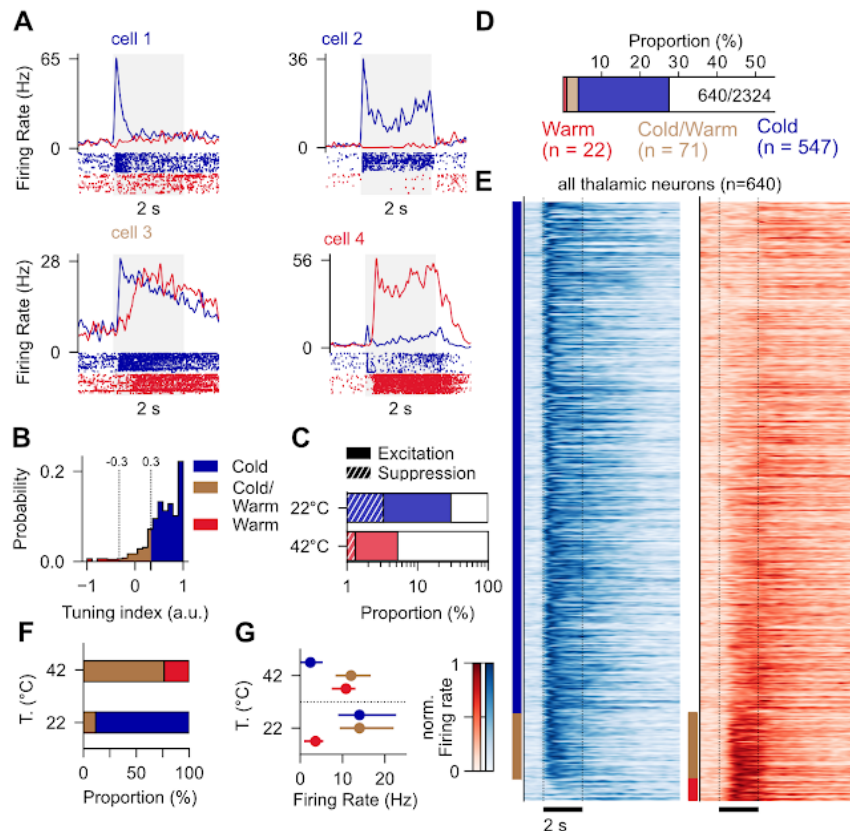


Figure 3.3.2-1 Characterization of response-types in thermally responsive thalamic cell population

- PSTH and raster plots of 4 thermally responsive cells that show either cooling specificity (cells 1 & 2), warming specificity (cell 4), or non-specific responses to both cooling and warming (cell 3). PSTHs and raster plots of cooling evoked responses are shown in blue. Red PSTHs and raster plots display warming-evoked responses. Grey bar indicated stimulus presentation window of 2 s.
- Probability distribution of thermal Tuning Index of all thermally responsive neurons. Dotted lines represent the classification borders for the individual response-types. Neurons with indices larger than 0.3 (blue shaded regions) are classified as "Cold", neurons with indices between -0.3 and 0.3 (copper shaded region) are classified as "Cold-Warm" and neurons with indices below -0.3 (red shaded regions) are labeled as "Warm".
- Proportion of cells that elicit an excitatory (blank) or suppressed (hatched pattern) sensory response to 22 °C (blue) or 42 °C (red) stimulation. Proportions were calculated from the total number of recorded cells.
- Proportion of thermally responsive cells (n = 640) that display either "Cold" (blue, n = 547), "Cold-Warm" (copper, n = 71), and "Warm" (red, n = 22) response-type. Proportion was calculated from the total number of recorded cells (n = 2324).

- E. Population of all thalamic cells ($n = 640$) responsive to cooling or warming sorted by decreasing Tuning Index. Each row displays the response of a single neuron to cooling (blue) and warming (red) and the firing rate was normalized with the maximum firing rate evoked by either cooling or warming. Colored ticks display response-type classification and uses same color-code as in D.
- F. Proportion of response-types activated by 42 °C or 22 °C stimulation. Proportions were calculated from the total number of cells that were activated by either warming or cooling.
- G. Baseline corrected firing rate distributions of the individual response-types to 42 °C and 22 °C thermal stimulation. Dots display median of distribution, error bar represent IQR.

Furthermore, "Cold" cells outnumbered "Cold-Warm" and "Warm" cells (Figure 3.3.2-1 D). From a total of 2324 recorded neurons, 547 neurons showed a selective cooling response ("Cold", 23 %), 71 neurons showed a response to both cooling and warming ("Cold-Warm", 3 %), and only 22 neurons elicited a selective warming response ("Warm", 1 %).

The neural responses to maximum warming (+10 °C from a 32 °C baseline temperature; red) and maximum cooling stimuli (-10 °C from a 32 °C baseline temperature; blue) across all three target structures are displayed in Figure 3.3.2-1 E. Neurons were grouped by their Tuning Index value. Cooling evoked both short-latency transient and short-latency sustained responses. Warming-evoked responses exhibited a stereotypical delayed response latency followed by a sustained response.

Across all three target nuclei, neural responses to cooling were predominantly driven by "Cold" neurons (89 %, $n = 547$ neurons), while "Cold-Warm" neurons accounted for only 11 ($n = 71$). The same "Cold-Warm" neurons responded to warming stimuli and comprised 76 % ($n = 71$) of the warming-responsive cells. Only 23 % ($n = 22$) of the warming-responsive cells were classified as "Warm" (Figure 3.3.2-1 F).

The average peak firing rates evoked by cooling and warming stimulation for each response-type are depicted in Figure 3.1.2 C. "Cold" neurons reached a median peak firing rate of 14 Hz (IQR; 9.2 - 22.4 Hz) at 22 °C and 2.4 Hz (0.4 - 4.9 Hz) at 42 °C. The neural response of "Cold-Warm" neurons exhibited a similar median peak firing rate of 14 Hz (9.6 - 21.7 Hz) during cooling stimulation compared to "Cold" neurons. Additionally, "Cold-Warm" neurons elicited a warming response with a median peak firing rate of 12 Hz (8.6 - 16.4 Hz) across all temperature-responsive neurons in the thalamus. "Warm"-classified neurons displayed a cooling response with a median peak firing rate of 3.6 Hz (1.2 - 5.2 Hz) and a warming response with 11 Hz (7.7 - 12.8 Hz).

In conclusion, the results suggest that cooling responses are carried by more cells than warming responses (Discussion chapter 4.3.1), with the neural representation of cooling mostly driven by "Cold" neurons followed by "Cold-Warm" neurons. Both types showed similar average peak-firing rates across responsive neurons. The "Cold" neurons presented two different temporal response types – transient and sustained cells. Warming responses were mainly driven by "Cold-Warm" neurons, with smaller contributions from "Warm" cells. Both response-types showed similar firing rates and exhibited a homogeneous and stereotypical temporal response profile.

3.3.3 Cooling and warming evoked sensory responses show distinct spatial distributions

The analysis of the dataset shown in the previous chapter was performed on the entire thalamic population (VPL, PO, PoT). In order to shed light on the spatial arrangement of the described response-type and encoding properties of individual thalamic nuclei, the following chapter will investigate the nucleus-specific subpopulations.

The population of responsive cells across the three thalamic structures consisted of three distinct response-types: "Cold" (blue), "Cold-Warm" (copper), and "Warm" (red) (Figure 3.3.3-1 A). The proportion of "Cold" cells formed the majority of responding cells in VPL (86.9 %), PO (86.9 %), and PoT (80.8 %). Secondly, the "Cold-Warm" cells were evenly distributed among the thalamic nuclei and were the second largest cell population in VPL (11.1 %), in PO (10.3 %), and in PoT (12.6 %). The smallest group was "Warm" neurons, accounting for 2.0 % in VPL, 2.8 % in PO, and 6.6 % in PoT. The distribution of response-types was similar across the three structures, revealing an overrepresentation of cells exhibiting cooling responses upon temperature stimulation and a very slight increase in the number of warming selective responses in PoT in relation to VPL and PO.

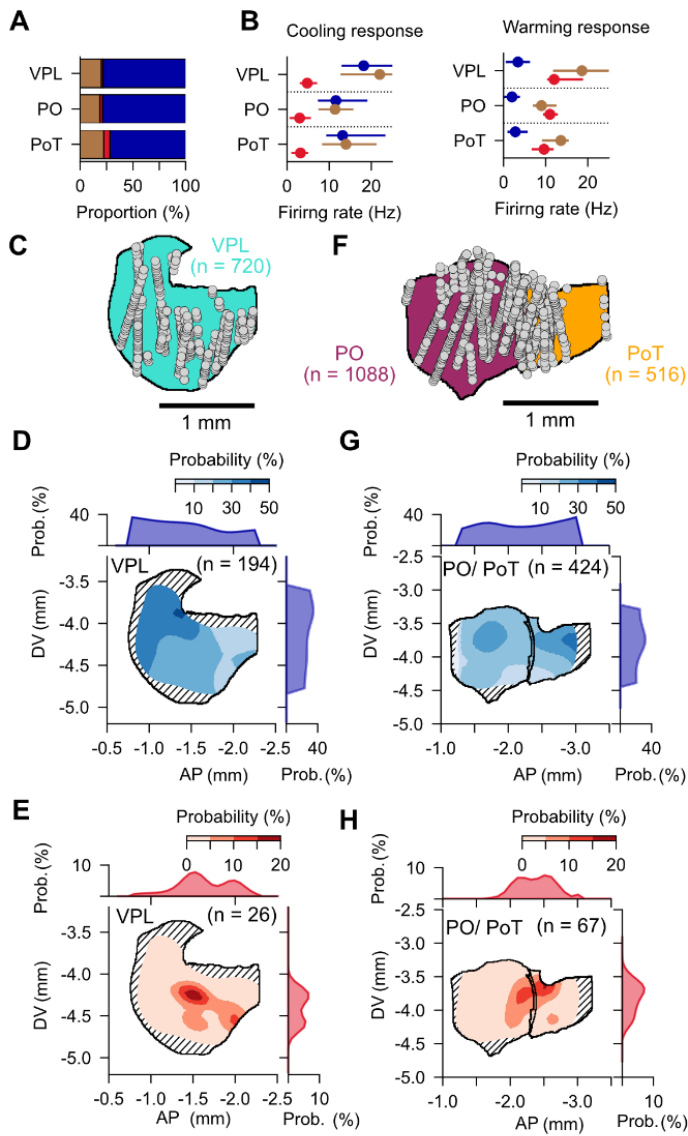


Figure 3.3.3-1 Spatial representation of cooling and warming evoked sensory response

- Proportion of response-types in VPL, PO and PoT. Proportion of "Cold" cells is shown in blue, "Cold-Warm" in copper and "Warm" in red. Proportions were calculated from all responsive cells.
- Baseline corrected firing rate distribution of response-types in VPL, PO, and PoT to cooling stimulation (left) and warming stimulation (right). Dots display median, error bars represent IQR. Same color code as in A.
- Position of all recorded single units (grey dots, n = 720) in VPL shown in a sagittal plane.
- Normalized spatial probability distributions of cooling-responsive ("Cold" & "Cold-Warm") neurons (n = 194). Normalization was performed with probability distribution of all recorded single units in that structure. Hatched pattern indicate region with insufficient cell count in null distribution for normalization.
- Same as D, for warming-responsive ("Cold-Warm", "Warm") cells (n= 26).
- Same as C for cells located in PO (n = 1088) and PoT (n = 516).
- Same as D for cooling-responsive cells located in PO and PoT (n = 424).
- Same as D for warming-responsive cells located in PO and PoT (n = 67).

When examining the baseline corrected peak firing rates for each response-type across the three thalamic target nuclei, it was observed that the sensory response to the maximum cooling stimulus (-10 °C) was mainly driven by "Cold" and "Cold-Warm" cells (Figure 3.3.3-1 B, left). In VPL, "Cold" cells exhibited a median firing rate of 18.2 Hz (IQR: 13.2 – 28.5 Hz). "Cold-Warm" cells exhibited a median firing rate of 22.0 Hz (20.3-29.1 Hz) and „Warm“ 4.8 Hz (3.3-6.9 Hz). A similar trend was seen in PO where "Cold" cells had median firing rates of 11.6 Hz (7.6 – 18.8 Hz), "Cold-Warm" cells had 11.4 Hz (7.7 – 14.3 Hz), and "Warm" cells only 3.0 Hz (0.9 – 5.4 Hz). PoT median firing rate in "Cold" cells was 13.2 Hz (9.6 - 23.1 Hz), "Cold-Warm" classified neurons showed 14.0 Hz (8.6 - 21.0 Hz), and "Warm" elicited 3.2 Hz (1.3 - 4.8 Hz) across the response-type class. For the maximum warming stimulus (42 °C), the response was primarily carried by "Warm" and "Cold-Warm" cells across all three thalamic target nuclei (Figure 3.3.3-1 B, right). For "Warm" cells, the firing rate was 12.0 Hz (11.0 – 19.4 Hz) in VPL, 11.8 Hz (10.8 – 12.2 Hz) in PO, and 9.5 Hz (6.9 – 11.6 Hz) in PoT. The response of "Cold-Warm" cells in VPL was stronger, with the median firing rate being 18.6 Hz (12.0 - 25.7 Hz), followed by PO with 9.0 Hz (1.23 - 12.3 Hz) and PoT with 13.6 Hz (9.4 - 15.2 Hz). In contrast, "Cold" cells exhibited lower firing rates, such as 3.4 Hz (0.8 - 6.0 Hz) in VPL, 2.0 Hz (0.4 - 3.6 Hz) in PO, and 2.8 Hz (1.2 - 5.5 Hz) in PoT.

Mapping the location of thermally responsive thalamic units onto the corresponding anatomical axis revealed sampling from the entire anterior-posterior axis of the individual thalamic target structures (Figure 3.3.3-1 C & F) with spatially localized regions showing very dense sampling. Sagittal plane spatial probability distributions were computed to analyze the spatial arrangement of cooling-responsive and warming-responsive neurons in the VPL (Figure 3.3.3-1 D & E) as well as PO and PoT (Figure 3.3.3-1 G & H). To account for variations in spatial sampling, the response distributions were normalized with the probability distribution of all recorded neurons within each respective structure. These normalized distributions provided an estimation of the proportion of cooling or warming-responsive neurons within each spatial bin. If the total neuron count in a bin was insufficient to accurately estimate the fraction, the bin was indicated as a hatched pattern in Figures 3.1.3 D, E, G, H.

Cooling responses were found to be widely distributed throughout VPL, with the highest probability (40 %) observed in the anterior region of VPL, indicating a significant concentration of cooling-responsive cells in that area (Figure 3.3.3-1 D). The probability distribution gradually decreased in posterior regions of VPL, suggesting a smaller fraction of cooling-responsive cells

(10 %). Conversely, warming responses in VPL exhibited a spatial localization in the posterior regions of the nucleus, as depicted in Figure 3.3.3-1 E. The maximum probability level for warming-selective responses reached 20 %.

The same analysis was conducted for the cell population in PO and PoT. Cooling responses were also found to be widely distributed throughout these thalamic structures (Figure 3.3.3-1 G). Interestingly, the highest probability of finding cooling-responsive cells was observed at the most posterior location in PoT (50 %). PO also contained a sharply demarcated region of high probability values (40 %) for cooling-responsive cells without a clear relation to the anterior-posterior location. In contrast, warming responses were spatially localized in the border region between PO and PoT, reaching a maximum probability level of 20 % (Figure 3.3.3-1 H).

These findings have shown that cooling evoked widespread activation across multiple thalamic nuclei, with spatially localized regions with high cooling-responsive cell concentrations. (Discussion chapter 4.4). Warming, on the other hand, activated spatially defined regions within VPL, PO, and PoT. The data therefore points towards spatially defined subgroups responsible for the selective processing of cooling or both cooling and warming.

3.3.4 Anterior and posterior subregions in thalamic nuclei show different thermal representation

The non-uniform spatial distribution of cooling and warming-responsive cells (see. 3.3.3) across and within thalamic nuclei raises the question of whether the anterior and posterior subregions in VPL and PO, as well as PoT as a whole structure, show distinct functional characteristics in their representation of cooling and warming. Therefore, the nucleus-specific subpopulations were further split by their anterior-posterior positions. This led to a total of 5 subgroups: anterior VPL (aVPL), posterior VPL (pVPL), anterior PO (aPO), posterior PO (pPO) as well as PoT. The subpopulation of PoT was not split since this structure is located at the most posterior border PO (Figure 3.3.4-1 A). This anatomical separation led to a relatively similar number of cells assigned to aVPL ($n = 114$) and pVPL ($n = 97$). Cell counts in PO differed,

and 114 cells were assigned to aPO and 177 cells to pPO. PoT cell count was 151 cells. (Figure 3.3.4-1 B)

In order to investigate if the subregion showed a significantly different thermal tuning, the subregion-specific Tuning Index was calculated and averaged over all thermally responsive cells in a subregion (Figure 3.3.4-1 C). Dots represent the median of the corresponding distributions, and the IQR is displayed as error bars. Interestingly, all distributions showed a cooling-preference thermal tuning indicated by median values larger than 0.5. However, comparing the subregion-specific distributions revealed that aVPL (median (IQR): 0.75 (0.55 - 0.90)) and aPO (0.78 (0.61 - 0.96)) showed even stronger cold tuning than the rest of the thalamic subpopulation (pVPL: 0.5 (0.30 - 0.68), pPO: 0.56 (0.33 - 0.81), PoT: 0.59 (0.37 - 0.83)) indicating a statistically (Mann-Whitney U test for pairwise comparison) different thermal tuning. This corresponds well with the results from the thermal map shown in Figure 3.3.3-1 D, G and E, H, which revealed that cooling-responsive neurons occurred more often in the anterior parts of VPL and PO, while warming-responsive cells were exclusively present in the posterior sections of VPL and PO, as well as in PoT.

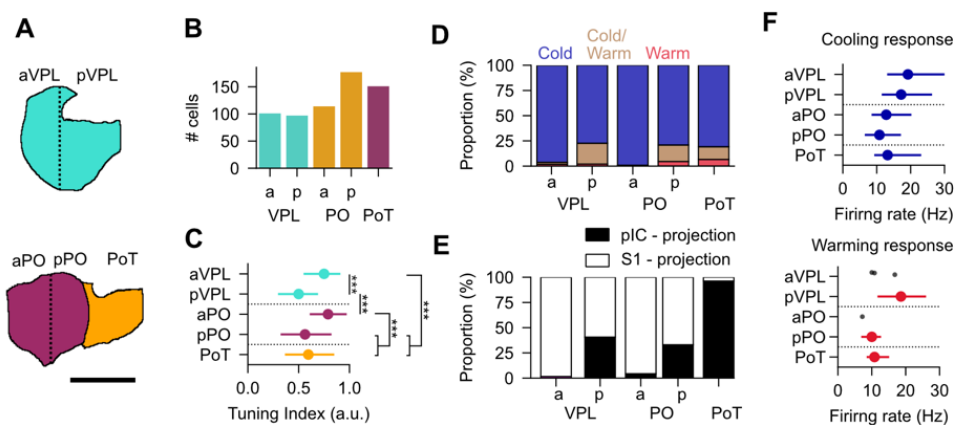


Figure 3.3.4-1 Subregion-specific thermal representations

- Schematics of VPL subdivisions (cyan), PO subdivision (bordeaux), and PoT (gold) in a sagittal plane. Black bar indicates 1mm.
- Cell count per subregion in VPL, PO, and PoT.
- Tuning Index distributions of thalamic subregions. Dots represent median, error bar IQR. Stars indicate $p < 0.001$. Mann-Whitney U test for pairwise comparison.
- Proportion of "Cold" (blue), "Cold-Warm" (copper), and "Warm" (red) cells per thalamic subregion.
- Proportion of pIC-projecting and S1-projecting cells in thalamic subregion. Data is reanalyzed from Chapter 3.1.

F. Baseline corrected firing rate distributions for cooling stimulation (top) and warming stimulation (bottom) for thalamic subregions. Dots represent median, error bar indicate IQR, black dots indicate individual datapoints.

In order to quantify the spatial distributions of cooling and warming-responsive neurons in thalamic subregions, the proportion of response-types per subregion is shown in Figure 3.3.4-1 D and indicates that “Cold” neurons were the most dominant response-type throughout the thalamus, providing an explanation for the preferred tuning to cooling. On the contrary, “Cold-warm” or “Warm” cells had larger concentrations in pVPL, pPO, and PoT. The presence of these response-types and the lack of them in the anterior region provided an explanation for the difference thermal tuning difference seen in Figure 3.3.4-1 C. Interestingly, if the same spatial grouping was applied to the anatomical dataset (see Chapter 3.1) it can be seen that within aVPL and aPO, almost 100 % of cells that send projections to S1 are situated there. On the other hand, PoT cells almost all sent thalamocortical projections to pIC. The posterior regions of VPL and PO had a mixed cell population of thalamocortical projection cells specific for S1 and pIC (Figure 3.3.4-1 E).

Finally, the baseline corrected firing rate distribution, shown as median and IQR, were plotted for each subregion (Figure 3.3.4-1 F) which allows the comparison of the response strength to the maximum cooling and warming stimuli across subregions. The cooling response (top) showed that both aVPL (19.2 Hz (13.2 - 30.4 Hz)) and pVPL (17.2 Hz (11.6 - 25.2 Hz)) demonstrated the strongest response to 22 °C stimulation, followed by PoT (12.8 Hz (9.2-22.0 Hz)). Both subregions in PO displayed the weakest firing rates (aPO: 12.7 Hz (8.8 - 19.9 Hz), pPO: 10.4 Hz (6.4 - 16.4 Hz)). Warming responses in pVPL (18.6 Hz (12.0 - 25.7 Hz)), pPO (10.0 Hz (7.2 - 12.4 Hz)) and PoT (10.8 (8.8 - 14.8 Hz)) showed a similar trend (bottom). pVPL displayed the largest warming-evoked firing rates, followed by PoT and pPO. Only three neurons in aVPL and one neuron in aPO showed warming-evoked sensory responses (black dots). The cell count was too small to parameterize the distribution, so individual data points were shown.

In summary, this chapter has quantified the heterogeneous distribution of cooling and warming-responsive neurons and demonstrated that the anatomical separation into anterior and posterior subpopulations resulted in distinct thermal tuning in these subregions mostly due to the presence of “Cold-Warm” neurons in posterior thalamic regions. This data is in line with results from the anatomical tracing that has shown that the anterior parts of VPL and PO

exclusively send projections to the cooling-selective S1, and the posterior regions of VPL and PO send projections to both S1 and the cooling- and warming-selective pIC (Chapter 3.1).

3.3.5 Thermal stimulation evokes diverse response profiles

In addition to the previously discussed response profiles, two other types of responses were observed in a small subset of neurons: neurons that exhibited a decrease in their firing rate (Figure 3.3.5-1 A-E), and neurons that had a selective offset response specifically during warming stimulation (Figure 3.3.5-1 F-I). Studies that investigated thermal encoding in the sensory periphery have proposed that suppression of neural firing could serve as an effective mechanism for encoding cooling and warming within the same cell and also that warming-selective suppression in Cold-fibers might play a crucial role in the perception of warming. (Burton, Forbes, and Benjamin 1970b; Paricio-Montesinos et al. 2020)

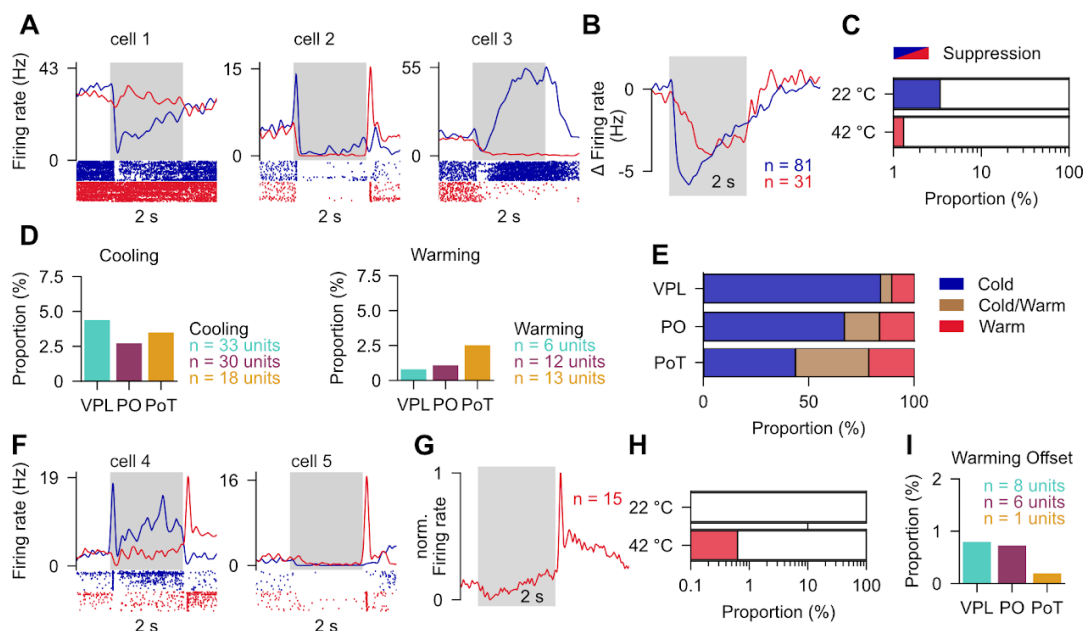


Figure 3.3.5-1 Thermal stimulation elicits suppressed sensory response as well as warming-specific offset responses

- Cooling and warming evoked PSTH and raster plots of thermally responsive cells that show a suppressed response profile specific to cooling (cell 1), warming (cell 3) and both cooling and warming (cell 2). Cooling evoked PSTH and raster plot is displayed in blue, warming in red. Grey bar indicated 2 s stimulus presentation window.*
- Baseline corrected population PSTH of all cooling (n = 81) and warming (n = 31) responsive cells that elicit a suppressed response. Same color-code as in A. Grey bar indicates stimulus presentation window.*
- Proportion of suppressed cells after cooling (22 °C) and warming (42 °C) stimulation. Same color-code as in A.*

- D. Proportion of cells with suppressed cooling (left) and warming (right) responses in VPL (cyan, cooling $n = 33$, warming: $n = 6$), PO (bordeaux, cooling: $n = 30$, warming: $n = 12$) and PoT (gold, cooling: $n = 18$, warming: $n = 13$).
- E. Proportion of suppressed cells that show cooling-specific (blue), warming-specific (red) and non-specific suppression (copper).
- F. Same as A for units that show a warming-specific offset response.
- G. Normalized population response of warming-specific offset response ($n = 15$) after warming stimulation. Grey bar indicates stimulus presentation.
- H. Proportion of warming specific and cooling specific offset response neurons.
- I. Proportion of warming-specific offset cells in VPL (cyan, $n = 8$), PO (bordeaux, $n = 6$) and PoT (gold, $n = 1$).

Figure 3.3.5-1 A provides three examples of cells that demonstrated a suppressed sensory response following cooling or warming stimulation. Cell 1 exhibited a cooling-specific decrease in neural firing, with the most significant decrease occurring within the first 500 ms after stimulus onset. Cell 2 displayed a more complex response profile, where cooling elicited a fast and short-duration transient response followed by a lack of firing throughout the stimulus presentation.

On the other hand, during warming stimulation, the thermal responses showed decreased neural firing during the stimulus, followed by an increase at the stimulus offset. Cell 3 exhibited a short-duration suppression during the initial phase of cooling stimulation followed by an excitatory response, while at warming stimulation, neural firing was completely abolished without an excitatory component.

Figure 3.3.5-1 B illustrates the population response of all neurons that exhibited a suppressed response to cooling or warming stimulation. The cooling-specific population ($n=81$, shown in blue) showed a rapid decrease in neural firing rate during the initial phase of sensory stimulation, with a maximum decrease of 5.8 Hz. This decrease is followed by a slow decay, returning to baseline activity within 4 s after sensory stimulation. On the other hand, the warming-specific population exhibited a delayed decrease in its neural firing rate, reaching a maximum decrease of 3.9 Hz. The fraction of cells showing a suppressed response, independent of any excitatory component, is depicted in Figure 3.3.5-1 B. The suppressive response profile to cooling stimulation occurred as the primary response profile in 3.2 % of all recorded cells, whereas when warming stimulation was applied, it occurred in 1.2 %. All together, similar to the excitatory response profile, cooling responses outnumbered warming responses across the thalamic population. To further analyze the cooling and warming-specific

populations, the cells were grouped based on their anatomical locations, and the individual fractions of cells showing suppression are presented in Figure 3.3.5-1 D. The highest proportion of suppressed neurons was found in VPL with 4.58 % (n=33), followed by PoT with 3.49 % (n=18) and PO with 2.76 % (n=30). Warming-specific neurons were most abundant in PoT with 2.51 % (n=13), followed by PO with 1.11 % (n=12) and VPL with 0.83 % (n=6).

Figure 3.3.5-1 E illustrates the fractions of cooling-specific suppression (blue) and warming-specific suppression (red), as well as the fraction of cells showing suppression to both cooling and warming (copper), for each target structure. The proportion of cooling-specific suppression was larger than warming-specific suppression across VPL, PO, and PoT. However, cooling-evoked suppression decreased from VPL (83.78 %) to PO (66.67 %) and PoT (43.48 %), while cold-warm-evoked suppression increased from VPL (5.40 %) to PO (16.67 %) and PoT (34.78 %). A similar trend was observed for warming-specific suppression, with VPL exhibiting the smallest fraction with 10.8 %, followed by PO with 16.67 % and PoT with 21.74 %.

In conclusion, although the overall proportion of cells showing a suppressed response-type was small, it is noteworthy that some cells displayed a robust decrease in their firing rate. In addition, just like with the excitatory population, warm-specific suppression was most pronounced in PoT. This response-type might be seen in relatively small numbers in the thalamus for multiple reasons. First, signaling in the peripheral nervous system might not completely follow a labeled-line scheme, and crosstalk on the level of the spinal cord could occur between an excitatory and suppressed channel, which could cancel out the suppressed channel. There are studies that have shown that crosstalk of fibers is a common mechanism in the spinal cord (Braz et al. 2014). Second, the thalamus is a heavily interconnected structure with other non-thalamic regions, and individual thalamic cells receive multiple sources of input, not just from the periphery but also from cortical regions (Alloway, Hoffer, and Hoover 2003; Mease and Gonzalez 2021; Deschênes, Veinante, and Zhang 1998; Alloway, Hoffer, and Hoover 2003). If the same thalamic cell is targeted by excitatory input from the cortex and suppressive input from the periphery, the suppressive input would be canceled, and that cell would appear to have an excitatory response. Lastly, it should be acknowledged that it is difficult to compare published data on response-types between the sensory periphery and central nervous system because of different experimental paradigms, separate recording preparations (*in-vivo*, *ex-vivo*), and other model organisms used in these studies.

Offset responses were another interesting response-type seen in the recordings of peripheral nerves in which they show selective activation at the offset of a sensory stimulus. Figure 3.3.5-1 F illustrates two examples of units exhibiting a warming offset response. Cell 4 showed no sensory response or suppression during warming stimulation; instead, an increase in neural firing was observed only at the offset of the response. On the other hand, cell 5 exhibited suppression during warming stimulation, but a distinct increase in neural firing was observed at stimulus offset, indicative of a warming offset response.

Across the thalamic population, a total of 16 cells were classified as warming-offset specific. Figure 3.3.5-1 G displays the population response for this group, which was characterized by a subtle increase in firing during stimulus presentation as well as a strong and short-duration increase in firing at the end of the stimulus plateau, specifically at stimulus offset. Interestingly, only warming stimulation elicited offset responses, with a small fraction of cells (0.68 %) following this response profile. Cooling stimulation, in contrast, did not show any sign of this response-type.

To further analyze the warming-offset specific population, the neurons were categorized based on their anatomical location. Figure 3.3.5-1 I depicts the number of cells in each nucleus: VPL ($n = 6$, 0.80 %) and PO ($n = 8$, 0.74 %) exhibited roughly equal numbers of neurons that showed this response profile. However, PoT only had one neuron (0.19 %) that followed this particular response pattern.

3.3.6 The thalamic representation of touch

Somatosensory stimuli including temperature and touch, get first detected on the skin and are forwarded to structures specialized for somatosensory information processing. However, the encoding of touch has been investigated in greater detail compared to temperature (Casas-Torremocha, Clascá, and Núñez 2017; Chien et al. 2017; Francis, Xu, and Chapin 2008b; Diamond, Armstrong-James, and Ebner 1992b). This opens the possibility of drawing comparisons between thermal and tactile encoding properties. Specifically, this chapter will investigate if temperature and touch are represented by distinct or the same cell populations, as well as if the spatial coverage of thalamic tactile activation differs from the regions that are

activated by thermal stimuli. This investigation will provide valuable insights into the functional organization principles neural circuits utilize to represent somatosensory stimuli of distinct modalities.

In a subset of experiments ($n = 40$ recordings), the animal received 40 Hz sinusoidal tactile stimulation applied to the backside of the right forepaw. The palm of the right forepaw was in contact with a gold-plated Peltier element, which was kept at a baseline temperature of 32 °C, and a 10 °C cooling stimulus was applied every 20 seconds (Figure 3.3.6-1 A).

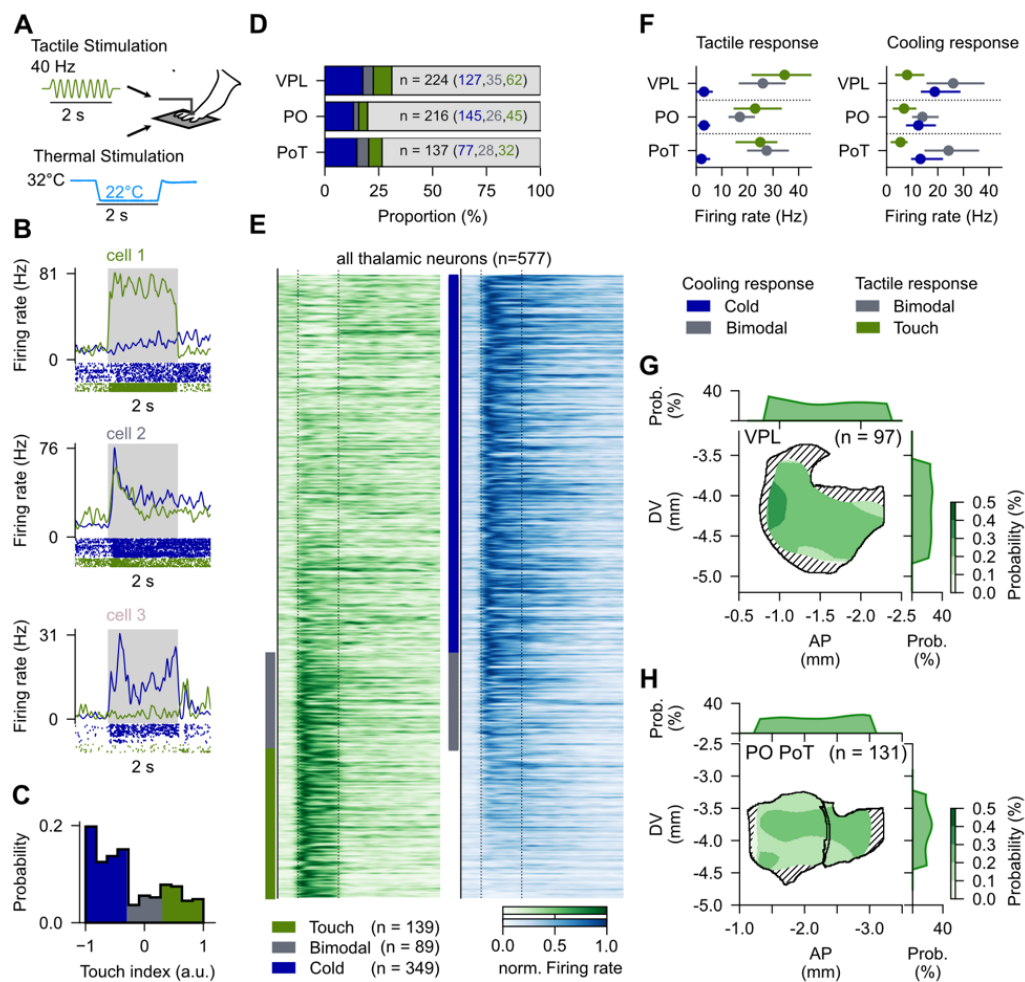


Figure 3.3.6-1 Characterization of the neural representations of temperature and touch

- Experimental paradigm. Paw-tethered mice receive cooling stimulation via a gold-plated Peltier element and tactile stimulation on the backside of the paw. 40 Hz sinusoidal frequency was applied for 2 s.
- PSTH and raster plot of example units that show tactile-specific (cell 1), cooling-specific (cell 3) non-specific sensory responses to both tactile and cooling (cell 2). Green PSTH and raster plot indicate tactile stimulation, blue displays PSTH and raster plot for cooling stimulation. Grey bar indicated stimulus presentation window.
- Probability distribution of Touch Index used for the classification of “Cold” (blue shaded region), “Bimodal” (grey shaded region) and “Touch” (green, shaded region).

- D. Proportion of “Cold” (blue), “Bimodal” (grey) and “Touch” (green) in VPL, PO, and PoT. Values were calculated from the total number of recorded cells located in these structures.
- E. Population of all thalamic cells ($n = 577$) responsive to cooling or tactile stimulation sorted by decreasing Touch Index. Each row displays the response of a single neuron to cooling (blue) and tactile (green). The firing rates were normalized to the maximum firing rate evoked by either stimulus. Colored ticks display response-type classification. Same color-code as in C.
- F. Baseline corrected firing rate distributions of “Thermal” (blue), “Bimodal” (grey) and “Touch” (green) in VPL, PO and PoT for tactile stimulation (left) and cooling stimulation (right). Dots represent median, error bar shows IQR.
- G. Normalized spatial probability distributions of tactile responsive (“Touch” & “Bimodal”) neurons ($n = 97$). Normalization was performed with probability distribution of all recorded cells in those structures. Hatched pattern indicate region with insufficient cell count in null distribution for normalization.
- H. Same as G for tactile responsive population in PO and PoT ($n = 131$).

The population of responsive cells exhibited three distinct response-types: “Touch” (Figure 3.3.6-1 B, cell 1, grey shading indicates stimulus presentation window), “Bimodal” (cell 2), and “Cold” (cell 3). Neurons belonging to the tactile responsive population (“Touch” + “Bimodal”) displayed both transient (cell 2) and sustained (cell 1) response-types. These tactile-responsive neurons exhibited certain characteristics similar to cooling responses observed in previous experiments (Figure 3.1.2), such as rapid and reliable spiking after stimulus onset. The classification of response-types was based on a metric labeled as Touch Index, which scaled the individual response strength of a neuron to tactile and cooling stimulation within the range of -1 to 1. Neurons with indices above 0.3 were classified as “Touch”, those with values between -0.3 and 0.3 were classified as “Bimodal”, and neurons with values below -0.3 were assigned to the “Cold” category (Figure 3.3.6-1 C).

Examining neural responses to tactile (40 Hz sinusoidal; green) and maximum cooling stimuli (-10 °C from 32 °C baseline temperature; blue) across all three target structures (Figure 3.3.6-1 D), it was observed that responsive units ($n = 577$) grouped by their response-type class displayed distinct characteristics. Transient and sustained responses were noted in the tactile-evoked responses. The response duration matched the stimulus application time. The response of the cooling-responsive population was characterized by transient-like and sustained-like response types with rapid onsets. The responses of the sustained-like response-types often persisted after stimulus termination, indicating a slow decay.

In VPL, PO, and PoT, the proportion of ‘Touch’ neurons formed 8.8 % ($n = 62$), 4.5 % ($n = 45$), and 6.4 % ($n = 32$) out of the cells recorded in the respective areas. “Bimodal” cell fraction constituted 5.0 % ($n = 35$) in VPL, 2.6 % ($n = 26$) in PO, and 5.6 % ($n = 28$) in PoT. The largest

fraction was attributed to the cooling-responsive cells, with 18.1 % ($n = 127$) in VPL, 14.4 % ($n = 145$) in PO, and 15.5 % ($n = 77$) in PoT. Combining the “Touch” and “Bimodal” cells, which form the tactile-responsive class, resulted in a total of 97 cells, corresponding to a proportion of 13.8 % in VPL. In PO, 71 out of 1002 cells (7.1 %) responded to tactile stimulation, and in PoT, 60 out of 498 recorded cells (12.0 %) exhibited tactile responsiveness (Figure 3.3.6-1 E). Plotting the baseline-corrected median peak firing rate for each response-type across the three thalamic target nuclei (Figure 3.3.6-1 F) revealed that the sensory response to the tactile stimulus was primarily driven by “Touch” and “Bimodal” cells. VPL had a median firing rate of 34.5 Hz (22.0 - 44.8 Hz) for “Touch” cells and 26.0 Hz (17.0 - 34.5 Hz) for “Bimodal” cells. For “Touch” cells in PO, the respective median firing rates were 23.0 Hz (15.0 - 33.0 Hz) and 17.0 Hz (13.0 - 22.5 Hz) for “Bimodal” cells. In PoT, the “Touch” cells had a median firing rate of 25.0 Hz (15.8 – 31.3 Hz), while “Bimodal” cells showed a firing rate of 27.5 Hz (20.3 - 35.8 Hz). Cells classified as “Cold” elicited firing rates of 3.0 Hz (-2.0 - 6.0 Hz) in VPL, 3.0 Hz (1.0 - 5.0 Hz) in PO, and 2.0 Hz (0.0 - 5.0 Hz) in PoT (Figure 3.3.6-1 F left). The sensory response to the maximum cooling stimulus (22 °C), was predominantly carried by “Bimodal” and “Cold” cells across all three thalamic target nuclei. “Cold” cells displayed similar firing rates across the structures, with 18.8 Hz (13.8 - 28.4 Hz) in VPL, 12.4 Hz (8.0 - 18.8 Hz) in PO, and 13.2 Hz (10.0 - 21.6 Hz) in PoT. Among “Bimodal” cells, VPL exhibited the highest firing rate with 26.0 Hz (16.0 - 37.8 Hz), followed by PoT with 24.2 Hz (15.2 - 35.7 Hz), and PO with 14.0 Hz (10.4 - 19.9 Hz). “Touch” cells across all structures reached firing rates of 8.0 Hz (3.7 - 14.2 Hz) in VPL, 6.8 Hz (2.8 - 11.2 Hz) in PO, and 5.4 Hz (2.0 - 7.8 Hz) in PoT (Figure 3.3.6-1 F left).

Spatial probability distributions were computed in the sagittal plane to analyze the spatial arrangement of tactile-responsive neurons in VPL (Figure 3.3.6-1 G), PO, and PoT (Figure 3.3.6-1 H). To account for variations in spatial sampling, the same normalization method as in Chapter 3.3.3 has been applied to the data. Tactile responses were found to be widely distributed throughout the thalamus, with the highest probability (40 %) observed in the anterior region of VPL, indicating a significant concentration of tactile-responsive cells in that area (Figure 3.3.6-1 G). The probability distribution gradually decreased in the posterior regions of VPL, suggesting a smaller fraction of tactile-responsive cells (10 %). Interestingly, the spatial extent of the tactile-responsive probability distribution showed significant overlap with the cooling-responsive distribution (Figure 3.3.3-1 D & G), exhibiting a weak but gradual decrease of responsive cells along the anterior-posterior axis of VPL. The same analysis

conducted for the cell population in PO and PoT revealed widely distributed tactile-responsive cells throughout these thalamic structures. Both PO and PoT exhibited regions with a high density of tactile-responsive cells (40 %), and no apparent relationship was observed between the probability distributions and the anterior-posterior location.

Taken together, this data has shown that cooling and tactile stimuli are encoded by both modality-specific cells as well as thermo-tactile-sensitive cells and that tactile stimulation evoked stronger firing rates compared to temperature stimulation. Furthermore, both modalities show great overlap in their spatial activation profiles, confirming the crucial role VPL, PO, and PoT have in the processing of somatosensory information (Discussion chapter 4.4.2).

3.4 Encoding of cooling and warming stimulus intensities across thalamic nuclei

In the previous chapter (see chapter 3.3), fundamental encoding properties of cooling and warming, as well as the spatial activation within the thalamus, were investigated. This chapter is going to examine if thermal stimuli are represented by distinct neural ensembles or by individual neurons scaling their activity in relation to the external stimulus (3.4.1) and if the encoding of stimulus amplitudes shows a nucleus or response-type specific profile (3.4.2). Finally, two key features of amplitude encoding are investigated: saturation (3.4.3) and sensitivity (3.4.4).

3.4.1 Thalamic temperature encoding is driven by stimulus intensity in the innocuous temperature range

Multiple models of thermal encoding have been proposed across the key nodes in the thermosensory system. At the level of the primary sensory afferents and the associated thermosensitive proteins, it is under debate if the encoding of cooling and warming stimuli

occurs in combinatorial and graded paradigms, respectively (F. Wang et al. 2018a). In the combinatorial coding paradigm, or the TRP-tiling model, different combinations of proteins, and therefore neurons, are activated at specific temperature ranges. This would lead to a specificity in the tuning profile of the neurons such that a neuron preferentially activates at a specific temperature (Figure 3.4.1-1A, left). The graded model presents an alternative whereby neurons respond primarily to an increasing stimulus intensity rather than eliciting a maximal response to a specific range of temperatures (Figure 3.4.1-1A, right). Here, I have referred to these two models as the “Specificity” model and the “Intensity” model.

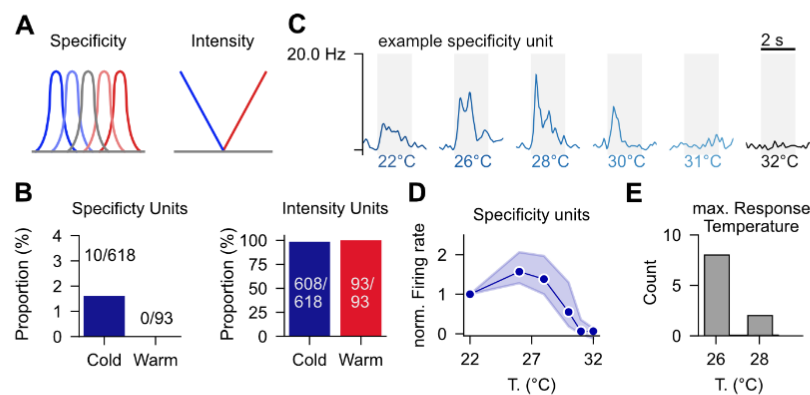


Figure 3.4.1-1 Thalamic thermal encoding is tuned to stimulus intensity, not stimulus specificity

- A. Schematic showing “Specificity” (left) and “Intensity” (right) coding schemes.
- B. Left: Proportion of neurons that follow a “Specificity” model in response to cooling (left; $n = 10$ of 618 cooling-responsive neurons) or warming (right; $n = 0$ of 93 warming-responsive neurons) stimulation. Right: Proportion of neurons that follow an “Intensity” model in response to cooling (left; $n = 602$ of 618 cooling-responsive neurons) or warming (right; $n = 93$ of 93 warming-responsive neurons) stimulation.
- C. Example unit following “Specificity” scheme.
- D. Normalized firing rate for all “Specificity” units ($n = 10$ units). Individual traces are normalized to response at maximum cooling intensity. Points display median; shaded region, 95 % confidence interval.
- E. Number of units with a maximum response amplitude at 26 °C ($n = 8$) or 28 °C ($n = 2$), respectively.

For cooling stimulation, I observed that only 1.61 % ($n = 10$) of neurons exhibited maximum tuning to temperatures below the maximum cooling amplitude and were classified as “Specificity” units (Figure 3.4.1-1 B, left). 98.9 % of thermosensitive thalamic neurons followed an intensity-based framework, where their responses monotonically increased with stimulus amplitudes (Figure 3.4.1-1 B, right). Furthermore, for warming stimulation, all neurons followed an intensity-based encoding scheme (Figure 3.4.1-1 B, right). Figure 3.4.1-1 C

presents an example unit that adheres to the “Specificity” framework, with the peak response already reached at 28 °C and the response strength decreasing with increasing cooling stimulus amplitudes. Among the subset of neurons classified as “Specificity” units, the majority exhibited maximal activation at intermediate temperatures (26 °C n = 8, 28 °C n = 2) (Figure 3.4.1-1 D & E). These findings suggest that within the investigated innocuous temperature range, temperature is encoded along an intensity axis rather than as a tuned feature. It has to be noted that the limited range of tested amplitudes within the innocuous temperature range probably evokes a smaller fraction of “Specificity” units compared to noxious cooling and warming stimuli (Discussion chapter 4.5.1). It is well known that sensory afferents are populated with TRP Channels that are tuned to the noxious temperature range, which wouldn't be activated by the tested temperature intensities (Voets et al. 2004a; Ramsey, Delling, and Clapham 2006; Venkatachalam and Montell 2007). Other studies that have applied painful stimuli have reported that noxious heat or cold is, to a certain extent, transmitted by separate subpopulations than those responding to innocuous thermal stimuli in the sensory periphery (Yarmolinsky et al. 2016a) and the spinal cord (Ran, Hoon, and Chen 2016a).

3.4.2 Various encoding profiles with anatomical specialization drive thermal encoding in the thalamus

As shown in chapter 3.4.1, the thermally responsive thalamic population scaled its neural firing monotonically with the amplitude of thermal stimuli within the innocuous temperature range. This allowed the examination of intensity-based encoding profiles at multiple scales, from the entire thalamic population to functional subtypes within thalamic nuclei, and how these functional ensembles encode stimuli of various intensities. Previous studies have not provided insights into the thalamic encoding of temperature amplitudes in the innocuous range, as mostly single amplitudes were tested in isolation, or the focus was set on the extremes of the intensity scale, i.e., noxious cold or heat.

Across the thermally responsive thalamic neuron population, a diverse range of encoding profiles was observed (see Figure 3.4.2-1 A). These profiles exhibited variations in the

saturation of sensory responses to cooling stimuli or the recruitment temperature at which cells initiated their sensory responses, particularly in response to warming stimulation. In certain example units, the tuning curve for cooling stimulations displayed a linear increase in response amplitude as stimulus temperature decreased (cell 1 - 3), suggesting an absence of saturation within the innocuous range. On the other hand, a subset of units showed tuning curves that were almost like a step function (cell 4) where the response was saturated at intermediate and high magnitudes of cooling stimuli (<28 °C). Warm stimulus tuning curves were typically not saturated in the innocuous thermal range (cells 3-5) suggesting the potential for the dynamic range extending to higher temperature.

The presented cooling-responsive units (cell 1-4) demonstrated significant firing in the low-amplitude stimulus range (> 28 °C), regardless of their response-type (cold, cold-warm) and encoding profile (linear, step-wise). Conversely, the warming-responsive cells initiated their firing in different stimulus intensity ranges: the low amplitude (< 40 °C) and high amplitude (\geq 40 °C) regimes. In two example units, a significant sensory response was observed at a stimulus temperature of 38 °C (cells 3 & 5). Another warming-responsive unit initiated its sensory response at 41 °C (cell 5).

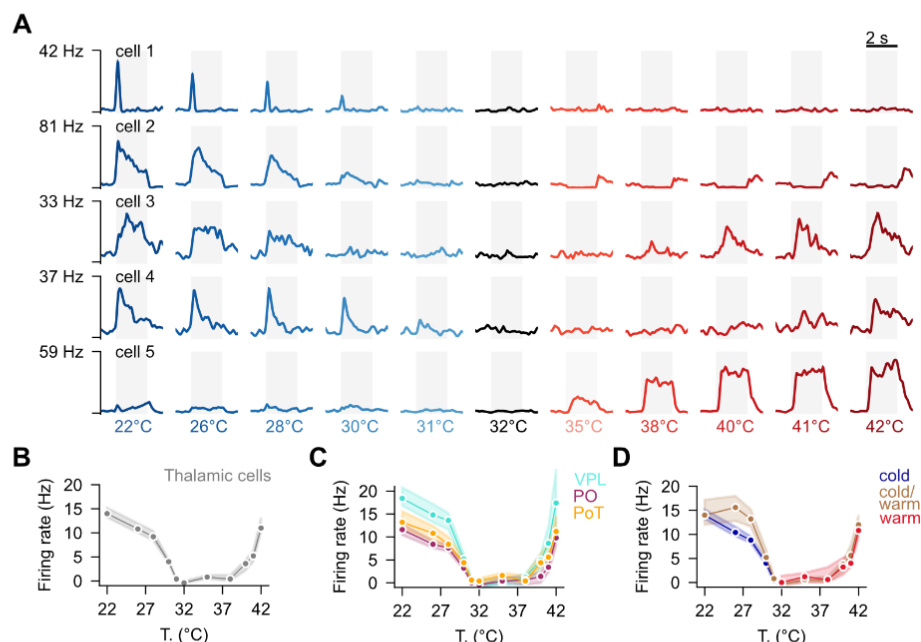


Figure 3.4.2-1 Temperature-evoked tuning curves show distinct encoding profiles

- A. Example unit PSTHs for graded encoding of temperature. Each row is one example unit, and each column is a single stimulus intensity. Grey shading indicates stimulus duration.

- B. Stimulus-evoked response amplitude for each stimulus intensity for the cooling-responsive ($n=618$) and warming-responsive ($n=93$) thalamic population. Dots display median, shaded area 95 % confidence interval.
- C. Stimulus evoked response amplitude for each stimulus intensity split by thalamic nuclei. Cooling-responsive neurons are shown for cooling stimuli (VPL: $n = 194$ neurons, PO: $n = 283$ neurons; PoT: $n = 141$ neurons), and warming-responsive neurons are shown for warming stimuli (VPL: $n = 28$ neurons, PO: $n = 38$ neurons; PoT: $n = 29$ neurons). Dots display median, shaded area 95 % confidence interval.
- D. Stimulus evoked response amplitude for each stimulus intensity split by response-types. "Cold" (blue) and "Cold-Warm" (copper) neurons are shown for cooling stimuli ("Cold": $n = 547$ neurons, "Cold-Warm": $n = 71$ neurons); and "Warm" (red) and "Cold-Warm" (copper) neurons are shown for warming stimuli ("Warm": $n = 22$ neurons, "Cold-Warm" $n = 71$) neurons. Dots display median, shaded area 95 % confidence interval.

The subsequent analysis of tuning curves for the cooling and warming-responsive populations (Figure 3.4.2-1 B), the populations segregated by anatomical region (Figure 3.4.2-1 C), and the populations split by response-type (Figure 3.4.2-1 D) aimed to investigate whether any of the aforementioned examples dominated the encoding schemes elicited by the thalamic nuclei or functional subgroups.

Across the thalamic population, cooling-responsive cells ($n=618$) exhibited a continuous increase in firing rate across the entire range of presented stimulus amplitudes, showing no apparent signs of saturation (Figure 3.4.2-1 B, Range: $22\text{ }^{\circ}\text{C}$ - $32\text{ }^{\circ}\text{C}$). The tuning curves of the cooling response population were characterized by a strong increase in neural firing in the low-amplitude stimulus range ($> 28\text{ }^{\circ}\text{C}$). The relationship between the increase in neural firing rate and stimulus amplitude weakened at $28\text{ }^{\circ}\text{C}$, and the population displayed only a weak but linear scaling of firing rate with decreasing stimulus amplitudes. In contrast, the warming-responsive population ($n=93$) demonstrated a different relationship between its firing rate and warming stimulus amplitudes. At low amplitudes ($< 40\text{ }^{\circ}\text{C}$), there was a slight increase in the firing rate, implying that the majority of warming neurons were probably tuned to high-amplitude warming. At $38\text{ }^{\circ}\text{C}$, the population exhibited a nearly exponential rise in firing rate versus stimulus amplitudes that increased up to the maximum temperature. This shape indicated that the warming population did not exhibit saturation even at the maximum temperature of $42\text{ }^{\circ}\text{C}$ (Figure 3.4.2-1 B, Range: $32\text{ }^{\circ}\text{C}$ - $42\text{ }^{\circ}\text{C}$).

Figure 3.4.2-1 C presents the thermally evoked tuning curves of VPL (cooling: $n = 194$; warming: $n = 28$, cyan), PO (cooling: $n = 283$; warming: $n = 38$, bordeaux), and PoT (cooling: $n = 141$; warming: $n = 29$, gold). A comparison of the three thalamic nuclei revealed that cooling-responsive cells exhibited similar encoding profiles independent of their anatomical location, resembling the shape of the tuning curve observed for the entire cooling-responsive

population. Furthermore, it was evident that the cooling-evoked firing rates are highest in VPL (cyan), followed by PoT (gold) and PO (bordeaux).

The warming-evoked tuning curves showed a slight increase in neural firing at low-amplitude warming stimuli (< 40 °C) in all three structures. The nucleus-specific tuning curves began to diverge in the high-amplitude stimulus range (> 40 °C). VPL (cyan) exhibited higher firing rates compared to PoT (gold) and PO (bordeaux) at the maximum stimulus temperature. In summary, the division by location did not provide evidence of anatomical specialization regarding the encoding profile of cooling stimuli. Only the response strength displayed a nucleus-specific relationship, with VPL being the strongest activated structure, followed by PoT and PO. For warming stimulation, a similar trend was observed, with no obvious difference in the tuning curve shape but variable response strength, with VPL showing stronger stimulus-evoked firing rates than PoT and PO at stimulus amplitudes over 40 °C.

Splitting the responsive population by response-type (Figure 3.4.2-1 D) revealed that the various encoding profiles observed in the example cells could be captured at the population level. Comparing the cooling-evoked tuning curves specific to "Cold" (blue) and "Cold-Warm" (copper) cells showed that "Cold" cells tended to exhibit tuning curves with a more linear shape than those elicited by "Cold-Warm" cells which resembled a step function. Recruitment in the low-amplitude cooling range was similar in both response-types (Range: 30 °C - 31 °C). Warming-evoked tuning curves indicated that the "Warm" (red) cells and "Cold-Warm" (copper) cells had almost the same encoding profiles.

In conclusion, this chapter has revealed that thermal encoding is carried out by various encoding profiles specific to cooling and warming stimulation. Cooling stimulation evoked neural responses in cells that varied in their encoding profiles with increasing cooling amplitudes. Interestingly, the different encoding profiles could be captured by the response-type specific separation (Figure 3.4.2-1 D) across the population, as indicated by the distinct shapes of tuning curves seen in "Cold-Warm" and 'Cold" cells. Across the thalamic population, the results revealed that the anatomical location only showed limited influence on the shape of the tuning curve but that the location was an indicator of the response strength to thermal stimulation, suggesting distinct streams of input varying in their neural gain. Warming stimulation has shown that on the single-unit level, variations in the thermal sensitivity appeared, with some neurons initiating their sensory response at small temperature changes and some neurons that were only activated by stimulus intensities larger than 40 °C.

The following chapters will focus on the saturation of the sensory response and the sensitivity to low-amplitude thermal stimuli, thereby investigating the significance of the response-types as well as the anatomical location for these thermal encoding characteristics.

3.4.3 Sensory response-types and anatomical location serve as an indicator of response saturation

The extent to which a neuron, a specific response-type, or an entire structure saturates its sensory response at different temperatures defines the range of possible intensity encoding capabilities and their functional role. In order to investigate the saturation of amplitude encoding in greater detail, I analyzed the fraction of cells that reached at least 80 % of the maximum response amplitude. This analysis was performed for the individual thalamic nuclei (Figure 3.4.3-1 A, left) and the sensory response-types (Figure 3.4.3-1 A, right). When the responsive cell population was grouped based on their anatomical position, no significant difference was found in the fraction of cells that reached their maximum response amplitudes across thalamic nuclei, except for a slightly higher fraction of saturated cells in PoT (gold) at 41 °C. However, when I divided the dataset by response-types, I observed a distinct relationship between the fraction of saturated cells and stimulus amplitude.

"Cold" cells showed a linear increase in the fraction of cells reaching maximum response with increasing cooling stimulus amplitude, indicating that even at high stimulus amplitudes, a significant number of cells continued to scale their sensory response with the stimulus intensity (Figure 3.4.3-1 A, right, blue). On the other hand, "Cold-Warm" (right, copper) classified cells exhibited a steep increase in the fraction of cells reaching their maximum response amplitudes at low stimulus amplitudes, with 85.9 % of cells showing a saturated response at 26 °C compared to 58.8 % in "Cold" cells.

For the warming-responsive groups ("Cold-Warm" and "Warm" cells) (copper, red), I observed that almost no cells reached their maximum response amplitude at low-amplitude warming stimuli. Only with increasing stimulus amplitudes did the fraction of saturated cells steeply increase, with the largest fraction of cells reaching their maximum response at 42 °C.

Furthermore, "Warm" (red) cells showed a slightly higher fraction of saturated cells at 40 °C compared to "Cold-Warm" cells (copper).

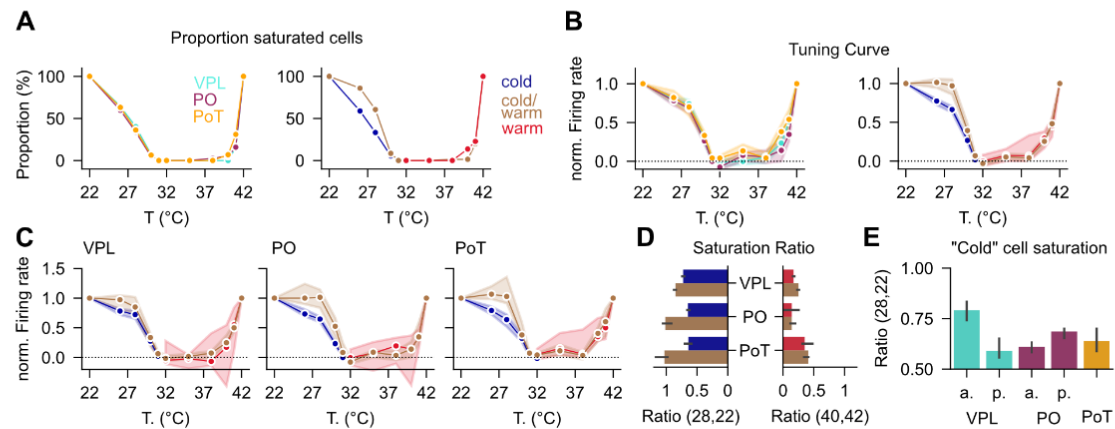


Figure 3.4.3-1 Saturation Profiles and Tuning Curves in Thalamic Neurons

- Fraction of cells reaching at least 80 % of maximum response amplitude plotted as a function of stimulus temperature for thalamic nuclei (left) and sensory response-types (right).
- Normalized tuning curves for the three thalamic nuclei (left) and response-types (right). Cooling- and warming-evoked firing rates were divided by the firing rates at maximum stimulus amplitudes, respectively. Dots display median, shaded area 95 % confidence interval.
- Normalized tuning curves for response-types and anatomical separation. Dots display median, shaded area 95 % confidence interval.
- Saturation Ratio analysis comparing warming and cooling evoked saturation of sensory responses for individual thalamic nuclei and response-types. Bar width represents median, error bar displays 95 % confidence interval.
- Saturation ratio of "Cold" cells split by anterior-posterior position in VPL and PO as well as PoT. Bar height represents median, error bar displays 95 % confidence interval.

To further investigate the shape of the tuning curves and the influence of the anatomical location, I generated normalized tuning curves for the three thalamic nuclei (Figure 3.4.3-1 B, left) and individual response-types (Figure 3.4.3-1 B, right). The firing rate of each neuron was normalized by dividing the response at any given amplitude with the response at maximum stimulus amplitude (22 °C for cooling-evoked firing and 42 °C for warming-evoked firing). The values were averaged over the groups of interest and plotted as medians with 95 % Confidence Intervals against stimulus amplitude. This analysis made it possible to investigate the shapes of the tuning curves in much more detail since neural populations tend to have large variance in firing rates. I found that all three thalamic nuclei exhibited very similar normalized tuning curves, with no obvious differences between them, confirming that the anatomical location had no effect on the tuning curve shapes for cooling stimulation. The same held true for low-

amplitude warming stimulation ($T < 40$ °C), which showed similar normalized firing rates across VPL, PO, and PoT. However, high-amplitude warming stimuli ($T = 40$ °C) elicited different normalized firing rates in the thalamic nuclei. PoT reached 38 % of its maximum firing rate (Figure 3.4.3-1 B, left, gold) at 40 °C, followed by VPL with 23 % (left, cyan) and PO with 14 % (left, bordeaux).

When I separated the data by response-types (Figure 3.4.3-1 B, right), I observed that both the "Cold" (blue) and "Cold-Warm" (copper) groups showed a strong increase in their normalized firing rates at low-amplitude cooling stimuli ($T > 28$ °C). The "Cold" group was at 66 % of the maximal firing rate, while the "Cold-Warm" group had already saturated its response at 28 °C (96 %). During high-amplitude cooling ($T < 28$ °C), the "Cold" population showed a linear increase with temperature decrease, while the response of the "Cold-Warm" group did not vary their firing with decreasing stimulus temperatures. The encoding of warming amplitudes followed a similar profile for both "Cold-Warm" and "Warm" cells, with a small increase in normalized firing rates at low-amplitude warming stimuli, followed by a stronger increase until reaching the maximum normalized firing rate at 42 °C confirming the results seen in the tuning curves generated with absolute firing rates (Figure 3.2.2 D).

To explore potential anatomical specializations of the individual response-types, I examined the normalized tuning curves for both response-type separation and anatomical separation (Figure 3.4.3-1 C). In all three thalamic structures, the tuning curves of "Cold-Warm" (copper) cells exhibited higher values for 26 °C and 28 °C stimuli compared to "Cold" (blue) cells. The difference in normalized firing rates at these temperatures increased from VPL (left) to PO (middle) and PoT (right), indicating that "Cold-Warm" cells in PoT showed the strongest saturation among the investigated structures. This anatomical specialization was also evident in the warming-evoked tuning curves, as PoT (right) exhibited slightly higher values at 40 °C and 41 °C for both "Cold-Warm" (copper) and "Warm" (red) cells compared to PO (middle) and VPL (left).

Parameterization of the tuning curves enabled estimation of the response saturation as the ratio between the evoked responses for the intermediate stimulus (cooling: 28 °C; warming: 40 °C) intensity and the highest intensity stimulus (cooling: 22 °C; warming: 42 °C). For example, if such a curve has a saturation ratio of 1, then the tuning curve is fully saturated at the intermediate stimulus value; otherwise that neuron still has capabilities to increase its firing at higher temperature amplitudes. Comparatively, saturation ratios of warming-

responsive cells (Figure 3.4.3-1 D, right) were largely below those of cooling-responsive cells (Figure 3.4.3-1 D, Left) across nuclei, demonstrating that cooling responses were more sensitive to a smaller range than warming responses. One should bear in mind, though, that cooling- versus warming-evoked saturation comparison is study-specific as it depends on the amplitudes that were tested, the intermediate stimulus amplitude, as well as on the adaption temperature at which the paw was kept. The intermediate cooling amplitude was defined as 28 °C, and the intermediate warming amplitude was defined as 40 °C. For this analysis, a temperature difference of 6 °C for cooling and 8 °C for warming was used as the intermediate temperatures step. The maximum temperature was adjusted to -10 °C and 10 °C which corresponded to 22 °C and 42 °C, respectively.

The saturation ratio of the cooling responses was lower for ‘Cold’ neurons (left, blue) than “Cool-warm” neurons (left, copper), pointing towards distinct functional roles in the encoding of stimulus intensities and agreeing with results from previous tuning curves observations (Figure 3.4.3-1 A, B, C see Discussion chapter 4.5). In addition, PoT “Cold-warm” registered the highest values compared to other nuclei. For warming stimulation, saturation ratio values did not differ significantly between “Warm” (red) and “Cold-warm” (copper) neurons, although the highest value was observed in PoT, followed by VPL and PO.

Figure 3.3.4-1 implies that “Cold” neurons in the thalamus were widely distributed not only across but also within the nuclei, whereas “Cold-Warm” and “Warm” cells had a specific spatial localization. In order to determine whether “Cold” neurons are saturated by the same profile independent of the location, I used the same spatial split as explained in section 3.3.4. Comparatively, the saturation ratio in the subregions of aVPL (cyan, left) and pVPL (cyan, right) displayed a significant difference – indicating that “Cold” cells found in the posterior part manifested weak saturation compared to those located at the anterior region of VPL. The saturation ratio of aPO (bordeaux, left) cells was slightly decreased compared to pPO (bordeaux, right), revealing an opposite tendency where posterior cells showed stronger saturation compared to anterior cells. PoT “Cold” (gold) cells exhibited an intermediate saturation ratio compared to anterior PO and posterior PO. Taken together, these results have shown that neural response saturation, which is an essential characteristic of the encoding of stimulus intensities, varied across the response-types and that similar response-types showed location-specific variations in the saturation level (Discussion chapter 4.5.3).

3.4.4 Sensitivity of thalamic nuclei to cooling and warming stimulation

The sensitivity of a neural ensemble to low-amplitude thermal stimuli can be regarded as an important feature necessary for a reliable and precise representation of external stimuli that are not considered painful. Humans (C. Stevens Kenneth K. Choo 1998) as well as mice (Paricio-Montesinos et al. 2020) have been shown to be able to detect tiny temperature changes. This behavioral capability points towards very temperature-sensitive neural circuits that represent these small-amplitude thermal stimuli.

In order to evaluate the sensitivity of thalamic nuclei (Figure 3.4.4-1 A) and response-types (Figure 3.4.4-1 B), cell recruitment was quantified as the fraction of cells reaching 20 % of the maximum firing rate and plotted against stimulus intensity. The recruitment profile for cooling stimulation exhibited similarity across nuclei, whereas warming stimulation showed distinct differences at low stimulus amplitudes (Figure 3.4.4-1 A). In the low-amplitude warming regime ($<40^{\circ}\text{C}$), cells in PO (bordeaux) and PoT (gold) were more likely to be recruited compared to VPL (cyan) (38°C ; PoT: 48.2 %, PO: 44.7 %, VPL: 15.3 %), suggesting variations in warm sensitivity among the nuclei. Figure 3.4.4-1 B demonstrates a similar recruitment profile for "Cold" (blue) and "Cold-Warm" (copper) cells, while warming-evoked recruitment exhibited slight differences between "Warm" (red) and "Cold-Warm" cells, with "Warm" cells showing increased recruitment fractions at low-amplitude warming.

Figure 3.4.4-1 C displays the fraction of low-amplitude (cooling $>28^{\circ}\text{C}$, warming $<40^{\circ}\text{C}$) recruited cells categorized by anatomical region and response-type. Cooling recruited cells consistently had larger fractions than warming recruited cells, irrespective of structure and response-type. It has to be noted that the cooling low-amplitude range was only a -2°C step from the baseline temperature of 32°C , the warming low-amplitude regime, however, was a 6°C temperature step. Even though the low amplitude regime was different for cooling and warming, cooling appeared to be more sensitive than warming, which is in line with the increased detectability of cooling compared to warming seen in behavioral studies (C. Stevens Kenneth K. Choo 1998; Paricio-Montesinos et al. 2020).

Within the cooling-responsive population (left), VPL exhibited the lowest fraction of recruited cells for both "Cold" (63.3 %) and "Cold-Warm" (59.0 %) cells. PO had the second-largest fraction, with 63.6 % "Cold" and 73.3 % "Cold-Warm" cells. PoT showed the largest fraction

with 73.3 % "Cold" and 78.9 % "Cold-Warm" cells. Warming-evoked recruitment (right) demonstrated a similar but stronger trend, with increasing fractions of "Cold-Warm" cells recruited from VPL (13.6 %) to PO (43.3 %) and PoT (42.1 %). This trend was also observed in the "Warm" classified cells, with PoT exhibiting the largest fraction of recruited cells (60.0 %), followed by PO (50.0 %) and VPL (25.0 %).

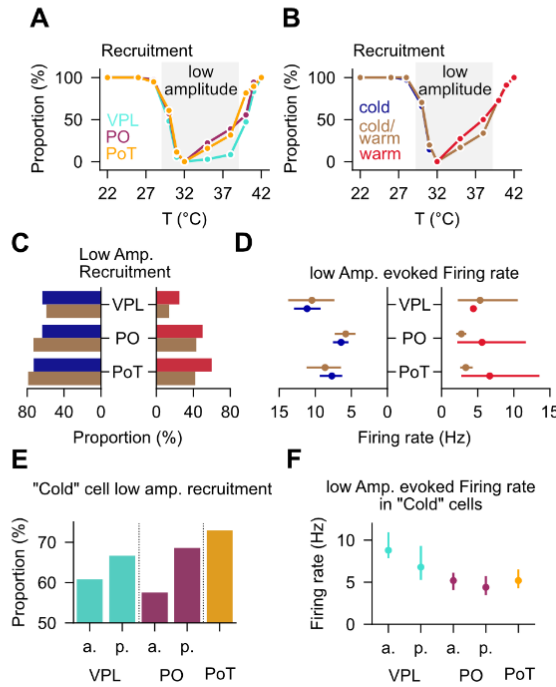


Figure 3.4.4-1 Sensitivity of thalamic nuclei and response-types to cooling and warming stimulation

- Recruitment profile of thalamic nuclei. Recruitment is defined as the proportion of cells that reached 20 % peak response amplitude.*
- Recruitment profile of response-types.*
- Fraction of low-amplitude recruited cells split by anatomical region and response-type.*
- Baseline-corrected firing rates of low amplitude recruited cells at respective recruitment temperatures. Dots display median, error bar show 95 % confidence interval.*
- Fraction of low-amplitude cooling recruited cells in thalamic subregions.*
- Baseline-corrected firing rate of thalamic subgroups at recruitment temperatures, Dots display median, error bar show 95 % confidence interval.*

To estimate the response strength of the low-amplitude recruited cells, Figure 3.4.4-1 D shows the baseline-corrected firing rates at stimulus recruitment temperatures, categorized by thalamic nuclei and response-type. The distribution of firing rates is shown as the median with the 95 % confidence interval. Cooling-evoked firing rates (left) were higher than warming-

evoked firing rates (right) in all three thalamic structures. Cooling-evoked firing rates of "Cold-Warm" (left, copper) cells were very similar to those of "Cold" (left, blue) cells in VPL ("Cold": 11.1 Hz, "Cold-Warm": 10.4 Hz), PO ("Cold": 6.4 Hz, "Cold-Warm": 5.78 Hz), and PoT ("Cold": 7.6 Hz, "Cold-Warm": 8.63 Hz). VPL "Cold" and "Cold-Warm" cells elicited the strongest firing rates compared to PO and PoT. Low-amplitude warming-evoked firing rates revealed that "Warm" (right, red) cells in PO and PoT exhibited stronger firing rates than "Cold-Warm" cells (right, copper), while in VPL, firing rates were comparable. Across structures, "Warm" (Figure 3.4.4-1 D, right, red) classified cells displayed similar firing rates with VPL 4.3 Hz, PO 5.6 Hz, and PoT 6.6 Hz as well as "Cold-Warm" with VPL 5.3 Hz, PO 2.7 Hz, and PoT 3.35 Hz.

To investigate the recruitment of the widespread "Cold" population in the low-amplitude range, the same spatial grouping described in chapter 3.2.3 was performed, and the fraction of low-amplitude cooling recruited cells is shown for each thalamic subregion (Figure 3.4.4-1 E). The aVPL (cyan, left) recruited 60.8 %, while the pVPL (cyan, right) recruited 66.6 %. This tendency of increased recruitment from the anterior to posterior position was also observed in PO/PoT. aPO (bordeaux, left) recruited 57.7 %, followed by pPO (bordeaux, right) with 68.5 % and PoT (gold) with 72.9 % in the low-amplitude range of cooling stimulation. Figure 3.4.4-1 F displays the baseline-corrected firing rate of these subgroups at 30 °C stimulation, showing that aVPL (Figure 3.4.4-1 F, cyan, left) elicited the strongest firing rates with 11.8 Hz compared to the rest of the thalamic population (pVPL: 10.2 Hz, aPO: 5.9 Hz, pPO: 6.75 Hz, PoT: 7.6 Hz). In summary, the results indicate that cooling stimulation recruited larger fractions of cells compared to warming, indicating increased sensitivity of the system to cooling. The cells that were recruited also showed stronger firing rates compared to those recruited by warming. The analysis and comparison of warming and cooling evoked sensitivities was conducted for distinct temperature steps. A low amplitude cooling range was defined as 32 °C to 30 °C and 32 °C to 38 °C for warming.

In PoT, the low-amplitude recruited cell fraction was slightly increased for the cooling response population, whereas evoked firing rates in the anterior part of VPL showed very strong responses. Warming stimulation evoked the strongest recruitment in PoT in the low-amplitude regime, as well as a slight tendency towards increased firing rates in these structures, making PoT the best-suited structure to transmit low-amplitude warming stimulus to downstream processing nodes (Discussion chapter 4.5.3).

3.5 Investigation of temporal response dynamics of thalamic nuclei

The following chapter will investigate and compare the temporal dynamics of cooling and warming-evoked sensory responses (3.5.1) and examine if the three thalamic nuclei VPL, PO, and PoT, follow a different temporal encoding profile for cooling and warming (3.5.2). In the next step, the population of responsive cells is investigated, and neurons with distinct temporal profiles are identified and mapped across the thalamic structures (3.5.3, 3.5.4). Finally, the temporal dynamics of tactile-evoked sensory responses are investigated and compared to cooling-evoked responses (3.5.5 and 3.5.6).

3.5.1 Cooling and warming elicit sensory responses with distinct temporal dynamics

Neural recordings conducted in the sensory afferents (Yarmolinsky et al. 2016a) and cortical regions (Vestergaard et al. 2023) have revealed that the application of cooling and warming stimuli elicits distinct sensory responses, particularly in terms of their temporal profiles. Cooling-induced sensory responses are characterized by precise timing, short latency, rapid rising times, and early peak response times. Furthermore, it was demonstrated that short-duration and long-duration sensory responses encode cooling stimuli. Conversely, warming-induced responses are mainly encoded with delayed response latencies, longer rising times and variable peak response times that indicate less temporal precision. The vast majority of recorded responses exhibited sustained responses (long-duration), whereas transient (short-duration) responses were rarely seen (Yarmolinsky et al. 2016a; Paricio-Montesinos et al. 2020; Vestergaard et al. 2023; A. D. Craig et al. 1994; Günter Schingnitz and Werner 1980a). In the next chapter, I will examine the sensory responses to cooling and warming in the distinct thalamic populations (VPL, PO, and PoT) to determine if similar temporal response characteristics hold true for the thalamus as they do in both the sensory periphery and cortex. The temporal dynamics of the neural response were investigated at the maximum cooling stimulus (-10 °C) and maximum warming stimulus (+10 °C) with the same experimental configuration as described in 3.3.2 (Figure 3.5.1-1 A).

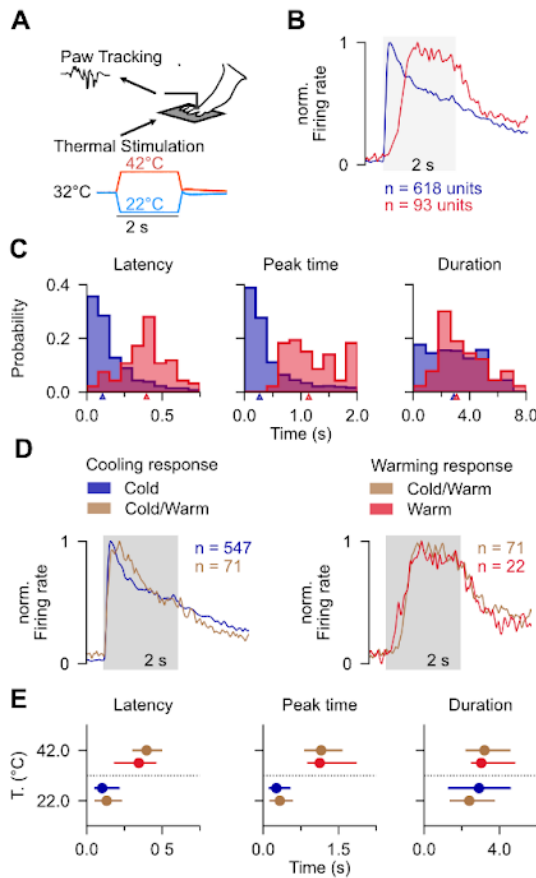


Figure 3.5.1-1 Characterization of cooling- and warming-evoked temporal dynamics

- A. Experimental paradigm. Thermal stimulation (+/- 10 °C) was applied to the right forepaw via a gold-plated Peltier element. Micro-movements were monitored by a force-feedback lever arm.
- B. Population PSTH of cooling-responsive (blue, $n = 618$) and warming-responsive (red, $n = 93$) thalamic cells to maximum cooling or warming stimulus, respectively. Grey bar displays stimulus-presentation window.
- C. Probability distributions for response latency (left), peak response time (middle) and response duration (right) of cooling (blue) and warming (red) responsive populations. Colored triangles display median of cooling and warming populations, respectively.
- D. Population PSTH for cooling (left) and warming (right) stimulation. The population was split by response-type and the cooling response was driven by “Cold” (blue, $n=547$) and “Cold-Warm” (copper, $n=71$) cells, warming response was driven by “Warm” (red, $n=22$) and “Cold-Warm” (copper, $n=71$) cells. Grey bar indicates stimulus presentation window.
- E. Distributions of response latencies (left), peak times (middle) and response durations (right) for cooling and warming evoked sensory responses split by response-type. “Cold” cells are shown in blue, “Cold-Warm” cells in copper, and “Warm” cells in red. Dots display median, error bar IQR.

The cooling and warming stimulus-evoked population PSTHs are presented in Figure 3.5.1-1 B. The cooling-responsive neuron population (blue, $n=618$) was utilized to construct a population response vector, where the averaged firing rate was normalized with the maximum average firing rate of that population. The cooling-responsive population consisted of two

response-types: "Cold" and "Cold-Warm" cells. The PSTH exhibited a short-latency response onset and rapid rising time, reaching the maximum response amplitude during the initial phase of the stimulus application (stimulus duration indicated by the grey bar). Subsequently, the PSTH decayed continuously until the baseline level was reached. The warming-responsive population response (red, n=93) contained "Warm" and "Cold-Warm" cells and had a different temporal profile compared to cooling. The warming population exhibited slower response onsets and peak times, which extended the initial period of the stimulus application. Additionally, the response was characterized by a weak decay during stimulus application and a strong decay at stimulus offset. To gain deeper insights into the temporal dynamics, the sensory responses of individual neurons were parameterized, enabling a comparative analysis of the onset latency, peak time, and duration of the sensory response for both cooling and warming stimuli. Figure 3.5.1-1 C displays the probability distributions of response latency (left), peak time (middle), and duration (right) for cooling-responsive neurons (blue) and warming-responsive neurons (red). The majority of cooling-responsive neurons (81.0 %; based on the area under the curve) exhibited latencies faster than 0.25 s, with almost the entire population (95.8 %) responding within the initial 0.5 s after stimulus onset. The median response latency for all cooling-responsive neurons is 0.104 s. In contrast, only a small fraction (13.9 %) of warming-responsive cells responded within the initial 0.25 s after stimulus onset, and the majority of the population exhibited onset latencies around 0.5 s upon warming stimulation. The median response latency for all warming-responsive neurons was 0.396 s. The probability distributions for the peak time of the response followed a similar trend. Most cooling-responsive neurons (83.0 %) reached their maximum response within 0.75 s after stimulus onset, with a median peak time of 0.286 s. Warming-responsive cells, however, reached their peak firing rate later compared to cooling-responsive cells, with peak times ranging from 0.75 s to 2 s (84.9 % of the population), corresponding to a median peak time of 1.14 s for the entire warming-responsive population.

The cooling-responsive population displayed a widespread distribution of response duration values, with 34.4 % of cells having shorter durations than 2 s and 65.6 % exhibiting long-duration (> 2 s) sensory responses. The median response duration for cooling-responsive cells was 2.88 s. On the other hand, the warming-responsive population indicated that only 18.3 % had response durations smaller than 2 s, while the majority of the population (81.7 %)

exhibited durations longer than 2 s. The median response duration for all warming-responsive cells was 3.08 s.

Next, I split the data into response-type groups in order to investigate if the distinct cooling- or warming-evoked temporal dynamics as well as the widespread distribution of cooling- evoked response durations were governed by "Cold", "Cold-warm" or "Warm" cells, respectively. A comparison was then made between the population PSTHs (Figure 3.5.1-1 D) and the response parameters (Figure 3.5.1-1 E) across these groups. The population PSTHs in response to a cooling stimulus (Figure 3.5.1-1 D, left) did not exhibit any apparent differences between the "Cold" (blue, n=547) and "Cold-Warm" (red, n=71) response-type groups. Both groups displayed a short-latency response onset, early peak time, and continuous decay after the maximum response amplitude was reached. Similarly, the warming response, driven by "Warm" (red, n=22) and "Cold-Warm" (copper, n=71) cells, showed no significant differences between the groups. It followed a similar temporal profile with a delayed response onset, a sustained-like period during stimulus application, and a rapid decay of the response after stimulus offset. Interestingly, the "Cold-Warm" response-type group exhibited a stimulus- specific temporal profile, suggesting that the response shape was not solely determined by the intrinsic properties of the cells but rather presented itself as a stimulus-specific feature.

Figure 3.5.1-1 E shows the response parameters for each response-type group at the maximum cooling or warming stimulus. The distributions of response parameters were represented as medians with interquartile ranges (IQR). The "Warm" response-type group displayed a response latency of 0.345 s (0.186 - 0.457 s), a peak time of 1.125 s (0.891 - 1.844 s), and a response duration of 3.032 s (2.536 - 4.781 s), which were comparable to the "Cold- Warm" response-type group with 0.397 s (0.309 - 0.494 s) for response latency, 1.154 s (0.837 - 1.559 s) for peak time, and 3.206 s (2.250 - 4.536 s) for response duration during warming stimulation. During cooling stimulation, the "Cold" response-type group exhibited, on average, similar response latency, peak time, and response duration to the "Cold-Warm" group, with values of 0.102 s (0.056 - 0.212 s) for response latency, 0.261 s (0.130 - 0.522 s) for peak time, and 2.914 s (1.32 - 4.551 s) for response duration, compared to 0.132 s (0.059 - 0.227 s), 0.33 s (0.145 - 0.568 s), and 2.397 s (1.404 - 3.701 s), respectively. Both "Cold" and "Cold-Warm" cells exhibited large IQRs and similar median values for response duration, indicating that the widespread distribution of the cooling-responsive population could not be explained by distinct temporal dynamics governed by the response-types. In addition, short-

duration and long-duration sensory responses were apparent in the “Cold” as well as “Cold-warm” groups due to large IQR values.

Additionally, the results indicated that sensory responses evoked by cooling and warming showed similar types of temporal coding as observed in the periphery and cortical regions. Response onsets and peaks were faster for the cooling stimuli than warming. In this case, both short- and long-duration responses encoded cooling; however, warming elicited long-duration sensory responses mainly. These results are in line with studies from the sensory periphery that have shown that cooling is transmitted through both fast and slow channels, while warming is transmitted solely through a slow conduction channel, emphasizing the functional role of the thalamus as a relay center of sensory information coming from the periphery (Darian-Smith, Johnson, and Dykes 1973; Darian-Smith et al. 1979; Duclaux and Kenshalo Dr 1980; Kenshalo and Duclaux 1977) (Discussion chapter 4.6.1).

3.5.2 Temporal response profiles vary across thalamic nuclei

In the preceding chapter, it was demonstrated that cooling and warming stimuli evoked distinct temporal profiles and, furthermore, that the distribution of response durations in the cooling-responsive thalamic population showed large variability. Both results could not be explained by the temporal tuning of “Cold”, “Cold-Warm” or “Warm” cells. The subsequent chapter aims to explore whether the variability in response duration and the distinct cooling and warming dynamics can be accounted for by the spatial location of responsive cells. To this end, the cooling and warming-responsive populations were divided based on their anatomical location, and their encoding profiles were investigated.

Figure 3.5.2-1 A displays the reconstructed anatomical boundaries of the three target structures: VPL (cyan), PO (bordeaux), and PoT (gold) in a sagittal plane. The colored dots represent the positions of three exemplary single units depicted in Figure 3.5.2-1 B, with the color-coding corresponding to their anatomical classification. Figure 3.5.2-1 B showcases the PSTHs of these three example cells in response to a temperature stimulus of 22 °C, starting from a baseline temperature of 32 °C (the grey bar indicates the duration of the stimulus). All three example cells exhibited short-latency response onsets and a rapid rise to the maximum firing rate. Cell 1 (VPL) displayed a response duration that extended beyond the stimulus

duration and followed a sustained-like profile. Cell 2 (PO) demonstrated a gradual decay of the response amplitude after reaching the initial peak, nearly returning to the baseline firing rate by the end of the stimulus presentation window. Cell 3 (PoT) exhibited a very brief response duration (<0.5s) and showed characteristics reminiscent of a transient-like response profile.

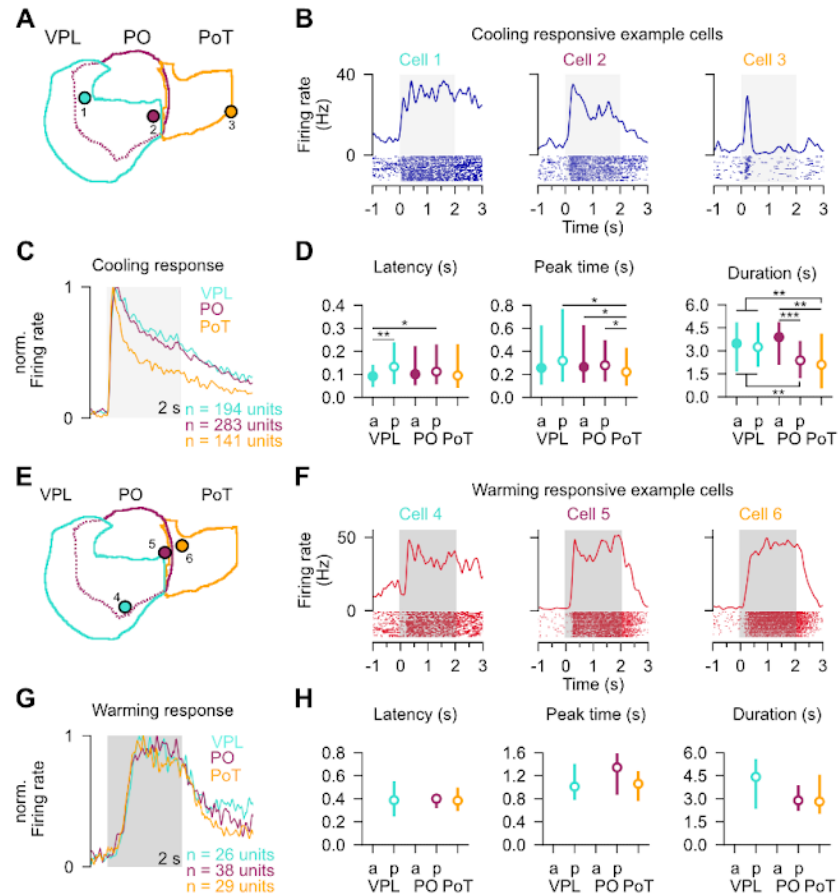


Figure 3.5.2-1 Characterization of sensory response dynamics across thalamic regions

- Schematic of VPL (cyan), PO (bordeaux) and PoT (gold) in a sagittal plane. Dots display position of cooling-responsive example units shown in **B**. Color-code corresponds to anatomical position.
- PSTH and raster plot of 3 cooling responsive units from distinct thalamic locations are shown in **A**. Grey bar indicates stimulus presentation window.
- Normalized population PSTH of cooling-responsive units grouped by their anatomical location. Cyan ($n = 194$) shows average VPL response, bordeaux ($n=283$) displays PO response, and gold ($n = 141$) presents PoT response. Grey bar indicates the stimulus presentation window.
- Distribution of cooling response latency (left), peak time (middle) and response duration (right) for thalamic subregions. Dots represent median, error bar IQR. Statistical significance is shown by stars (* $p < 0.05$, ** $p < 0.01$, *** $p < 0.001$, pairwise comparison with Mann Whitney U test).
- Same as **A**, for warming-responsive cells shown in **F**.
- Same as **F** for 3 warming-responsive cells from distinct thalamic locations shown in **E**.

G. Same as G, for VPL (cyan, n = 26), PO (bordeaux, n = 38) and PoT (n = 29).

H. Same as D, for warming evoked response parameters.

The reduction of the sensory response duration along the anterior-posterior axis observed in the example units can be generalized to the population level. Figure 3.5.2-1 C presents the normalized population PSTHs from VPL (cyan; n=194), PO (bordeaux; n=283) and PoT (gold; n=141). The population responses within each structure were characterized by short-latency response onsets and a rapid rise within the initial 0.5 s of stimulus application, exhibiting minimal variability across structures. However, the decay of the sensory population responses displayed nucleus-specific temporal characteristics. While the responses in VPL and PO decayed with similar time constants, the response in PoT decayed much more rapidly, resulting in shorter response durations across the population of responsive neurons.

Figure 3.5.2-1 D provides a more detailed examination of the temporal response parameters (latency, peak time, and duration) segregated by anatomical subregions. Among the five groups, aVPL exhibited the shortest response latency on average, with a value of 0.092 s (0.050 - 0.135 s), indicating a significantly faster onset latency compared to pVPL (0.133 s; 0.064 - 0.232 s) and pPO (0.112 s; 0.063 - 0.224 s). PoT (0.095 s; 0.049 - 0.225 s) and aPO (0.101 s; 0.059 - 0.211 s) demonstrated intermediate onset latencies relative to all five subregion groups. When comparing the distributions of peak times, PoT (0.221 s; 0.112 - 0.419 s) exhibited the fastest peak times, followed by aVPL (0.256 s; 0.123 - 0.613 s). pVPL (0.318 s; 0.148 - 0.756 s), aPO (0.265 s; 0.141 - 0.617 s), and pPO (0.279 s; 0.150 - 0.486 s) had significantly longer peak times compared to PoT. Regarding response duration, more variability was observed across subregions. The most posterior regions, PoT (2.096 s; 0.640 - 4.024 s), and pPO (2.368 s; 1.311 - 3.546 s) exhibited significantly shorter response durations than aVPL (3.475 s; 1.725 - 4.763 s), pVPL (3.245 s; 2.049 - 4.761 s), and aPO (3.890 s; 2.169 - 4.790 s).

Collectively, this analysis has elucidated distinct temporal dynamics exhibited by the posterior thalamic nucleus (PoT) relative to the other four subregions. Specifically, PoT demonstrated sensory responses characterized by shorter latencies, earlier peak times, and shorter response durations. Additionally, anterior subregions (aVPL and aPO) exhibited shorter latencies and peak times compared to their posterior counterparts (pVPL and pPO). Notably, the

considerable variability in response durations across the entire population of cooling-responsive neurons could be attributed to nucleus-specific temporal tuning.

Figure 3.5.2-1 E presents the sagittal reconstruction of VPL (cyan), PO (bordeaux), and PoT (gold), along with the estimated positions of three warming-responsive example cells depicted in Figure 3.5.2-1 F. The color-coded dots indicate their respective anatomical classifications. The PSTHs of these cells in Figure 3.5.2-1 F illustrate their responses to a 42 °C temperature stimulus initiated from a baseline temperature of 32 °C (gray bar indicates stimulus duration). All three cells exhibited a delayed response latency (~200 ms), followed by a robust and steep increase in firing rate until reaching the peak firing rate. Moreover, all cells exhibited sustained-like response profiles, with Cell 4 (VPL) persisting beyond the stimulus offset. Cells 5 (PO) and 6 (PoT) displayed temporal profiles tied to the stimulus application, with a rapid decay of the response upon stimulus offset, returning to their baseline firing rate within 3 s of stimulus onset.

On a population level, the sensory responses of VPL (n=26), PO (n=38), and PoT (n=29) neurons exhibited highly similar temporal profiles resembling the responses of Cells 5 and 6. These profiles entailed a delayed response onset, sustained firing throughout the stimulus application, and a fast decay of the response after stimulus offset (Figure 3.5.2-1 G). Comparisons of the distributions of response latency, peak time, and response duration confirmed the homogeneity across the nuclei, with no significant differences observed in any of the three response parameters.

In summary, the investigation of response dynamics in cooling- and warming-responsive neurons revealed distinct encoding patterns for both stimuli that are independent of the anatomical location. All thalamic regions investigated here displayed faster onsets and peak-times for cooling stimulation compared to warming stimulation. Cooling stimuli elicited temporally sharp responses predominantly in the posterior subregions (pPO and PoT), while a sustained-like response profile characterized aPO as well as the entire VPL nucleus, as indicated by long response durations. This suggests that peripheral cooling channels with distinct temporal dynamics show a region-specific input to thalamic nuclei (Discussion chapters 4.6.1, 4.6.2).

Furthermore, warming-responsive neurons across all thalamic structures exhibited a uniform temporal response profile, displaying only subtle variations among the thalamic regions.

3.5.3 Three temporal profiles govern the sensory response to cooling and warming

In order to explain the reduction in the sensory response duration of the cooling response and the homogeneity of the warming response across thalamic nuclei, the input received by each thalamic nucleus from the periphery must be considered. Previous studies (Yarmolinsky et al. 2016a) have demonstrated that cooling of the tongue evokes three distinct temporal response profiles in the orofacial nerves of rodents. These profiles are as follows: (1) a transient-like profile characterized by short-latency and short-duration neural firing ("Transient"), (2) a sustained-like profile with either short or long latency and long-duration firing of the nerve ("Sustained"), and (3) a temporal profile that exhibits characteristics of both aforementioned profiles ("Mixed"). The 'Mixed response' is defined by transient-like firing at the start of sensory stimulation and sustained neural firing after the decline of this initial period that often outlasts the sensory stimulation. Conversely, warming responses are solely encoded by sustained-like responses in the orofacial nerve, exhibiting delayed onset latency and long-duration neural firing (Figure 3.5.3-1 A).

To quantify the temporal response profiles, two metrics have been developed: the "Sharpness Index" and the "Duration Index". A "Sharpness Index" was defined as the ratio of the peak firing rate that occurred in response to sensory stimulation within the first 500 ms and the average firing rate over a 0.5s time window starting at the point defined by the peak time multiplied by a factor of 2. A "Transient" or "Mixed" profile showed "Sharpness Indices" near 1. The exception was neurons showing no pronounced transient-like response in their initial phase and was labeled as "Sustained", which received "Sharpness Indices" close to 0. The "Duration Index" scaled the duration of a sensory response between -1 and 1 by calculating the ratio of the peak firing rates within the first and final second of sensory stimulation. "Transient" neurons received values close to 1, whereas "Sustained" and "Mixed" neurons received values around 0.

In the subsequent analysis, both metrics were applied to the cooling- and warming-responsive thalamic populations to identify neurons that exhibited temporal profiles similar to those observed in the periphery (Figure 3.5.3-1 B, left). Plotting the "Sharpness Index" against the "Duration Index" for all cooling-responsive (blue) and warming-responsive (red) neurons

revealed the following observations: (1) a subset of points fell within the maximum "Duration Index" range ($D.I = 1$) with positive "Sharpness Index" values (brown shaded region), (2) a subset of points occupied the region with maximum "Sharpness Index" ($S.I = 1$) and "Duration Index" values between -1 and 1 (salmon shaded region), (3) the majority of cooling-responsive neurons populated the region with intermediate "Sharpness Index" and "Duration Index" values (purple shaded region), and (4) the warming-responsive neurons exhibited a less dispersed point cloud with values around 0 for both the "Sharpness Index" and "Duration Index" (purple shaded region).

The distributions of both the "Duration Index" and "Sharpness Index" displayed a bimodal shape, with a significant fraction of cells exhibiting maximum values for both metrics (Figure 3.5.3-1 B, right). In order to separate the neurons with either maximum "Sharpness Index" or "Duration Index" values, two boundaries at 0.85 have been defined (left: salmon and brown rectangle, right: dotted line). Cooling-responsive neurons falling within the defined boundaries were classified as either "Transient" ($D.I > 0.85$, $n = 87$) or "Mixed" ($S.I > 0.85$, $D.I < 0.85$, $n = 58$). The remaining cooling-responsive cells were classified as the "Sustained" group ($n = 473$). Almost all warming-responsive cells belonged to the "Sustained" group ($n = 92$), with only 1 cell falling into the "Mixed" category.

Figure 3.5.3-1 C illustrates the population responses to cooling (left) and warming (right) stimuli of neurons grouped based on the temporal classification. The "Transient" group exhibited a temporal profile with a short latency and steep increase in the initial phase of stimulus application. After reaching its peak value, the response quickly decayed and returned to the baseline level within the stimulus duration (brown, $n = 87$). The "Mixed" population displayed an initial transient-like profile that transitioned into a sustained-like profile during the latter part of sensory stimulation (salmon, $n = 58$). The temporal profile of the "Sustained" group was characterized by a short-latency response onset and a slow decay of the response after reaching its peak value (purple, $n = 473$). The population response of warming-responsive neurons resembled the stereotypical warming response, exhibiting a delayed onset, sustained activity throughout stimulus presentation, and rapid decay after stimulus offset (Figure 3.5.3-1 C, right). Figure 3.5.3-1 D and E present the response latency and response duration for the defined temporal groups (dots represent individual neurons, black dot represents the median, and error bars represent the IQR). Most neurons assigned to the "Transient" group had response latencies between 30 and 100 ms (0.051 s (0.043 - 0.090 s)),

with only a small subset of cells showing response latencies longer than 100 ms. The "Mixed" group exhibited slightly slower latencies (0.073 s (0.045 - 0.105 s)) with a larger spread of data points. The "Sustained" group, on the other hand, displayed a wide range of response latencies, with neurons exhibiting both fast and slow responses (0.124 s (0.069 - 0.247 s)). In the warming-responsive "Sustained" group, most neurons exhibited long response latencies (0.396 s (0.304 - 0.479 s)). The response duration (Figure 3.5.3-1 E) of the defined groups revealed that neurons classified as "Transient" had the shortest average sensory response duration (0.384 s (0.223 - 0.811 s)). The "Mixed" group had its median response duration at 2.806 s (0.565 – 4.556 s) which was shorter compared to the "Sustained" type (3.259 s (2.058 - 4.632 s)) after cooling stimulation. The response duration of the "Sustained" group during warming stimulation (3.080 s (2.276 - 4.608 s)) showed an equivalent duration to the "Sustained" cooling group. Ultimately, these two types of response parameters enabled me to classify the corresponding temporal profiles into separate classes. Since this analysis aimed to explain the temporal sharpening of the sensory response to cooling from anterior to posterior regions within the thalamus and to confirm that the response-type is not a defining factor for the temporal profile of the sensory response, the next step was to divide the responsive population by response-types (Figure 3.5.3-1 F) as well as anatomical location (Figure 3.5.3-1 G) and to investigate the proportions of cells in those groups. Splitting the data into response-type groups for cooling stimulation revealed that the majority of "Cold" (74.7 %) and "Cold-Warm" (90.1 %) cells were classified as "Sustained." Only 14.9 % of "Cold" and 7.0 % of "Cold-Warm" cells were labeled as "Transient," and the smallest fraction of "Cold-Warm" cells were labeled as "Mixed" with 2.9 %, similar to the "Cold" cells, which comprise 10.4 %. On the other hand, warming stimulation showed that almost all cells classified as "Cold-Warm" and "Warm" belonged to the "Sustained" group, with only 1 cell classified as "Mixed" and a complete absence of "Transient" cells among the response-types.

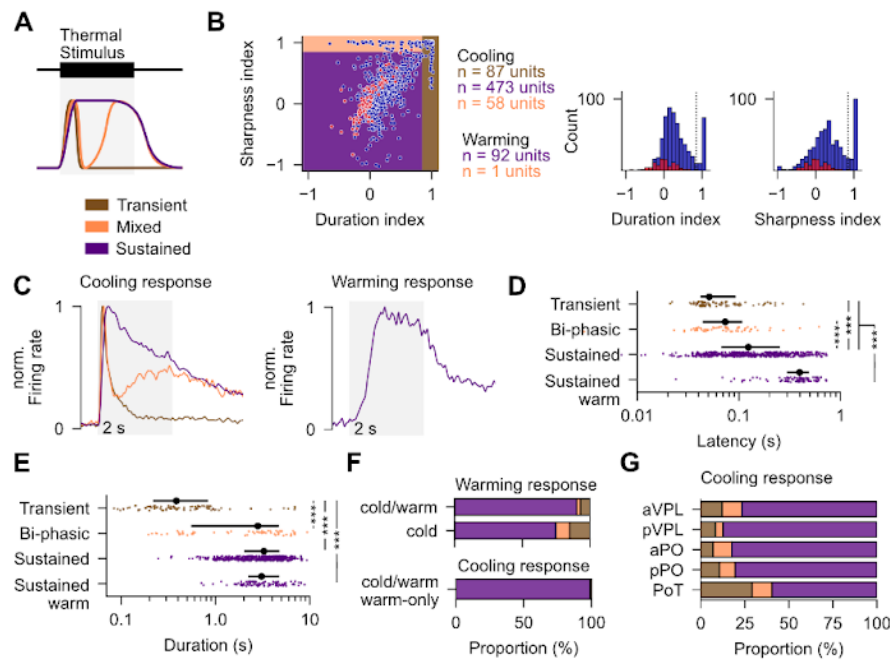


Figure 3.5.3-1 Characterization and spatial distribution of temporal response profiles across thalamus

- Schematic of thermally evoked response profiles in sensory afferents: "Transient" (brown), "Mixed" (salmon) and "Sustained" (purple).
- Left, two-dimensional feature space defined by "Sharpness Index" and "Duration Index". The points represent the values of cooling-responsive (blue) and warming-responsive (red) neurons. Colored regions show boundary line (0.85) for "Transient", "Mixed" and "Sustained" neurons. Right, unidimensional histograms of Sharpness Indices (right) and Duration Indices (left) for cooling (blue) and warming responsive cells. Boundary line is represented by dashed line.
- Normalized population PSTH for "Transient", "Mixed" and "Sustained" neurons evoked by cooling (left) and warming (right) stimulation. Same color-code as A. Grey bar indicates stimulus presentation window.
- Distribution of cooling-evoked response latency for "Transient", "Mixed" and "Sustained" groups as well as warming-evoked "Sustained warm" groups. Colored dots display latencies of individual neurons. Black dots show median, error bar IQR. Stars indicate statistical significance, evaluated with Mann Whitney U test for pairwise comparisons (* $p<0.05$, ** $p<0.01$, *** $p<0.001$).
- Same as D for response duration.
- Proportion of "Transient", "Mixed" and "Sustained" neurons in "Cold-Warm", "Cold" response-type groups as well as warming-responsive population ("Cold-Warm" + "Warm").
- Proportion of "Transient", "Mixed" and "Sustained" neurons in thalamic subregions.

Figure 3.5.3-1 F illustrates the uneven distribution of temporal dynamic types across thalamic subregions. The proportion of "Transient" cells increased from aVPL (12.1 %) to pVPL (8.4 %), and from aPO (7.0 %) to pPO (10.6 %). Notably, PoT stood out with a significantly higher proportion of "Transient" cells, accounting for 29.0 % of cooling-responsive cells in PoT. The distribution of "Mixed" cells was relatively similar across subregions, with a slight overrepresentation in aVPL (11.1 %) compared to the other subregions: pVPL (4.2 %), aPO

(10.5 %), pPO (2.3 %), and PoT (11.3 %). The "Sustained" group predominated in all five thalamic subregions: aVPL (76.8 %), pVPL (87.4 %), aPO (82.5 %), pPO (87.1 %), and PoT (59.7 %).

The substantial proportion of "Transient" cells in PoT could account for the observed sharper sensory response to cooling depicted in Figure 3.3.2-1. This finding pointed out to the existence of separate input channels dedicated to the investigated thalamic structures. Since aVPL, pVPL, aPO, and pPO mainly consisted of "Sustained" cells, these structures might only receive a singular input from the periphery; in contrast, PoT would receive two different input streams with transient and sustained characteristics. These input channels have been extensively documented in the literature (Darian-Smith, Johnson, and Dykes 1973; Darian-Smith et al. 1979; Yarmolinsky et al. 2016a; Ran, Hoon, and Chen 2016a), aligning with studies investigating spinothalamic projections to the thalamus, which identified PoT as the primary recipient (Zhang, Davidson, and Giesler 2006) (Discussion chapter 4.6.2).

3.5.4 The sharpening of the sensory response from anterior to posterior thalamic regions

The classification of temporal response-types depicted in Figure 3.5.3-1 focused solely on cells exhibiting the maximum "Duration-Index" or "Sharpness-Index," resulting in an unequal distribution of cell subsets, with the majority assigned to the "Sustained" group. The following analysis will focus on this group and investigated if neurons within that subset showed homogenous dynamics or presented themselves as distinct subsets within a coarsely defined functional group.

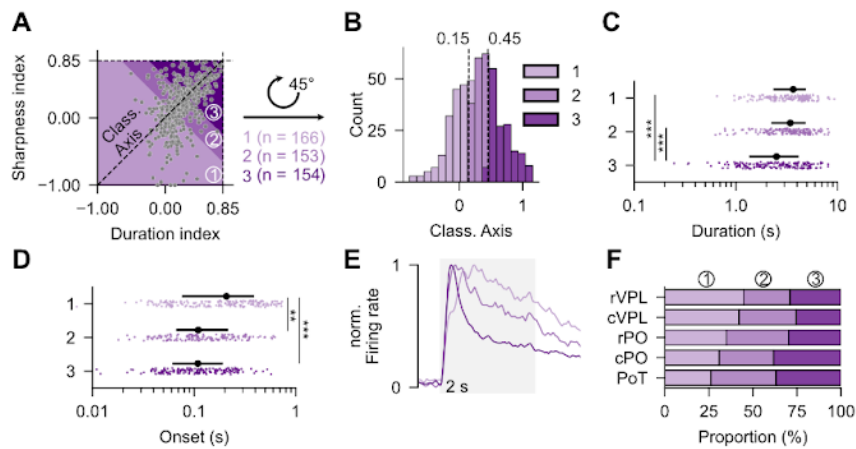


Figure 3.5.4-1 Non-homogenous temporal dynamics in "Sustained" group

- A. Two-dimensional feature space defined by Sharpness Index and Duration Index. Points display values of individual "Sustained" neurons. Colored regions indicate boundaries for grouping into classes 1,2 and 3. Black dotted diagonal indicated classification axis ("Class. Axis").
- B. Histogram of "Class. Axis" values. Position of each neuron in A. was rotated by 45° and projected onto the Class. Axis. Color-code same as A.
- C. Distribution of "Sustained" neuron groups 1- 3. Colored dots display durations of individual neurons. Black dots show median, error bar IQR. Stars indicate statistical significance, evaluated with Mann Whitney U test for pairwise comparisons (* $p<0.05$, ** $p<0.01$, *** $p<0.001$).
- D. Same as C for response latency.
- E. Normalized population PSTH for groups 1- 3 classified neurons evoked by thermal stimulation. Same color code as A. Grey bar indicates stimulus presentation window.
- F. Proportion of grouped neurons in thalamic subregions. Same color code as A.

Figure 3.5.4-1 A illustrates the positioning of individual "Sustained" neurons in the two-dimensional feature space defined by the "Sharpness-Index" and the "Duration-Index" from Figure 3.3.3. The data points are aligned along a diagonal line (dotted line in Figure 3.5.4-1 A, "Class. Axis"), which was used for subsequent population grouping. Each data point was rotated by 45° in a clockwise direction and projected onto the resulting x-axis (Figure 3.5.4-1 B, A, 'Class. Axis'). The distribution observed in Figure 3.5.4-1 B was divided into three groups of comparable sample sizes (1: n = 166, 2: n = 153, 3: n = 154) using arbitrary boundaries set to 0.15 and 0.45, respectively.

Next, the response duration (Figure 3.5.4-1 C) as well as the response latencies (Figure 3.5.4-1 D) were compared across groups. The response duration (Figure 3.5.4-1 C) exhibited a decreasing trend from group 1 (3.66 s (2.407 - 4.756 s)) to group 2 (3.426 s (2.294 - 4.734 s)), with the shortest duration observed in group 3 (2.510 s (1.384 - 4.049 s)). A similar tendency was observed for the response latencies, with group 1 displaying the longest latencies at 0.208

s (0.077 - 0.380 s). Group 2 (0.110 s (0.068 - 0.211 s)) showed slightly longer latencies than group 3, which exhibited latencies of 0.109 s (0.063 - 0.186 s). Population response vectors plotted for each group confirmed these results (Figure 3.5.4-1 D), showing that group 1 exhibited the longest response duration, while duration decreased in group 2 and was shortest in group 3.

Analyzing the distribution of each "Sustained" subgroup across thalamic nuclei revealed the following: Firstly, cells grouped into group 1 - characterized by long-latency and long-duration sensory responses on average - were primarily located in aVPL (44.7 %), with proportions steadily decreasing along the anterior-posterior axis and reaching a minimum in PoT (26.2 %). Secondly, group 3 cells - characterized by short-latency and short-duration sensory responses were predominantly found in pPO (38.2 %) and PoT (36.9 %), with the smallest proportions in aVPL (28.9 %) and pVPL (25.3 %). Thirdly, the fraction of group 2 cells was evenly distributed across thalamic subregions. Overall, this analysis demonstrated that the large "Sustained" group exhibited variability in its temporal response parameters.

Moreover, it could be shown that increased values for the Duration Index and Sharpness Index corresponded to fast and short responses but smaller values indicated long and delayed responses. Though, one should note that the data did not show separate functional groups but spaned a continuum. An increased percentage of neurons belonging to group 1 was observed in VPL (aVPL and pVPL), whereas the highest percentage of group 3 neuron cells was seen in posterior regions (POp and PoT). These results have shown that even the coarsely defined "Sustained" group demonstrates a region-specific temporal tuning: posterior regions demonstrate sharper responses as opposed to anterior regions, where responses are more sustained.

3.5.5 Temporal dynamics of tactile evoked sensory response vary across thalamus

The spatial representation of touch and cooling stimuli in the thalamus exhibits widespread activation and significant overlap, as depicted in Figure 3.3.6-1. The temporal profiles of cooling-evoked sensory responses displayed non-homogeneous dynamics across thalamic

structures due to the distribution of different temporal response-profiles within thalamic nuclei. To determine whether this finding is specific to temperature or an anatomical characteristic of thalamic structures, the temporal dynamics of tactile-evoked responses are investigated in the following chapter.

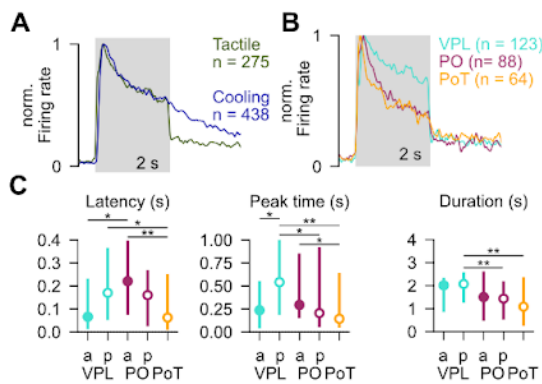


Figure 3.5.5-1 Characterization of tactile-evoked response dynamics across thalamic regions

- A. Normalized population PSTHs of cooling-responsive (blue, $n = 438$) as well as tactile-responsive (green, $n = 275$) populations. Grey bar indicates stimulus presentation window.
- B. Normalized population PSTH of tactile responsive units grouped by their anatomical locations. Cyan ($n = 123$) shows average VPL response, bordeaux ($n=88$) displays PO response, and gold ($n = 64$) presents PoT response. Grey bar indicates stimulus presentation window.
- C. Distribution of tactile response latency (left), peak time (middle) and response duration (right) for thalamic subregions. Dots represent median, error bar IQR. Statistical significance is shown by stars (* $p < 0.05$, ** $p < 0.01$, *** $p < 0.001$, pairwise comparison with Mann Whitney U test).

Figure 3.5.5-1 A presents the population responses of the entire thalamic population ($n=438$) to cooling and tactile stimulation (grey rectangle indicating stimulus duration).

For each of these modalities, the initial phase of the response had a short-latency onset and rapid build-up to peak response. However, at the end of the stimulus, response to tactile stimulation rapidly diminished while cooling responses persisted for a few seconds after the stimulus ended. Subsequently, the tactile-responsive population was divided based on anatomical regions, and the population responses of VPL (cyan, $n=123$), PO (bordeaux, $n=88$), and PoT (gold, $n=64$) are shown for tactile stimulation in Figure 3.5.5-1 B. All structures showed similar fast-rising times to peak response in the initial phase of the sensory response. However, the decay phase showed a clear difference between VPL, PO, and PoT. VPL had a

slow decay giving it more of a sustained-like character than PO and PoT decays, which were more rapid. Interestingly, all three thalamic structures displayed a sudden and complete decay of the response at stimulus offset. To provide a detailed description of the sensory response dynamics within these structures, the distributions of response parameters (latency, peak time, and response duration) were compared across thalamic subregions in Figure 3.5.5-1 C. Comparing response latency distributions across thalamic subregions (Figure 3.5.5-1 C, left) revealed that the fastest response latencies were observed in aVPL and PoT, with 0.066 s (0.018 - 0.225 s) and 0.062 s (0.015 - 0.245 s), respectively. Both subregions exhibited significantly different distributions compared to aPO (0.220 s (0.081 - 0.391 s)), which had the slowest average response latency distribution. Interestingly, both posterior regions in VPL as well as PO showed intermediate response latency distributions (pVPL: 0.170 s (0.058 - 0.360 s), pPO: 0.160 s (0.031 - 0.263 s)). These findings contrasted with those for cooling stimulation, where tactile-evoked responses were fastest in the most anterior and posterior thalamic nuclei. Cooling activation showed a more homogeneous spread across thalamic subregions and a trend towards short response onsets in pVPL. Generally, average response latencies after tactile stimulation were faster compared to cooling stimulation.

Analyzing peak time distributions across thalamic subregions revealed that PoT (0.143 s (0.063 - 0.6255 s)) and pPO (0.205 s (0.068 - 0.906 s)) exhibited the shortest average peak times, followed by aVPL (0.236 s (0.055 - 0.5385 s)). However, no statistical differences were observed between these peak time distributions. On the other hand, aPO (0.294 s (0.165 - 0.836 s)) displayed slower average peak times, significantly different from the fastest subregion PoT. The subregion that stood out in this comparison is pVPL (0.541 s (0.201 - 1.009 s)), as it exhibited, on average, the slowest peak times and a significantly different peak time distribution compared to the three leading subregions (PoT, pPO, and aVPL).

Examining the response duration distributions revealed that PoT (1.085 s (0.314 - 2.303 s)) exhibited, on average, the shortest response durations, followed by pPO (1.434 s (0.584 - 2.124 s)) and aPO (1.502 s (0.525 - 2.553 s)). Both aVPL (2.012 s (0.917 - 2.278 s)) and pVPL (2.071 s (1.314 - 2.513 s)) displayed, on average, longer response durations compared to the other subregions, confirming the population response observed in Figure 3.5.5-1 B.

Comparing the response parameters across thalamic subregions for tactile and cooling stimulation revealed the following: First, both aVPL and PoT were the subregions that

exhibited the earliest activation, as indicated by the faster response latency distributions relative to pVPL, aPO, and pPO.

Second, PoT showed the shortest response peak times, while pVPL is characterized by the longest peak times regardless of sensory modality. Third, PoT exhibited more transient cooling and tactile-evoked responses on average, compared to other thalamic sub-regions, specifically aVPL and pVPL, which showed increased response duration.

3.5.6 Tactile response is governed by three temporal response-profiles

In the following chapter, the tactile responsive population is investigated in greater detail with a focus on the spatial distribution of temporal dynamic types in order to explain the subregion-specific differences in the temporal response parameters we have seen across the thalamic nuclei.

For each tactile-evoked response, the "Sharpness Index" and "Duration Index" were calculated and plotted against each other (Figure 3.5.6 1 A). The data points in the two-dimensional feature space occupied distinct regions corresponding to their temporal response profiles. Similar to the cooling-evoked responses, a subset of tactile responses exhibited a "Duration Index" close to 1, forming a cluster indicated by the brown rectangle. These cells were classified as the "Transient" group ($n=81$). Another subset of cells had a "Sharpness Index" close to 1 and were classified as the "Mixed" group ($n=39$). The remaining data points with intermediate values of "Duration Index" and "Sharpness Index" were assigned to the "Sustained" group ($n=155$). The boundaries defining the individual temporal types were set at 0.85, similar to those used in the thermal investigation. The distribution of the "Sharpness Index" and "Duration Index" displayed a bimodal shape, and the defined boundaries allowed for the separation of the respective parts of each distribution (Figure 3.5.6 1 A, right).

Plotting the response latency for the three temporal response-profile groups (Figure 3.5.6 1 B) revealed that the "Transient" group exhibited the fastest response on average, with a latency of 0.028 s (0.005 - 0.068 s), followed by the "Mixed" group with a latency of 0.071 s (0.01 - 0.253 s), and the "Sustained" group with a latency of 0.204 s (0.032 - 0.351 s). However, all groups had cells with very short latencies (2-10 ms), resulting in tactile-evoked responses

that, on average, were faster than the cooling-evoked responses across the thalamic structures. The response duration (Figure 3.5.6 1 C) showed that the majority of the "Transient" group responded within 2 s after stimulus onset, with an average duration of 0.498 s (0.280 - 0.797 s). The "Mixed" and "Sustained" groups responded with significantly longer durations, averaging around 1.646 s (0.593 - 2.182 s) and 2.126 s (1.973 - 2.568 s), respectively. Figure 3.5.6 1 D displays the PSTHs of the temporal response profiles evoked by tactile stimulation. The "Transient" group (brown, n=81) exhibited a short-latency response in the initial phase of stimulus presentation, followed by a rapid decay of the response. At stimulus offset, the population response had almost returned to its baseline activity. The "Mixed" group (salmon, n=39) also showed a short-latency response in the initial phase of stimulus application, with a slightly delayed peak response compared to the "Transient" group. The response in the "Mixed" group had a sustained component after reaching the initial peak, and it did not display the secondary peak observed for thermal encoding. The "Sustained" group (purple, n=155) showed a short-latency response without an initial transient response. The response remained close to its maximum throughout the sensory stimulation and exhibited a rapid decay at stimulus offset.

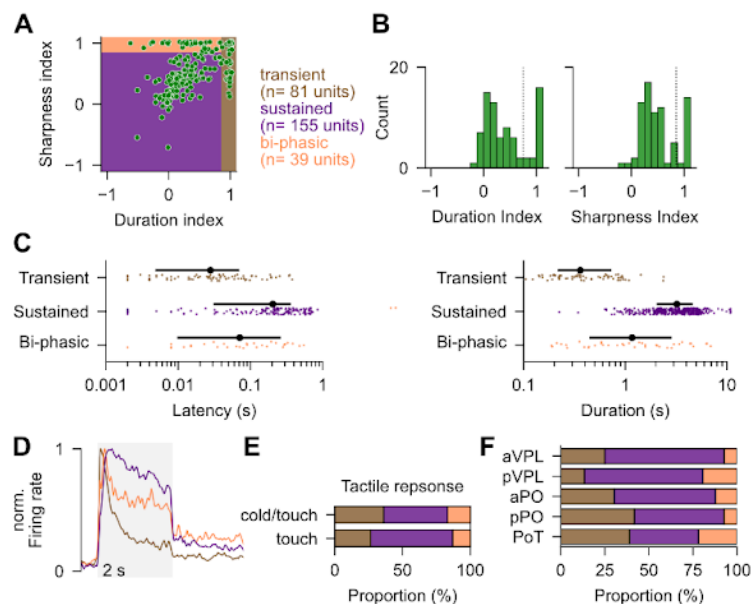


Figure 3.5.6 1 Characterization and spatial distribution of temporal dynamics type across thalamus

- A. Left, two-dimensional feature space defined by Sharpness Index and Duration Index. Points display values of individual tactile responsive (green) neurons. Colored regions indicate boundaries (0.85) for the classification of "Transient", "Mixed" and "Sustained" neurons. Right, one dimensional histograms of Duration Indices (left) and Sharpness Indices (right) for tactile (green) responsive neurons. Dotted line represents boundaries used for classification in two-dimensional feature space.

- B. Distribution of tactile evoked response latency for "Transient", "Mixed" and "Sustained" groups. Colored dots display latencies of individual neurons. Black dots show median, error bar IQR. Stars indicate statistical significance, evaluated with Mann Whitney U test for pairwise comparisons (* p<0.05, ** p<0.01, *** p< 0.001).
- C. Same as B for response duration.
- D. Normalized Population PSTH for "Transient", "Mixed" and "Sustained" neurons evoked by tactile stimulation. Same color-code as A. Grey bar indicates stimulus presentation window.
- E. Proportion of "Transient", "Mixed" and "Sustained" neurons in "Cold/Touch" and "Touch" response-type groups.
- F. Proportion of "Transient", "Mixed" and "Sustained" neurons split by thalamic subregions.

Across the three thalamic nuclei, the proportions of temporal response profiles were comparable for the two distinct response-types: "Cold-touch" neurons had 35.9 % "Transient", 16.8 % "Mixed", and 47.3 % "Sustained" neurons (Figure 3.5.6 1 E). The population of "Touch" neurons consisted of 26.3 % "Transient", 12.9 % "Mixed", and 60.8 % "Sustained" neurons. Interestingly, similar to thermal stimulation, the response-type was not an indicative factor for the distribution of the temporal profile. In the next step, the proportion of temporal types is displayed for each thalamic subregion (Figure 3.5.6 1 F). Similar to thermal stimulation, VPL (both aVPL and pVPL) exhibited the highest fraction of "Sustained" cells, which were characterized by longer response durations (aVPL: 67.8 %, pVPL: 67.1 %). The proportion of "Transient" cells was highest in pPO (41.8 %) and PoT (39.0 %), explaining the temporal differences observed in Figure 3.3.5. Interestingly, the spatial distribution of temporal types followed the same trend regardless of the stimulus (thermal or tactile), suggesting that the difference in temporal dynamics is more likely an anatomical rather than a stimulus-specific feature.

4. Discussion

4.1 Anatomical tracing of thermal circuits

The tracing experiments (see Chapters 3.1.2, 3.1.3) were primarily designed to anatomically delineate and compare the two thalamocortical circuits for cooling-related sensory transmission and in order to anatomically identify the thalamic nuclei. This was achieved through injections into the forepaw cooling representation of S1 and the pIC, both functionally defined by widefield imaging during thermal stimulation. Nonetheless, prior studies have suggested that pIC encodes not only cooling but also warming stimuli. Additionally, it was observed that the cooling representation within the pIC is situated in close spatial proximity to the representations of tactile and auditory sensory modalities (Sawatari et al. 2011; Vestergaard et al. 2023). The employment of relatively large-volume injections of CTB and AAV raises the possibility that not only cooling-related neurons but also tactile, warming, and auditory-responsive neurons could have been labeled by these injections. Similarly, analogous outcomes could arise from injections into the S1, where prior research demonstrated an overlap between tactile and cooling representations (Milenkovic et al. 2014).

It is important to acknowledge that the findings presented in this study do not exclusively pertain to cooling-specific neural circuits. Instead, they afford comprehensive insights into the broader connectivity patterns within thalamocortical circuits. These circuits play a pivotal role in transmitting temperature-related information between nodes of the thermal processing chain. Consequently, the outcomes contribute significantly to our understanding of the intricate anatomical framework that underpins thalamocortical communication in relaying temperature-associated sensory data.

4.1.1 Thalamocortical projections to S1 and pIC

The data presented in chapter 3.1.2 has shown that the two cortical representations of temperature in S1 and pIC show region-specific connectivity with three somatosensory-related thalamic nuclei, VPL, PO, and PoT. Interestingly, the thalamocortical projections to S1

or pIC arise from distinct and spatially localized thalamic regions. S1 receives significantly more thalamocortical projections from VPL and PO than pIC. (Figure 3.1.2-1 B). This data is in line with results from the literature, as the projections from VPL and PO to S1 have extensively been investigated (Casas-Torremocha et al. 2022).

The connectivity of pIC has been investigated as well, with the posterior somatosensory thalamic nucleus (PoT in rodents and the homologous region VMpo in monkeys) identified as one of the major sources of thalamocortical projections to pIC (Kimura, Imbe, and Donishi 2010; Gehrlach et al. 2020; Bud Craig 2014). In addition to PoT, it has also been shown that VPL and PO send thalamocortical projections to pIC (Z.-H. Zhang and Oppenheimer 2000; Gehrlach et al. 2020). Overall, the presented results are in good agreement with published tracing studies that have investigated thalamocortical projections to S1 and pIC.

Within the three thalamic nuclei VPL, PO, and PoT, it was shown that S1 receives selective input from anterior thalamic regions, whereas pIC receives selective input from posterior thalamic regions, namely PoT. The medial subregions send thalamocortical collaterals either to pIC or S1 (see 3.1.2-1 D). A comparison to already published data is difficult in that regard due to a lack of studies that performed dual injections in two sensory cortices that are involved in the processing of the same modality. However, one of the most recent studies (Gehrlach et al. 2020) that investigated the thalamic projections to pIC has shown that pIC receives input from cells that are located at positions from -1.5 mm to -3 mm relative to Bregma, which the researchers assigned to the PO complex. In the analysis performed in the present study, these positions align with the anatomical location we have identified as the output region for thalamocortical pIC projections. (Figure 3.1.2-1 D). The same study also identified thalamocortical projections to pIC from the VB (note Gehrlach et al. 2020 labeled VP) that span from -1.5 mm to -2.5 mm relative to Bregma. Our analysis has found projections from VB spanning from -1.5 mm to – 2.2 mm relative to Bregma. Even though this study did not trace connectivity from S1, the positions of thalamocortical projections to pIC overlap with the locations we have identified.

Taken together, a comparison to other studies that investigated thalamocortical projections suggests that pIC receives input from VPL, PO, and PoT. Second, the thalamic input to both thermal representations is separate and direct, suggesting that there may be two segregated pathways that mediate feedforward thermal information transfer.

4.1.2 Corticothalamic projections from S1 and pIC

In chapter 3.1.3. it was shown that corticothalamic projections from S1 and pIC are widespread and label multiple thalamic regions. An in-depth investigation of the projections led to the conclusion that S1 developed increased projection strength to VPL and PO compared to pIC. Additionally, PoT is the only thalamic region that received selective pIC projections. Within the thalamic nuclei the corticothalamic projections are more overlapping than the regions sending thalamocortical projections to S1 and pIC. To account for this discrepancy, one must realize that the corticothalamic projections had been visualized by AAV-based labeling. While this approach is highly effective in labeling axonal projections, it does not specifically label synaptic boutons, and therefore the analysis of axonal projections will include fibers of passage as well as terminating fibers. Future use of tools that label presynaptic sites, e.g., synaptophysin-cre-based viruses (Beier et al. 2015; Lerner et al. 2015) could help resolve this and identify thalamic structures that receive synaptic input from S1 or pIC. Although the corticothalamic projections were more widespread than the areas that send thalamocortical projections, relatively similar regions were identified.

4.2 Thalamic inactivation during thermal detection task

Chapter 3.2 of the present study reveals findings regarding the impact of reversible pharmacological inactivation of the thalamic thermal representation on thermal detection behavior. The results demonstrate a robust impairment in thermal detection performance (see 3.2.1) upon thalamic inactivation. Remarkably, this impairment is specific to thermal detection, and the site of pharmacological inactivation has minimal influence on the strength and stimulus-specificity of the impairment (see 3.2.2). The results of the behavioral inactivation indicate a causal relationship between thalamic activity and the thermal detection capabilities of the animal. Nonetheless, they also provide reason for the discussion of two points. First, past investigations revealed weak effects on thermo-discrimination behaviors after thalamic inactivation. The discrepancy of these weak effects found in previous studies

and the profound impairment observed in the present study will be explained in the course of this chapter (4.2.1).

The present study also adds evidence to the participation of various thalamic nuclei in thermosensory processing. In addition, these thalamic regions are also independently connected to thermal cortices. Such a finding implies the existence of redundant pathways that relay perceptually significant sensory information to cortical regions in case one pathway is inactivated. The purpose of Chapter 4.2.2. is to explain the complete impairment of thermal detection even though multiple pathways might be involved in the transmission of thermal information.

4.2.1 Comparison with previous studies of thalamic inactivation in thermal detection tasks

Previous studies ($n = 4$) that have investigated thermal discrimination behaviors in various model organisms after thalamic inactivation have reported only mild impairments. One study has performed thalamic lesioning in cats and engaged the animals 6 – 9 days after surgery in a floor temperature discrimination task (Norrsell and Craig 1999). The study found after post-hoc identification of the lesion site that the animals with mild behavioral impairments showed incomplete lesioning of the somatosensory thalamus, indicating the importance of on-target inactivation when performing behavioral impairment experiments. The present study only included animals in the dataset in which on-target inactivation was confirmed by post-hoc reconstruction of the injection site.

Interestingly, the same study found that the animal with complete a lesion of the thalamic structure showed a strong behavioral impairment. However, the performance of the animal did recover after multiple experimental sessions. A similar effect was seen in monkey lesion experiments in which the animal recovered its thermal discrimination performance over the course of multiple days (Cragg and Downer 1967) after showing initial impairment of the behavior. A more recent study that investigated object detection in mice using their whiskers has seen a comparable recovery. It was shown that mice quickly recovered their performance after lesioning of Barrel Cortex (Hong et al. 2018). The permanent inactivation is therefore difficult to interpret as plasticity or homeostatic mechanisms of the brain might be triggered

over time due to irreversible disruption of an entire structure (Otchy et al. 2015), which wouldn't be triggered by a short-lasting reversible inactivation of neural structures like the one used in the present study (Lomber 1999).

Another study that examined the effect of reversible inactivation of the somatosensory thalamus in a temperature discrimination task also reported only a weak behavioral impairment (Duncan et al. 1993). The researchers injected Lidocaine into VB and found a concentration-dependent behavioral impairment. Interestingly, the researchers performed multi-unit extracellular recordings in close vicinity of the position they had placed the injection cannula at and were able to record neural spikes even after administration of Lidocaine in the thalamus. This partial inactivation of thalamic activity could be an explanation for the weak behavioral impairment. Lidocaine has been shown to result in a less effective reduction of neural spiking compared to Muscimol, which was used in the present study (Van Duuren et al. 2007).

The last study that performed thalamic lesions in a temperature discrimination essay examined the capability of an animal to learn the task in the absence of VPL and didn't investigate the performance of an animal that had already learned the task (Finger and Frommer 1970). They have shown that the electrolytic lesion of VPL had only a minor influence on task learning. Other studies have found that rodents are capable of learning sensory discrimination tasks in the absence of their primary sensory cortices (Hong et al. 2018) or motor-related behavioral tasks in the absence of their primary motor cortex (Pack et al. 2020). The neural mechanisms that govern task learning are different from the experimental paradigm used in the present study and, thus, hard to compare.

In summary, this chapter has stressed that the behavioral phenotypes seen in thalamic inactivation studies are ambiguous, and therefore, comparisons to the phenotypes of the present study become problematic. This might be due to un-specific inactivation in the thalamus, an irreversible inactivation approach, incomplete reversible inactivation, and differences in the learning paradigm.

4.2.2 Influence of inactivated region on strength and stimulus-specificity in thermal detection behavior

The present study has found that inactivation of the posterior region in VPL or PoT led to a robust impairment of thermal detection performance that was not stimulus-specific (i.e., one injection could influence cooling or warming perception). Taking into account that thermal information is represented by multiple thalamic nuclei that send information to two cortical temperature-sensitive cortices, S1, and pIC, one could assume that the redundancy of the pathways should enable the mouse to perform a thermal detection task even if one thalamic processing node is inactivated.

One possible explanation is the use of muscimol. Injections of muscimol led to the spread of the GABA-blocker into the surrounding tissue of the injection site. This could especially be a problem in the thalamus, as it is a densely packed structure with many nuclei in close proximity and diverse functions. The main inhibitory thalamic nuclei RT is adjacent to VPL, and injections could have affected RT inhibitory drive onto the entire thalamus (Roy et al. 2022), which would have led to non-physiological thalamic function and, therefore, possibly results in unspecific impairment of thermal detection behavior. However, the study has performed control experiments in which VPL was inactivated in acoustic-trained animals and no behavioral impairment could be seen. RT has been shown to send collateral to the auditory thalamus (Bartlett 2013), so one would assume that the effect of RT inactivation on somatosensory or auditory detection is similar. Another possibility could be the spread of muscimol from VPL to PoT after VPL injections or the spread from PoT to VPL after PoT injections. Considering the distance between the injection sites and the border of the other thalamic structure (~ 0.5 mm) this might seem unlikely but not impossible. Further experiments with improved visual control of the spread of muscimol bound to a fluorescent protein could help in resolving that issue (Allen et al. 2008).

Another explanation of the strong behavioral impairment seen in the present study takes the densely interconnected and dynamic nature of the brain, especially of the thermal system, into consideration. In a system with multiple processing nodes and strong connectivity, perturbation of the physiological function of one might affect the processing of another downstream processing node (Otchy et al. 2015). An example in the thermal system of this

interference are studies that performed pharmacological inactivation and optogenetic inhibition of S1 that resulted in impaired warming and cooling detection (Paricio-Montesinos, n.d.). Interestingly, S1 lacks a warming representation but is connected with other cortical and thalamic regions that process warming information (Bokiniec et al. 2018; Vestergaard et al. 2023; Milenkovic et al. 2014). Under the assumption that the creation of a sensory percept depends on multiple cortical and thalamic structures to act precisely in concert, any perturbation of that functional interplay could create major deficits in sensory perception. In chapter 3.1, it was presented that the posterior region of VPL and PoT both project to pIC, both regions are necessary for thermal detection (see 3.2), and that both thalamic regions represent cooling and warming stimuli (see Results 3.3) but that their temporal encoding profiles are different (see Results 3.5). This could be interpreted that the structures extract different features from a sensory stimulus and send nucleus-specific information to downstream cortical areas that are utilized for building a sensory percept, similar to the ‘two-stream hypothesis’ in vision and audition (Belin and Zatorre 2000; Goodale and Milner 1992) and that perturbation of one thalamocortical information stream comprises the physiological function of the recipient structure, which in turn negatively affects sensory perception.

Taken together, the robust impairment of thermal detection could be attributed to the limited spatial control of muscimol and the non-specific inactivation of multiple thalamic regions, as well as the disturbance of a heavily connected system like the thermal system in rodents. More experiments are necessary to distinguish the perceptual relevance as well as physiological function of the thermal processing nodes in order to understand a complex mechanism like sensory perception.

4.2.3 Conclusion and future direction

The behavioral experiments in this present study have shown that the somatosensory thalamus plays a crucial role in thermal detection behavior. More experiments are necessary to investigate the specific role of the individual thalamic nuclei and their downstream cortical projection targets in such a behavioral experiment. Future studies need to improve the spatial control over the inactivated area without sacrificing the efficiency of neural activation. The

recent development of potassium-selective channelrhodopsin provides spatial control of the inactivating, and they are efficient inhibitory constructs that effectively shut down neural transmission with axonal photo stimulation (Vierock et al. 2022) thereby ensuring the necessary spatial control.

4.3 Thermal tuning of thalamic nuclei

The identification of sensory-tuned neurons is a fundamental and necessary step in understanding the encoding of sensory information by neural ensembles. The existence of distinct cell populations that respond selectively to a specific stimulus provides an easy readout of the sensory identity by downstream processing units.

The present study investigated the thermal tuning to cooling and warming on a single cell level sampled from multiple thalamic nuclei. While thermally tuned cells to cooling and warming, as well as thermally non-tuned cells were found, the data gives rise to the discussion of two points. First, all thalamic nuclei that were investigated in this study showed a dominant thermal tuning to cooling compared to warming. Chapter 4.3.1 will compare the outcome of the present study to already published work and provide explanations for the observed cooling bias of the thalamic population. Second, the proportion of warming-selective neurons was unexpectedly low across the thalamic nuclei. Chapter 4.3.2 aims to provide explanations for this result and discusses the functional implication of such a sparse warming-specific representation.

4.3.1 Overrepresentation of cooling compared to warming

The neural recordings performed in the present study, presented in chapters 3.3.2, 3.3., 3.3.4, and 3.3.5, revealed that cooling and warming of the forepaw are represented by a significant number of cells, respectively. However, the proportion of cells showing cooling responses outnumbered warming-responsive cells. This result was consistent for the entire thalamic population (Fig. 3.3.2-1), on the level of individual thalamic nuclei (Fig. 3.3.3-1) as well as on

the level of thalamic subregions (Fig. 3.3.4-1). Furthermore, the overrepresentation of cooling responsiveness was not only represented in cells that show an excitatory response but also in cells that exhibit a suppressed response to thermal stimulation (see 3.3.5-1). In order to evaluate the cooling bias seen in the present study, one has to consider the representation of cooling and warming in the sensory periphery that transmits thermal information to the thalamus. Thermal information is initially detected by receptors of the TRP family that are embedded in the skin (M. Caterina and Pang 2016). Cooling and warming-selective receptors form spatial clusters (cold-spots, warm-spots) that showed increased sensitivity and detectability of thermal stimuli compared to other regions of the skin (Adair 1999a; Blix 1882). Studies that have investigated the spatial distribution of these thermal spots have consistently shown that cold spots outnumber warm spots independent of the body part and model organism (Leem, Willis, and Chung 1993; Arens and Zhang 2006; Dallenbach 1927). A similar cooling bias was seen in electrophysiological recordings of sensory afferents innervating the limbs in monkeys, humans, and rodent model organisms (Gentle 1989; Darian-Smith et al. 1979; Darian-Smith, Johnson, and Dykes 1973; F. Wang et al. 2018a) as well as in recent imaging studies of the spinal cord in rodents (Ran, Hoon, and Chen 2016b). It, therefore, seems likely that the overrepresentation seen in the present study is a consequence of a cooling-biased functional architecture that is already present in the sensory periphery.

Within the following paragraph, a collection of already published studies on thalamic temperature encoding is presented and compared to the results of the present study. Multiple studies have examined the neural representation of temperature in the thalamus in anesthetized preparations and found diverse results in terms of the representation of cooling and warming. Key factors that defined the representations were the stimulation site (e.g., Limb, Scrotum), the model organism (e.g., Rat, cat, monkey, human) as well as the tested temperature range (e.g., innocuous, noxious).

The body part that was thermally stimulated had a strong impact on the neural representation of temperature in the rats' VB in an anesthetized preparation. Interestingly, while stimulation of the scrotum evoked cooling and warming responses, limb stimulation completely lacked a warming representation (Günter Schingnitz and Werner 1980b; Sakata, Morimoto, and Murakami 1989; Kanosue et al. 1985; Hellon and Misra 1973; Hellon and Taylor 1982; Jahns 1975). In the context of noxious thermal stimulation, PoT, and VB have been shown to encode painful heat stimuli in anesthetized rats after limb stimulation (Gauriau and Bernard 2004a;

William D Willis et al. 2002). Only in higher model organisms like cats and monkeys, researchers were able to find innocuous warming-responsive neurons (Burton, Forbes, and Benjamin 1970a; Martin and Manning 1971) after thermal stimulation of the limb within the cats' and monkeys' homolog structures of PoT.

This body of work shows contrary results to the present study since innocuous warming stimulation of the paw evoked a sensory response in the thalamus after limb stimulation. However, a comparison of these results is challenging for multiple reasons. First, all studies that have been conducted in rodent model organisms have been performed under anesthesia, which has a strong impact on multiple nodes of the thermal processing chain, like the sensory afferents that transmit thermal information (Raithel et al. 2018) and the thalamus, which relays thermal information to the cortex (Huh and Cho 2013) and could therefore cause the lack of warming responses seen in these studies and explain the discrepancy of the reported thermal representation of already published work to the present result. Second, studies that found warming responses in anesthetized rodents performed thermal stimulation of the scrotum (Günter Schingnitz and Werner 1980b). Even though only very limited data on the spatial distribution of TRP channels across the rodents' body surface is available, human studies that have tested cooling and warming sensitivity in relation to the stimulated body area found that the hand palm shows significantly less sensitivity to warming than areas close to the scrotum (Luo et al. 2020) and could therefore explain the lack of warming after limb stimulation and the presence of warming responses after scrotum stimulation. It is unclear whether rodents display the thermal maps after stimulation of other body parts. the presence of an increased number of warming-sensitive neurons after thermal scrotum stimulation suggests that they do, and this makes comparison to the present study that focused on paw stimulation difficult. Third, painful heat stimuli were observed to evoke neural responses in rodents. However, recent studies have found that painful heat stimuli activate dedicated sensory afferents and spinal cord fibers compared to innocuous warming stimuli (Ran, Hoon, and Chen 2016b; F. Wang et al. 2018b).

When combined, these findings conclude that the presence of cooling exceeds that of warming at various stages of the thermal processing chain. This was shown across a range of model organisms, with some studies showing no signs of warming at all. One reason that may explain the cooling bias observed in the present study is that this study is conducted in warm-blooded animals.

This group of animals is characterized by a relatively stable body core temperature as well as a constant temperature in the extremities (Gordon 2017). In order to elicit a thermal response, a stimulus must have a significant deviation from the skin temperature. Usually, the thermal statistics of the environment are cold-biased compared to the skin temperature which could have led to the development of the thermal system to be stronger tuned to cold rather than warm processing. Another possible explanation for the overrepresentation of cooling might be that cold temperatures lead to increased energy expenditure compared to warm temperatures in warm-blooded subjects (Ocobock 2016). From an evolutionary perspective, it might have been more important for an animal to be able to detect cold temperatures than warm temperatures, as cold temperatures present a greater threat to the animal's survival.

4.3.2 Low proportion of “Warm” cells and its functional implication

A recent imaging study that investigated thermal encoding in pIC has found that warming shows a robust representation by a large population of warming-selective (“Warm”) cells which is contradictory to the results shown in the present study (Vestergaard et al. 2023). One might have expected a higher number of warming-selective cells under the assumption that the thalamus is the main origin of sensory information to cortical areas and that temperature information follows this thalamocortical pathway. The next chapter will address this difference, provide a possible explanation for the contrasting results about the representation of warming in the cortex compared to the thalamus, and finally, consider the functional consequences of a sparse representation of warming.

One explanation for the discrepancy between the cortical temperature representation seen in pIC and the thalamic representation displayed in the present study is that thermal information is not exclusively transmitted via the thalamus to the cortical processing area but uses a parallel pathway via the LPN and the amygdala to pIC. Thermal information is transmitted via spinal cord lamia I fibers to the thalamus but also to the LPN (Hachisuka, Koerber, and Ross 2019; Li et al. 2006; Cechetto, Standaert, and Saper 1985; Hylden, Anton, and Nahin 1989; A. D. Craig, Zhang, and Blomqvist 1999; Kumazawa et al. 1975; Al-Khater and Todd 2009; A. D. Craig and Dostrovsky 2001; Bester et al. 2000; W. D. Willis et al. 2001). The

LPN sends projections to the amygdala, which shows strong connectivity with pIC (Nakamura and Morrison 2010; 2008; Gehrlach et al. 2020; Bokiniec et al. 2018; 2023). Furthermore, innocuous thermal stimuli are encoded in the LPN (Nakamura and Morrison 2010; 2008), and even though the amygdala has mainly been associated with the processing of noxious thermal stimuli, it is not unlikely that the structure contains neurons responsive to innocuous stimuli (Corder et al. 2019; Neugebauer and Li 2002).

A general assumption of the spinal-parabrachial pathway is that it is involved in the evocation of thermoregulatory responses linked to a discrepancy between body core temperature and ambient temperature. After all, temperature changes have to be registered by thermal receptors, and it seems possible that this pathway is triggered by the stimulation paradigm used in the present study. Nevertheless, more experiments are needed to determine whether the thermal coding in LPN consists of innocuous warming-selective neurons that would point to parallel thermosensory pathways.

Alternatively, the low proportion of warming-selective neurons throughout the thalamus in comparison to the cortical temperature representation in pIC could be due to the fact that the thalamocortical input to pIC is filtered by cortical circuits in a stimulus-specific manner. This would imply that the low fraction of warming-selective neurons is an inherent feature of the thalamus that is distinct from the cortex. The results have shown that cooling is encoded by thalamic “Cold” and “Cold-Warm” cells in the posterior regions of VPL, PO, and PoT. If the “Cold” cells activate a layer 4 feed-forward inhibition circuit in pIC that gates the thalamocortical input from “Cold-Warm” cells, this cell would only be able to activate the cortical recipient cells when a warming stimulus is applied and would therefore appear as warming tuned cell. Multiple requirements must be met for a system to engage in such a feedforward inhibitory circuit that would shape the thermal tuning of a layer 4 pIC cell. First, there must be a “Cold” cell-specific projection onto inhibitory cells located in the recipient layer of pIC. While there is plenty of evidence that thalamocortical projection cells activate inhibitory neurons in layer 4 throughout the entire neocortex (Swadlow 2003; 2002), no data is available for the thermal system, especially in regards to functional response-type specific projections. Second, the “Cold” cell projection onto layer 4 inhibitory neurons must be precisely timed, and proceed the thalamocortical signal from “Cold-Warm” cells as an additional synapse is involved in the feed-forward circuit and both signals must coincide at the layer 4 recipient cell. Third, the inhibitory drive onto the layer 4 recipient cell must be strong

in order to effectively keep the recipient cell below the spiking threshold for the duration of stimulus application. The investigation of the temporal response dynamics has shown that “Cold-Warm” cells mainly show sustained firing throughout the stimulus presentation eliciting high firing rates. While multiple studies have shown that thalamocortical feed-forward circuits are able to modulate a sensory response which leads to increased specificity and tuning of sensory cortical neurons compared to thalamic neurons, there is no evidence in the literature of such a complete and strong inhibition of layer 4 inhibitory neurons that would be necessary for the proposed circuit mechanism to transform the signal of a thalamic “Cold-Warm” cell to a cortical “Warm” cell.

4.4 Spatial representation of somatosensory stimuli

The results presented in chapters 3.3.3 and 3.3.6 have shown that cooling, warming, and tactile stimulation of the forepaw evoked neural responses in the three thalamic nuclei VPL, PO, and PoT. Numerous studies confirm that somatosensory stimuli, including innocuous cooling and tactile stimulation, are represented in VPL (Günter Schingnitz and Werner 1980b; Turecek, Lehnert, and Ginty 2022; Abraira and Ginty 2013), PO (Sanganahalli et al. 2022) and PoT (A. D. Craig et al. 1994; Gauriau and Bernard 2004a). Furthermore, the anatomical tracing experiments have shown (chapter 3.3.1) dense labeling of S1- and pIC- projection neurons spanning a large extent within VPL, PO, and PoT. Together, these results strongly indicate the functional engagement of these thalamic nuclei in the encoding and relay of somatosensory information towards cortical processing centers.

The following chapter aims to discuss the spatial extent of the representation of warming, cooling, and tactile stimulation. This examination takes the peripheral input these structures receive into account and will also underscore the constraints of the present study, particularly regarding the potential impact of corticothalamic feedback on the spatial delineation of the investigated somatosensory stimuli.

4.4.1 The spatial representation of warming

Warming stimuli evoked neural responses in neurons that were exclusively localized in the posterior part of VPL as well as the border region of posterior PO and PoT (chapter 3.3.3). The anterior region in VPL and PO showed no evidence of warming-evoked activity across the neural population. Interestingly, the anatomical tracing experiments (chapter 3.1) have shown that pIC receives thalamic projections from the posterior region in VPL and PO as well as from PoT, and studies have shown that pIC is thermally tuned to both warming and cooling. In consideration of the thalamic function as a relay structure of sensory information, the spatial representation of warming is in line with the anatomical tracing (chapter 3.3.4). Other studies that investigated the sensory representation across thalamic nuclei associated pVPL as well as the border region of pPO and PoT with the representation of noxious tactile and painful temperature stimuli (X. Zhang, Davidson, and Giesler 2006; X. Zhang and Giesler 2005 ;Francis, Xu, and Chapin 2008; Turecek, Lehnert, and Ginty 2022). The transmission of painful sensory stimuli from the sensory periphery to the central nervous system has traditionally been associated with the Spinothalamic tract, and spinothalamic projections from lamina I - the spinal cord layer in which Spinothalamic tract fibers are located - were shown to terminate in pVPL (Hodge and Apkarian 1990) as well as in the border region of pPO and PoT (Al-Khater, Kerr, and Todd 2008). A key component of the Spinothalamic tract is input from non-myelinated C-fibers that are activated by noxious mechanical and thermal stimuli but also by innocuous warming stimuli (Hallin, Torebjork, and Wiesenfeld 1982) due to the expression of TRP channels (Silverman et al. 2020) in the primary afferents. Hence, innocuous warming stimuli appear to be detected by TRP channels situated in non-myelinated C-fibers, and the thermal information is conveyed to the Spinothalamic tract that terminates at the level of the thalamus in pVPL and pPO/PoT, areas that have been classically associated with the processing painful stimuli. From there, the information is sent via thalamocortical projections topic for further processing. Taken together, the results presented in that chapter are in good agreement with retrograde tracing from pIC, as well as the projection targets from Spinothalamic tract lamina I fibers of the spinal cord, and provide valuable and additional insights into the somatosensory tuning of thalamic structures.

4.4.2 The spatial representation of cooling and touch

Functional mapping of cooling and tactile-evoked sensory responses upon forepaw stimulation demonstrated a strong and widespread cellular activation that spanned large areas in VPL, PO, and PoT. It was remarkable that cooling produced increased cellular activation in the anterior subregion of VPL and PoT, while tactile stimulation led to a uniform spatial activation in VPL, PO, and PoT. The results provide reasons for the discussion about potential causes for the widespread representation of cooling and tactile compared to the spatially localized warming representation.

As stated in the previous chapter, warming stimuli are exclusively transmitted via C-fibers and the Spinothalamic tract to thalamic nuclei that were traditionally associated with the encoding of painful stimuli. Tactile stimulation, on the other hand, activates a larger variety of sensory afferents including C-fibers but also A β - and A δ -fibers. These fibers synapse onto spinal cord fibers that belong to the Spinothalamic tract but also the Dorsal Column-Medial Lemniscal pathway (Abraira and Ginty 2013; Turecek, Lehnert, and Ginty 2022). This additional activation of an ascending somatosensory pathway might, in part, account for the larger area activated by tactile stimulation, taking into account that the two pathways terminate at different thalamic locations (Ralston and Ralston 1994; W. D. Willis and Westlund 1997). However, the two ascending pathways signal distinct features of a tactile stimulus. While the Dorsal Column-Medial Lemniscal pathway is associated with features like fine touch, vibration, and proprioception, the Spinothalamic tract signals features that are rather associated with the nociceptive spectrum of tactile stimulus features like crude touch (Al-Chalabi, Reddy, and Gupta 2023). Given the strong vibratory stimulus that spans the entire surface of the dorsal side of the paw, it is possible that both pathways are activated at the same time, which could explain why responses could be recorded in several nuclei.

The cooling of the skin activates two types of sensory afferents, C-fibers, and A δ -fibers. Both fiber types synapse in the dorsal horn of the spinal cord on second-order neurons that are associated with the Spinothalamic tract and travel on distinct fibers to the thalamic nuclei (Ma 2010; A. D. Craig and Bushnell 1994). In there the cooling and warming-responsive C-fibers terminations are located in the posterior part of VPL and PoT and the cooling-selective A δ -fibers terminals could be responsible for the widespread cooling representation (chapter.

3.3.4). Another possible explanation for this cooling-selective widespread activation could be the salience of the cooling stimuli (-10 °C) that could lead to non-specific activation of the thalamic nuclei similar to the widespread activation painful stimuli elicit in neural structures (Hayes and Northoff 2012). In favor of this hypothesis are the results shown in Figure 3.4.4-1, which show that PoT and posterior VPL have the highest fraction of low-amplitude cooling recruited cells, which would align with the main targets of the Spinothalamic tract. Systematic tracing of functionally defined cooling-selective fibers from the spinal cord would help to resolve this controversy and provide useful insights into the functional architecture of somatosensory ascending pathways that non-noxious stimuli utilize. Another explanation for the widespread cooling-selective representation also applies to the tactile representation and considers that the thalamus and cortex are heavily interconnected structures (Rikhye, Wimmer, and Halassa 2018) that could lead to the activation of thalamic neurons by cortical feedback induced by strong sensory drive like a -10 °C cooling or vibrotactile stimuli applied to the entire paw. This hypothesis could, in part, explain the widespread activation seen in PO, as it has been shown that this nucleus receives most of its input from the cortical region and not from the sensory periphery (Diamond, Armstrong-James, and Ebner 1992b; S. M. Sherman 2016; Sampathkumar et al. 2021). This hypothesis also exposes one of the limitations of the present study; that it examines thalamic encoding in the context of active cortical circuits that may influence thalamic processing. An additional explanation for the widespread cooling representation could be that the cooling of the skin not only activates C-fibers and A δ -fibers but also a subset of temperature-responsive low-threshold mechanoreceptors (Abraira and Ginty 2013). This type of fiber also terminates in the superficial layers of the skin and sends sensory information via the Dorsal Column-Medial Lemniscal pathway to the thalamus. If thermal information is transmitted via this pathway, the overlap between the cooling and tactile representations could be explained. However, recordings from primary sensory afferents have shown that these receptors mainly respond to noxious thermal stimuli with delayed response latencies. This, in turn, would lead to delayed sensory responses in the thalamus. However, these responses were rarely seen in the investigated population.

Therefore, at present, a possible interpretation of the larger extent of cooling and touch representation compared to warming could be an additional input channel to the thalamus utilized by cooling and touch and not by warming. The study exclusively used paw stimulation and saw widespread activation, with thermal hotspots in the posterior parts of VPL and PO as

well as PoT. It remains to be tested if stimulation of other body parts will also lead to such widespread activation with spatially distinct hotspots compared to paw stimulation.

4.5 The encoding of temperature amplitudes

The encoding of stimulus intensities in a robust and reliable fashion is a fundamental and critically important feature of a sensory system, protecting animals not just against exposure to high-intensity, potentially damaging stimuli but also enabling the detection of even minor changes in a sensory environment. This chapter is going to focus on the discussion of two intensity encoding-related characteristics: the saturation to high-amplitude stimuli and its functional implication (chapter 4.5.2), as well as the sensitivity to low-amplitude stimuli and its anatomical specification (chapter 4.5.3).

4.5.1 Low proportion of “Specificity” neurons

Analysis of encoding profiles in response to incremental changes in stimulus amplitudes revealed that a predominant proportion of neurons responsive to cooling or warming stimuli exhibit an almost linear relationship between their firing rates and the magnitudes of the applied stimuli (referred to as "Intensity"). Conversely, a minor subset of cooling-responsive cells displayed discernible firing selectivity confined within a specific temperature range ("Specificity") (chapter 3.4.1), peaking at lower temperature amplitudes than the maximum temperature amplitude and showing significantly reduced firing rates at the maximum temperature as compared to the peak firing rate. Ion channels of the TRP family drive the detection of temperature changes on the skin. The receptors are localized in primary sensory afferents and show specific activation profiles that are tuned to certain temperature ranges (Ferrandiz-Huertas et al. 2014; H. Wang and Siemens 2015).

As depicted in Figure 4.5.1-1, most of the channels exhibit either maximal activity at noxious temperature levels (i.e., $T < 15^{\circ}\text{C}$, $T > 42^{\circ}\text{C}$) or remain highly active as the stimulation magnitude increases. However, it is important to note that the present study considered only

temperatures within the innocuous thermal range. The significant proportion of the units exhibiting the “Intensity” profile might be due to this experimental constraint. Further experiments that test the full thermal range (innocuous and noxious) will help to further refine the examination of the encoding profiles the thermal system utilizes.

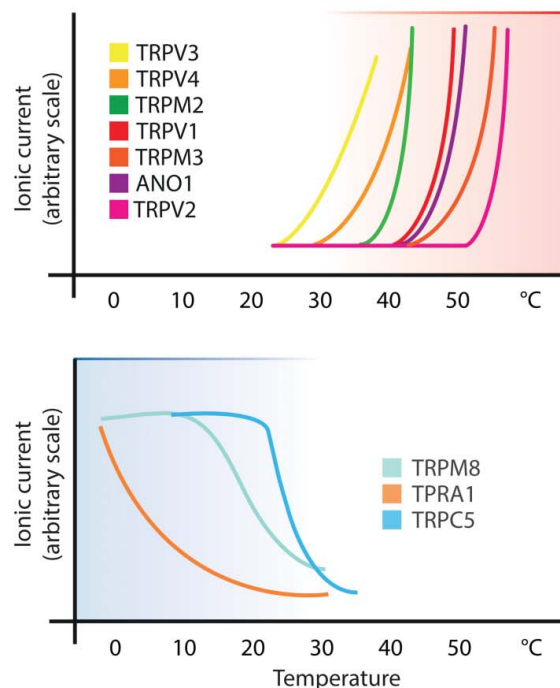


Figure 4.5.1-1 The diagrams schematically illustrate the temperature activation profiles of warm/hot-sensitive ion channels (upper panel) and cold-sensitive channels (lower panel) inherent to primary afferent neurons specialized in temperature perception. Edited from H. Wang and Siemens 2015

4.5.2 Encoding profile of “Cold-Warm” neurons in comparison to “Cold” neurons

The examination of encoding profiles spanning the thalamic nuclei has revealed that neurons categorized as "Cold" exhibit a graded scaling of their firing rates with decreasing stimulus amplitudes. In contrast, the tuning curves of "Cold-Warm" neurons demonstrate saturation at temperature amplitudes lower than 28 °C, resulting in statistically comparable firing rate distributions within the range of 22 °C to 28 °C. This result was independent of the thalamic nuclei and therefore points towards a functional specialization of "Cold-Warm" and "Cold"

neurons in the thermal system. Under the assumption that stimulus intensities are encoded in a firing rate-dependent manner, “Cold” cells are well suited to precisely encode cooling amplitudes in comparison to “Cold-Warm” neurons and might therefore play a crucial role in the perception of stimulus intensities (Muniak et al. 2007; Winter, Robertson, and Yates 1990). The interpretation of the tuning curves of “Cold-Warm” neurons and their physiological role is more complicated. Because the neurons have a small dynamic range, they would seem to be ideally suited to act as “cooling stimulus detectors”, responding to slight changes in the temperature. The non-specific thermal tuning to cooling and warming, however, conflicts with this hypothesis because the stimulus identity cannot be decoded by downstream processing nodes without complex circuit mechanisms, as discussed in Chapter 4.3.2. This neuron type could also have another physiological function to detect stimulus-related features, such as identifying the place of stimulation. Thermally non-tuned neurons could perform this function, but only if separate neural populations are activated in a stimulus-site-specific manner. Since the forepaw was exclusively stimulated in the present study, this hypothesis can't be tested. The final hypothesis on the physiological function of the saturating response curves of “Cold-Warm” neurons considers the coexistence of saturating and linear intensity encoders within a sensory system. Both functionally specialized subsets of cells would ensure both, a robust and sensitive detection of small-amplitude stimuli in combination with reliable and precise encoding of stimulus intensities (Gollo 2017). In favor of this hypothesis are the increased detectability and decreased perceptual thresholds for cooling compared to warming (Paricio-Montesinos et al. 2020), which could, in part, be explained by the activity of saturating “Cold-Warm” cells.

4.5.3 Increased sensitivity of PoT to low amplitude warming stimuli

The investigation into the recruitment patterns and firing rates evoked by low-amplitude cooling and warming stimuli (chapter 3.4.4) showed that low-amplitude cooling stimuli recruit a similar number of cells among thalamic nuclei with a minor bias towards recruiting more cells in the posterior regions. Nonetheless, low-amplitude stimulus-evoked firing rates are quite distinct between structures, indicating higher response strength in VPL. Warming stimuli

recruited different numbers of cells, with an increased proportion in PO and PoT but with relatively similar firing rates.

The disparity in low-amplitude cooling-induced firing rates between VPL and both PO and PoT remains consistent across response types, signifying an inherent anatomical specialization. This specialization in response strength to both low and high-amplitude stimuli (Fig. 3.4.2) may be elucidated by their functional roles within two discrete ascending sensory pathways that were initially described in the whisker system of rodents: the lemniscal and paralemniscal pathways (Rodriguez-Moreno et al. 2018; Mo et al. 2017; Bureau, Paul, and Svoboda 2006). While structures assigned to the lemniscal pathway (VPL) are characterized by a strong and precise neural response to sensory stimulation, thalamic structures belonging to the paralemniscal pathway (PO) often show delayed and weak neural responses (Diamond, Armstrong-James, and Ebner 1992a). Besides their functional differences, the thalamic nuclei also showed diversity in their layer-specific cortical projections. While thalamic projections of the lemniscal pathways mainly terminate in layer 4, paralemniscal terminals are found in layers 1 and 5 of the same cortical area (El-Boustani et al. 2020). The relatively small firing rates seen in PoT compared to VPL are more challenging to interpret due to the lack of data on its cellular and synaptic properties, functional involvement in ascending sensory pathways, and only limited data on the evoked sensory response upon innocuous somatosensory stimulation. Only the projection target in its primary cortical target, pIC, points towards paralemniscal-like functional properties as most of the terminations end in layer 1 (Casas-Torremocha et al. 2019), which could explain the reduced firing rates compared to VPL. However, this hypothesis would not be in line with the increased number of responsive cells in PoT compared to VPL after warming stimulation. Since the paralemniscal pathway is rather associated with modulatory activity on the sensory information-bearing lemniscal pathway (Mo et al. 2017).

The increased number of responsive cells, especially in the posterior region of the thalamus, could be explained by an increased density of Spinothalamic tract fibers terminating in PoT and PO compared to VPL. Interestingly, this hypothesis has been extensively discussed in the context of pain processing and spinothalamic input from lamina I and II of the spinal cord (William D Willis et al. 2002). However, this debate was mainly concerned with the existence of spinothalamic projections to VPL and didn't provide data on the density or the number of synaptic contacts in these regions.

4.6 Temporal dynamics

The investigation of the temporal response profile provides valuable insights into which features of a stimulus the neuron is tuned to and which information content can be extracted by a single neuron or neural ensemble. This might therefore be an important investigation in order to understand the physiological function of neural structures.

The following chapter will discuss the temporal encoding of the entire thalamic population of cooling and warming (4.6.1) and further investigate the anatomical specialization of VPL, PO, and PoT in the encoding of a cooling stimulus (4.6.2)

4.6.1 Temporal dynamics of cooling and warming encoding

The investigation of the temporal dynamics of cooling and warming-evoked sensory responses revealed that cooling elicits, on average, significantly shorter response latencies and peak response times than warming (chapters 3.5.1, 3.5.3). This result is in line with results from multiple studies that have examined the temporal profile of cooling and warming responses at different nodes of the thermal system, from the sensory periphery to the cortex (Darian-Smith, Johnson, and Dykes 1973; Darian-Smith et al. 1979; Vestergaard et al. 2023). There are multiple factors that could be responsible for the temporal difference. Cooling stimuli are transmitted by non-myelinated C-fibers as well as myelinated A δ -fibers, whereas warming exclusively utilizes non-myelinated C-fibers. These fibers are characterized by significantly different conduction velocities due to myelination (Adriaensen et al. 1983; Harper and Lawson 1985). Interestingly, the difference in response latency is also present in cells that respond to both cooling and warming. Taking into consideration, that non-myelinated C-fibers send input to these neurons, other factors than the conduction velocity of the ascending fibers must play a role. Anatomical studies have shown that cold receptors and warm receptors are located at different depths in the skin of humans (Adair 1999b; Ezquerra-Romano and Martínez 2016), with warm receptors populating deeper levels of the skin compared to cold receptors. Taking into account that heat transfer is limited by the velocity of heat diffusion through biological tissue, warm-receptors could potentially be activated at a later point compared to cold-

receptors (Rodríguez de Rivera et al. 2022; Dar et al. 2022). Another possibility for the increased response latency for warming compared to cooling is related to the biophysical properties of the temperature receptors, specifically the kinetics of the channel opening. It has been shown that TRPM8, in comparison to TRPV1, shows faster opening kinetics (Voets et al. 2004b).

Another pronounced difference between temporal dynamics of cooling and warming-evoked activity regards the duration of the response. Only long-duration sustained responses are triggered by warming, whilst cooling manifests as short-duration transient as well as long-duration sustained responses (chapters 3.5.1, 3.5.2, 3.5.3). The additional temporal profile seen in cooling responses is most likely driven by fast cooling specific input from A δ -fibers and has been described in the sensory periphery as well as at the cortical level (Darian-Smith, Johnson, and Dykes 1973; Darian-Smith et al. 1979; Vestergaard et al. 2023). The encoding of different sensory features has been associated with these two fundamentally different temporal profiles of cooling responses. While the temporal properties of transient cells are well suited to encode dynamic features of thermal stimulation, especially the change in temperature, sustained cells are better equipped to encode features like the stimulus amplitude and duration of the stimulus application (Maksymchuk et al. 2022; Vestergaard et al. 2023).

4.6.2 Anatomical specification of temporal response properties

The temporal tuning shows anatomy-specific characteristics. While aVPL showed, on average, the fastest response latencies for cooling and tactile responses, the posterior regions pPO and PoT were characterized by the shortest response durations for cooling and tactile responses. Warming responses were more homogenous than cooling or tactile responses but showcased a slight tendency to be shortest in pPO and PoT (chapters 3.5.2, 3.5.5). A likely explanation for the decreased response durations seen in the posterior regions of pPO and PoT for cooling and tactile stimulation is the increased proportion of transient cells (chapters 3.5.3, 3.5.6). It has been shown that cooling, as well as tactile information, is transmitted by fibers that resemble the temporal profile seen in the transient subpopulation (Yarmolinsky et al. 2016b;

Emanuel et al. 2021), and the increased proportion in pPO and PoT might be an indicator of increased input of these peripheral fibers. Another possible explanation for the transient population could be related to the inhibitory activity of RT, which gets activated by an excitatory sensory response. It has been shown that RT connects in a function-specific manner with distinct thalamic nuclei (Roy et al. 2022), and increased RT connectivity with pPO and PoT compared to VPL may explain the difference in the duration of the response. Nonetheless, no data exists showing increased projections of RT towards the posterior regions.

Taken together, the data has revealed that the temporal profiles of sensory responses are location-specific, which points towards anatomy-specific encoding of distinct thermal features across the thalamus.

5. Conclusion and future direction

5.1 Conclusion

The present study had the aim to investigate the cellular and spatial representation of temperature across multiple thalamic nuclei and to examine the behavioral relevance of these regions in a sensory detection task. The study has used a combination of anatomical tracing methods, neural inactivation during a thermal perception task, as well as extracellular electrophysiology, and came to the following key results:

- The anatomy of the thermal circuitry shows region-specific connectivity with cortical areas, specifically with the posterior thalamic regions primarily sending thalamocortical projections to pIC and the anterior thalamic regions sending projections to S1.
- Inactivation of the posterior thermal representations in the identified thalamic regions profoundly affects thermal detection, and therefore, activity in these structures may be behaviorally relevant to the animal.
- Cooling-selective neurons predominate thermal representation in the anterior regions of VPL and PO, whereas the posterior representations in VPL and PO and in PoT contain both neurons responding to cooling and warming.

- In the encoding of stimulus amplitudes “Cold” cells are widespread and the posterior regions in which “Cold-Warm” cells are located show a unique response-type-specific encoding profile.
- Increased sensitivity to low-amplitude warming stimuli is due to increased numbers of responsive cells in posterior regions in PO and PoT.
- The anterior region in VPL shows the strongest response strength compared to the rest of the thalamic region that was investigated in the present study.
- The posterior region of PoT showed an increased proportion of cells that are transiently responding to thermal and tactile stimuli, while the other thalamic regions were dominated by sustained cells.

5.2 Future direction

The present study has shown that thalamic temperature is represented by multiple thalamic subpopulations that show distinct anatomical and functional characteristics. The data presented in the study provides the basis for further investigations into the functional architecture of thalamocortical pathways and an in-depth investigation of thalamic encoding and processing. The following chapter provides ideas for future experiments that could broaden our understanding of thermal processing in the thalamus but also of general principles for how the brain encodes sensory information.

The anatomical and functional data showed two thermal representations that might have distinct functions for thermosensory perception. In this regard, I suggest a sequence of behavioral experiments that will examine the role of different thalamic nuclei for thermal perception. The experiments need to increase the spatial specificity of the manipulation compared to those shown in the present study by selectively inactivating thalamocortical projections to S1 or pIC. At the cortical level, presynaptic inhibition of thalamocortical axons could facilitate this. Such inactivation could be carried out in a comparatively more challenging behavioral paradigm than the one used in the current study. For instance, a thermal discrimination task could be relevant paradigm to determine whether thalamic nuclei are engaged differentially in stimulus detection or discrimination. Due to the cooling-selective

thermal tuning in the anterior regions of the thalamus that send thalamocortical projections to S1 and the cooling and warming tuning of posterior regions of the thalamus that send projections to pIC, I propose that the posterior regions in the thalamus are well equipped to encode the stimulus identity. The outcome of these experiments could provide evidence that thermal information is channeled in a parallel fashion through the thalamus and that each channel has a specific functional role in sensory perception.

Second, our functional data suggests widespread activation across multiple thalamic nuclei in response to stimulation of the forepaw. It is, however, well known that the thalamus has a well-developed somatotopic map. Thus, I suggest examining whether thalamic neurons are activated on such a global scale during stimulation of other body parts or if there are spatially localized cell ensembles as in the case of warming stimulation. In the situation of global activation, such experiments would improve the understanding of the somatotopic organization of thalamic neurons which would utilize a more complex activity scheme than a binary code. The possible directions of such investigations could include comparing the onset latencies and peak response times that may be faster if selective receptive fields of single thalamic neurons are stimulated. Moreover, this experiment should be conducted when the reciprocals connected cortical areas are inactivated to exclude the possibility of feedback activity that would result in nonspecific activation of thalamic neurons. These experiments would especially be suited to investigate the thermal representation in PO, as this structure receives its main input from the cortex.

6. Bibliography

- Abraira, Victoria E., and David D. Ginty. 2013. "The Sensory Neurons of Touch." *Neuron* 79 (4): 618–39. <https://doi.org/10.1016/j.neuron.2013.07.051>.
- Adair, Robert K. 1999a. "A Model of the Detection of Warmth and Cold by Cutaneous Sensors through Effects on Voltage-Gated Membrane Channels." *Proceedings of the National Academy of Sciences* 96 (21): 11825–29. <https://doi.org/10.1073/pnas.96.21.11825>.
- Adriaensen, H, J Gybels, H O Handwerker, and J Van Hees. 1983. "Response Properties of Thin Myelinated (A-Delta) Fibers in Human Skin Nerves." *Journal of Neurophysiology* 49 (1): 111–22. <https://doi.org/10.1152/jn.1983.49.1.111>.
- Al-Chalabi, Mustafa, Vamsi Reddy, and Sonu Gupta. 2023. "Neuroanatomy, Spinothalamic Tract." In *StatPearls*. Treasure Island (FL): StatPearls Publishing. <http://www.ncbi.nlm.nih.gov/books/NBK507824/>.
- Al-Khater, Khulood M., Robert Kerr, and Andrew J. Todd. 2008. "A Quantitative Study of Spinothalamic Neurons in Laminae I, III, and IV in Lumbar and Cervical Segments of Rat Spinal Cord." *The Journal of Comparative Neurology* 511: 1–18.
- Al-Khater, Khulood M., and Andrew J. Todd. 2009. "Collateral Projections of Neurons in Laminae I, III, and IV of Rat Spinal Cord to Thalamus, Periaqueductal Gray Matter, and Lateral Parabrachial Area." *Journal of Comparative Neurology*, no. 515: 629–46.
- Allard, Julien. 2019. "Physiological Properties of the Lamina I Spinoparabrachial Neurons in the Mouse." *The Journal of Physiology* 597 (7): 2097–2113. <https://doi.org/10.1113/JP277447>.
- Allen, Timothy A., Nandakumar S. Narayanan, Dianna B. Kholodar-Smith, Yanjun Zhao, Mark Laubach, and Thomas H. Brown. 2008. "Imaging the Spread of Reversible Brain Inactivations Using Fluorescent Muscimol." *Journal of Neuroscience Methods* 171 (1): 30–38. <https://doi.org/10.1016/j.jneumeth.2008.01.033>.
- Alloway, Kevin D., Zachary S. Hoffer, and John E. Hoover. 2003. "Quantitative Comparisons of Corticothalamic Topography within the Ventrobasal Complex and the Posterior Nucleus of the Rodent Thalamus." *Brain Research* 968 (1): 54–68. [https://doi.org/10.1016/s0006-8993\(02\)04265-8](https://doi.org/10.1016/s0006-8993(02)04265-8).
- Apkarian, Av, and T Shi. 1994. "Squirrel Monkey Lateral Thalamus. I. Somatic Nociresponsive Neurons and Their Relation to Spinothalamic Terminals." *The Journal of Neuroscience* 14 (11): 6779–95. <https://doi.org/10.1523/JNEUROSCI.14-11-06779.1994>.
- Arens, E., and H. Zhang. 2006. "The Skin's Role in Human Thermoregulation and Comfort." In *Thermal and Moisture Transport in Fibrous Materials*, 560–602. Elsevier. <https://doi.org/10.1533/9781845692261.3.560>.
- Baker, M. A. 1971. "Spontaneous and Evoked Activity of Neurones in the Somatosensory Thalamus of the Waking Cat." *The Journal of Physiology* 217 (2): 359–79. <https://doi.org/10.1113/jphysiol.1971.sp009576>.
- Bartlett, Edward L. 2013. "The Organization and Physiology of the Auditory Thalamus and Its Role in Processing Acoustic Features Important for Speech Perception." *Brain and Language* 126 (1): 29–48. <https://doi.org/10.1016/j.bandl.2013.03.003>.
- Bautista, Diana M., Sven-Eric Jordt, Tetsuro Nikai, Pamela R. Tsuruda, Andrew J. Read, Jeannie Poblete, Ebenezer N. Yamoah, Allan I. Basbaum, and David Julius. 2006. "TRPA1

- Mediates the Inflammatory Actions of Environmental Irritants and Proalgesic Agents." *Cell* 124 (6): 1269–82. <https://doi.org/10.1016/j.cell.2006.02.023>.
- Beier, Kevin T., Elizabeth E. Steinberg, Katherine E. DeLoach, Stanley Xie, Kazunari Miyamichi, Lindsay Schwarz, Xiaojing J. Gao, Eric J. Kremer, Robert C. Malenka, and Liqun Luo. 2015. "Circuit Architecture of VTA Dopamine Neurons Revealed by Systematic Input-Output Mapping." *Cell* 162 (3): 622–34. <https://doi.org/10.1016/j.cell.2015.07.015>.
- Belin, Pascal, and Robert J. Zatorre. 2000. "'What', 'Where' and 'How' in Auditory Cortex." *Nature Neuroscience* 3 (10): 965–66. <https://doi.org/10.1038/79890>.
- Bester, Hervé, Victoria Chapman, Jean-Marie Besson, and Jean-François Bernard. 2000. "Physiological Properties of the Lamina I Spinoparabrachial Neurons in the Rat." *Journal of Neurophysiology* 83 (4): 2239–59. <https://doi.org/10.1152/jn.2000.83.4.2239>.
- Blix, Magnus. 1882. "Experimentela Bidrag till Losning Af Fragan Om Hudnervernas Specifika Energi." *Uppsala Lakfor. Forh*, no. 18: 87–102.
- Bocarsly, Miriam E., Wan-chen Jiang, Chen Wang, Joshua T. Dudman, Na Ji, and Yeka Aponte. 2015. "Minimally Invasive Microendoscopy System for in Vivo Functional Imaging of Deep Nuclei in the Mouse Brain." *Biomedical Optics Express* 6 (11): 4546. <https://doi.org/10.1364/BOE.6.004546>.
- Bokiniec, Phillip, Clarissa J Whitmire, Tobias M Leva, and James F A Poulet. 2023. "Brain-Wide Connectivity Map of Mouse Thermosensory Cortices." *Cerebral Cortex* 33 (8): 4870–85. <https://doi.org/10.1093/cercor/bhac386>.
- Bokiniec, Phillip, Niccolò Zampieri, Gary R Lewin, and James FA Poulet. 2018. "The Neural Circuits of Thermal Perception." *Current Opinion in Neurobiology* 52 (PLoS Biol 10 2012): 98–106. <https://doi.org/10.1016/j.conb.2018.04.006>.
- Braz, João, Carlos Solorzano, Xidao Wang, and Allan I. Basbaum. 2014. "Transmitting Pain and Itch Messages: A Contemporary View of the Spinal Cord Circuits That Generate Gate Control." *Neuron* 82 (3): 522–36. <https://doi.org/10.1016/j.neuron.2014.01.018>.
- Browne, Tyler J., Kelly M. Smith, Mark A. Gradwell, Jacqueline A. Iredale, Christopher V. Dayas, Robert J. Callister, David I. Hughes, and Brett A. Graham. 2021. "Spinoparabrachial Projection Neurons Form Distinct Classes in the Mouse Dorsal Horn." *Pain* 162 (7): 1977–94. <https://doi.org/10.1097/j.pain.0000000000002194>.
- Bud Craig, A.D. 2014. "Topographically Organized Projection to Posterior Insular Cortex from the Posterior Portion of the Ventral Medial Nucleus in the Long-Tailed Macaque Monkey: VMpo Input to Posterior Insula." *Journal of Comparative Neurology* 522 (1): 36–63. <https://doi.org/10.1002/cne.23425>.
- Bureau, Ingrid, Francisca von Saint Paul, and Karel Svoboda. 2006. "Interdigitated Paralemniscal and Lemniscal Pathways in the Mouse Barrel Cortex." *PLOS Biology* 4 (12): e382. <https://doi.org/10.1371/journal.pbio.0040382>.
- Burton, Harold, Donna J. Forbes, and Robert M. Benjamin. 1970a. "Thalamic Neurons Responsive to Temperature Changes of Glabrous Hand and Foot Skin in Squirrel Monkey." *Brain Research* 24 (2): 179–90. [https://doi.org/10.1016/0006-8993\(70\)90099-5](https://doi.org/10.1016/0006-8993(70)90099-5).
- Burton, Harold, Shin-Ichi Terashima, and Joan Clark. 1972. "Response Properties of Slowly Adapting Mechanoreceptors to Temperature Stimulation in Cats." *Brain Research* 45 (2): 401–16. [https://doi.org/10.1016/0006-8993\(72\)90471-4](https://doi.org/10.1016/0006-8993(72)90471-4).

- C. Stevens Kenneth K. Choo, Joseph. 1998. "Temperature Sensitivity of the Body Surface over the Life Span." *Somatosensory & Motor Research* 15 (1): 13–28. <https://doi.org/10.1080/08990229870925>.
- Casas-Torremocha, Diana, Francisco Clascá, and Ángel Núñez. 2017. "Posterior Thalamic Nucleus Modulation of Tactile Stimuli Processing in Rat Motor and Primary Somatosensory Cortices." *Frontiers in Neural Circuits* 11: 69. <https://doi.org/10.3389/fncir.2017.00069>.
- Casas-Torremocha, Diana, César Porrero, Javier Rodriguez-Moreno, María García-Amado, Joachim H. R. Lübke, Ángel Núñez, and Francisco Clascá. 2019. "Posterior Thalamic Nucleus Axon Terminals Have Different Structure and Functional Impact in the Motor and Somatosensory Vibrissal Cortices." *Brain Structure and Function* 224 (4): 1627–45. <https://doi.org/10.1007/s00429-019-01862-4>.
- Casas-Torremocha, Diana, Mario Rubio-Teves, Anna Hoerder-Suabedissen, Shuichi Hayashi, Lucía Prensa, Zoltán Molnár, Cesar Porrero, and Francisco Clasca. 2022. "A Combinatorial Input Landscape in the 'Higher-Order Relay' Posterior Thalamic Nucleus." *The Journal of Neuroscience*, September, JN-RM-0698-22. <https://doi.org/10.1523/JNEUROSCI.0698-22.2022>.
- Casey, K. L., S. Minoshima, T. J. Morrow, and R. A. Koepp. 1996. "Comparison of Human Cerebral Activation Pattern during Cutaneous Warmth, Heat Pain, and Deep Cold Pain." *Journal of Neurophysiology* 76 (1): 571–81. <https://doi.org/10.1152/jn.1996.76.1.571>.
- Casey, Kenneth L., and Thomas J. Morrow. 1983. "Ventral Posterior Thalamic Neurons Differentially Responsive to Noxious Stimulation of the Awake Monkey." *Science* 221 (4611): 675–77. <https://doi.org/10.1126/science.6867738>.
- Caterina, M. J., M. A. Schumacher, M. Tominaga, T. A. Rosen, J. D. Levine, and D. Julius. 1997. "The Capsaicin Receptor: A Heat-Activated Ion Channel in the Pain Pathway." *Nature* 389 (6653): 816–24. <https://doi.org/10.1038/39807>.
- Caterina, Michael, and Zixuan Pang. 2016. "TRP Channels in Skin Biology and Pathophysiology." *Pharmaceuticals* 9 (4): 77. <https://doi.org/10.3390/ph9040077>.
- Cechetto, David F., David G. Standaert, and Clifford B. Saper. 1985. "Spinal and Trigeminal Dorsal Horn Projections to the Parabrachial Nucleus in the Rat." *The Journal of Comparative Neurology* 240 (2): 153–60. <https://doi.org/10.1002/cne.902400205>.
- Chien, Jui, Anna Korzeniewska, Luana Colloca, Claudia Campbell, Patrick Dougherty, and Frederick Lenz. 2017. "Human Thalamic Somatosensory Nucleus (Ventral Caudal, Vc) as a Locus for Stimulation by INPUTS from Tactile, Noxious and Thermal Sensors on an Active Prosthesis." *Sensors* 17 (6): 1197. <https://doi.org/10.3390/s17061197>.
- Chung, J. M., D. J. Surmeier, K. H. Lee, L. S. Sorkin, C. N. Honda, Y. Tsong, and W. D. Willis. 1986. "Classification of Primate Spinothalamic and Somatosensory Thalamic Neurons Based on Cluster Analysis." *Journal of Neurophysiology* 56 (2): 308–27. <https://doi.org/10.1152/jn.1986.56.2.308>.
- Clasca, Francisco, Alfonso Llamas, and Fernando Reinoso-Suarez. 1997. "Insular Cortex and Neighboring Fields in the Cat: A Redefinition Based on Cortical Microarchitecture and Connections with the Thalamus." *The Journal of Comparative Neurology* 384 (3): 456–82. [https://doi.org/10.1002/\(SICI\)1096-9861\(19970804\)384:3<456::AID-CNE10>3.0.CO;2-H](https://doi.org/10.1002/(SICI)1096-9861(19970804)384:3<456::AID-CNE10>3.0.CO;2-H).
- Corder, Gregory, Biafra Ahanonu, Benjamin F. Grewe, Dong Wang, Mark J. Schnitzer, and Grégory Scherrer. 2019. "An Amygdalar Neural Ensemble That Encodes the

- Unpleasantness of Pain." *Science* 363 (6424): 276–81. <https://doi.org/10.1126/science.aap8586>.
- Cottrell, D. F. 1984. "Conduction Velocity and Axonal Diameter of Alimentary C Fibres." *Quarterly Journal of Experimental Physiology (Cambridge, England)* 69 (2): 355–64. <https://doi.org/10.1113/expphysiol.1984.sp002811>.
- Cragg, B.G., and J.de C. Downer. 1967. "Behavioral Evidence for Cortical Involvement in Manual Temperature Discrimination in the Monkey." *Experimental Neurology* 19 (4): 433–42. [https://doi.org/10.1016/0014-4886\(67\)90163-X](https://doi.org/10.1016/0014-4886(67)90163-X).
- Craig, A. D. (Bud). 2014. "Topographically Organized Projection to Posterior Insular Cortex from the Posterior Portion of the Ventral Medial Nucleus in the Long-Tailed Macaque Monkey: VMpo Input to Posterior Insula." *Journal of Comparative Neurology* 522 (1): 36–63. <https://doi.org/10.1002/cne.23425>.
- Craig, A. D., and M. C. Bushnell. 1994. "The Thermal Grill Illusion: Unmasking the Burn of Cold Pain." *Science* 265 (5169): 252–55. <https://doi.org/10.1126/science.8023144>.
- Craig, A D, M C Bushnell, E -T Zhang, and A Blomqvist. 1994. "A Thalamic Nucleus Specific for Pain and Temperature Sensation." *Nature* 372 (6508): 770–73. <https://doi.org/10.1038/372770a0>.
- Craig, A. D., and J. O. Dostrovsky. 2001. "Differential Projections of Thermoreceptive and Nociceptive Lamina I Trigeminothalamic and Spinothalamic Neurons in the Cat." *Journal of Neurophysiology* 86 (2): 856–70. <https://doi.org/10.1152/jn.2001.86.2.856>.
- Craig, A.D. (Bud). 2003. "PAIN MECHANISMS: Labeled Lines Versus Convergence in Central Processing." *Annual Review of Neuroscience* 26 (1): 1–30. <https://doi.org/10.1146/annurev.neuro.26.041002.131022>.
- Craig, A.D., En-Tan Zhang, and Anders Blomqvist. 1999. "A Distinct Thermoreceptive Subregion of Lamina I in Nucleus Caudalis of the Owl Monkey." *The Journal of Comparative Neurology* 404 (2): 221–34. [https://doi.org/10.1002/\(SICI\)1096-9861\(19990208\)404:2<221::AID-CNE7>3.0.CO;2-N](https://doi.org/10.1002/(SICI)1096-9861(19990208)404:2<221::AID-CNE7>3.0.CO;2-N).
- Dallenbach, Karl M. 1927. "The Temperature Spots and End-Organ." *The American Journal of Psychology* 39 (1/4): 402. <https://doi.org/10.2307/1415426>.
- Dar, Javid Gani, Mir Ajiaz, Ibrahim M. Almanjahie, and Arundhati Warke. 2022. "Estimation of Heat Diffusion in Human Tissue at Adverse Temperatures Using the Cylindrical Form of Bioheat Equation." *Mathematics* 10 (20): 3820. <https://doi.org/10.3390/math10203820>.
- Darian-Smith, I, K O Johnson, and R Dykes. 1973. "'Cold' Fiber Population Innervating Palmar and Digital Skin of the Monkey: Responses to Cooling Pulses." *Journal of Neurophysiology* 36 (2): 325–46. <https://doi.org/10.1152/jn.1973.36.2.325>.
- Darian-Smith, I., K. O. Johnson, C. LaMotte, Y. Shigenaga, P. Kenins, and P. Champness. 1979. "Warm Fibers Innervating Palmar and Digital Skin of the Monkey: Responses to Thermal Stimuli." *Journal of Neurophysiology* 42 (5): 1297–1315. <https://doi.org/10.1152/jn.1979.42.5.1297>.
- Davidson, Steve, Hannah Moser, and Glenn Giesler. 2014. "Ascending Pathways for Itch." In *Itch: Mechanisms and Treatment*, edited by E. Carstens and Tasuku Akiyama. Frontiers in Neuroscience. Boca Raton (FL): CRC Press/Taylor & Francis. <http://www.ncbi.nlm.nih.gov/books/NBK200921/>.
- Davidson, Steve, Hai Truong, and Glenn J. Giesler. 2010. "Quantitative Analysis of Spinothalamic Tract Neurons in Adult and Developing Mouse." *The Journal of Comparative Neurology* 518 (16): 3193–3204. <https://doi.org/10.1002/cne.22392>.

- Davis, J. B., J. Gray, M. J. Gunthorpe, J. P. Hatcher, P. T. Davey, P. Overend, M. H. Harries, et al. 2000. "Vanilloid Receptor-1 Is Essential for Inflammatory Thermal Hyperalgesia." *Nature* 405 (6783): 183–87. <https://doi.org/10.1038/35012076>.
- Davis, Karen D., Chun L. Kwan, Adrian P. Crawley, and David J. Mikulis. 1998. "Functional MRI Study of Thalamic and Cortical Activations Evoked by Cutaneous Heat, Cold, and Tactile Stimuli." *Journal of Neurophysiology* 80 (3): 1533–46. <https://doi.org/10.1152/jn.1998.80.3.1533>.
- Deschênes, Martin, Pierre Veinante, and Zhong-Wei Zhang. 1998. "The Organization of Corticothalamic Projections: Reciprocity versus Parity." *Brain Research Reviews* 28 (3): 286–308. [https://doi.org/10.1016/S0165-0173\(98\)00017-4](https://doi.org/10.1016/S0165-0173(98)00017-4).
- Diamond, Mathew E., Michael Armstrong-James, and Ford F. Ebner. 1992a. "Somatic Sensory Responses in the Rostral Sector of the Posterior Group (POm) and in the Ventral Posterior Medial Nucleus (VPM) of the Rat Thalamus." *Journal of Comparative Neurology* 318 (4): 462–76. <https://doi.org/10.1002/cne.903180410>.
- Duclaux, R., and Sr. Kenshalo Dr. 1980. "Response Characteristics of Cutaneous Warm Receptors in the Monkey." *Journal of Neurophysiology* 43 (1): 1–15. <https://doi.org/10.1152/jn.1980.43.1.1>.
- Duncan, G. H., M. C. Bushnell, J. L. Oliveras, N. Bastrash, and N. Tremblay. 1993. "Thalamic VPM Nucleus in the Behaving Monkey. III. Effects of Reversible Inactivation by Lidocaine on Thermal and Mechanical Discrimination." *Journal of Neurophysiology* 70 (5): 2086–96. <https://doi.org/10.1152/jn.1993.70.5.2086>.
- Egan, Gary F., John Johnson, Michael Farrell, Robin McAllen, Frank Zamarripa, Michael J. McKinley, Jack Lancaster, Derek Denton, and Peter T. Fox. 2005. "Cortical, Thalamic, and Hypothalamic Responses to Cooling and Warming the Skin in Awake Humans: A Positron-Emission Tomography Study." *Proceedings of the National Academy of Sciences* 102 (14): 5262–67. <https://doi.org/10.1073/pnas.0409753102>.
- El-Boustani, Sami, B. Semihcan Sermet, Georgios Foustoukos, Tess B. Oram, Ofer Yizhar, and Carl C. H. Petersen. 2020. "Anatomically and Functionally Distinct Thalamocortical Inputs to Primary and Secondary Mouse Whisker Somatosensory Cortices." *Nature Communications* 11 (1): 3342. <https://doi.org/10.1038/s41467-020-17087-7>.
- Emanuel, Alan J., Brendan P. Lehnert, Stefano Panzeri, Christopher D. Harvey, and David D. Ginty. 2021. "Cortical Responses to Touch Reflect Subcortical Integration of LTMR Signals." *Nature* 600 (7890): 680–85. <https://doi.org/10.1038/s41586-021-04094-x>.
- Ezquerra-Romano, Ivan, and Ángel Martínez. 2016. "Highway to Thermosensation: A Traced Review, from the Proteins to the Brain." *Reviews in the Neurosciences* 28 (January). <https://doi.org/10.1515/revneuro-2016-0039>.
- Feldman, Sanford G., and Lawrence Kruger. 1980. "An Axonal Transport Study of the Ascending Projection of Medial Lemniscal Neurons in the Rat." *Journal of Comparative Neurology* 192 (3): 427–54. <https://doi.org/10.1002/cne.901920305>.
- Ferrandiz-Huertas, Clotilde, Sakthikumar Mathivanan, Christoph Wolf, Isabel Devesa, and Antonio Ferrer-Montiel. 2014. "Trafficking of ThermoTRP Channels." *Membranes* 4 (3): 525–64. <https://doi.org/10.3390/membranes4030525>.
- Finger, Stanley, and Gabriel P Frommer. 1970. "Effects of Cortical and Thalamic Lesions on Temperature Discrimination and Responsiveness to Foot Shock in the Rat." *Brain Research* 24 (1): 69–89. [https://doi.org/10.1016/0006-8993\(70\)90274-x](https://doi.org/10.1016/0006-8993(70)90274-x).

- Fitzmaurice, Marnie C., Vivian M. Ciaramitaro, Larry A. Palmer, and Alan C. Rosenquist. 2003. "Visual Detection Deficits Following Inactivation of the Superior Colliculus in the Cat." *Visual Neuroscience* 20 (6): 687–701. <https://doi.org/10.1017/S095252380320609X>.
- Francis, Joseph T, Shaohua Xu, and John K Chapin. 2008a. "Proprioceptive and Cutaneous Representations in the Rat Ventral Posterolateral Thalamus." *Journal of Neurophysiology* 99 (5): 2291–2304. <https://doi.org/10.1152/jn.01206.2007>.
- Francis, Joseph T., Shaohua Xu, and John K. Chapin. 2008b. "Proprioceptive and Cutaneous Representations in the Rat Ventral Posterolateral Thalamus." *Journal of Neurophysiology* 99 (5): 2291–2304. <https://doi.org/10.1152/jn.01206.2007>.
- Gauriau, Caroline, and Jean-François Bernard. 2004a. "Posterior Triangular Thalamic Neurons Convey Nociceptive Messages to the Secondary Somatosensory and Insular Cortices in the Rat." *Journal of Neuroscience* 24 (3): 752–61. <https://doi.org/10.1523/jneurosci.3272-03.2004>.
- Gauriau, Caroline, and Jean-François Bernard. 2004b. "A Comparative Reappraisal of Projections from the Superficial Laminae of the Dorsal Horn in the Rat: The Forebrain." *The Journal of Comparative Neurology* 468 (1): 24–56. <https://doi.org/10.1002/cne.10873>.
- Gehrlich, Daniel A, Caroline Weiand, Thomas N Gaitanos, Eunjae Cho, Alexandra S Klein, Alexandru A Hennrich, Karl-Klaus Conzelmann, and Nadine Gogolla. 2020. "A Whole-Brain Connectivity Map of Mouse Insular Cortex." *eLife* 9 (September): e55585. <https://doi.org/10.7554/eLife.55585>.
- Gentle, Michael J. 1989. "Cutaneous Sensory Afferents Recorded from the Nervus Intramandibularis of Gallus Gallus Vardomesticus." *Journal of Comparative Physiology A* 164 (6): 763–74. <https://doi.org/10.1007/BF00616748>.
- Giuffrida, R., and A. Rustioni. 1992. "Dorsal Root Ganglion Neurons Projecting to the Dorsal Column Nuclei of Rats." *The Journal of Comparative Neurology* 316 (2): 206–20. <https://doi.org/10.1002/cne.903160206>.
- Gollo, Leonardo L. 2017. "Coexistence of Critical Sensitivity and Subcritical Specificity Can Yield Optimal Population Coding." *Journal of The Royal Society Interface* 14 (134): 20170207. <https://doi.org/10.1098/rsif.2017.0207>.
- Goodale, Melvyn A., and A. David Milner. 1992. "Separate Visual Pathways for Perception and Action." *Trends in Neurosciences* 15 (1): 20–25. [https://doi.org/10.1016/0166-2236\(92\)90344-8](https://doi.org/10.1016/0166-2236(92)90344-8).
- Gordon, Christopher J. 2017. "The Mouse Thermoregulatory System: Its Impact on Translating Biomedical Data to Humans." *Physiology & Behavior* 179 (October): 55–66. <https://doi.org/10.1016/j.physbeh.2017.05.026>.
- Gottschlich, K -W, and J Werner. 1985. "Effects of Medial Midbrain Lesions on Thermoresponsive Neurons in the Thalamus of the Rat." *Experimental Brain Research* 57 (2): 355–61. <https://doi.org/10.1007/bf00236541>.
- Green, Barry G. 2004. "Temperature Perception and Nociception." *Journal of Neurobiology* 61 (1): 13–29. <https://doi.org/10.1002/neu.20081>.
- Guest, Steve, Fabian Grabenhorst, Greg Essick, Yasheng Chen, Mike Young, Francis McGlone, Ivan De Araujo, and Edmund T. Rolls. 2007. "Human Cortical Representation of Oral Temperature." *Physiology & Behavior* 92 (5): 975–84. <https://doi.org/10.1016/j.physbeh.2007.07.004>.
- Güler, Ali Deniz, Hyosang Lee, Tohko Iida, Isao Shimizu, Makoto Tominaga, and Michael Caterina. 2002. "Heat-Evoked Activation of the Ion Channel, TRPV4." *The Journal of*

- Neuroscience: The Official Journal of the Society for Neuroscience* 22 (15): 6408–14. <https://doi.org/10.1523/JNEUROSCI.22-15-06408.2002>.
- Guo, Zengcai V., Hidehiko K. Inagaki, Kayvon Daie, Shaul Druckmann, Charles R. Gerfen, and Karel Svoboda. 2017. "Maintenance of Persistent Activity in a Frontal Thalamocortical Loop." *Nature* 545 (7653): 181–86. <https://doi.org/10.1038/nature22324>.
- Hachisuka, Junichi, H. Richard Koerber, and Sarah E. Ross. 2019. "A Labeled-Line for Cold from the Periphery to the Parabrachial Nucleus." Preprint. Neuroscience. <https://doi.org/10.1101/633115>.
- Halassa, Michael M. 2023. *The Thalamus*. Cambridge, United Kingdom: Cambridge university press.
- Hallin, R G, H E Torebjork, and Z Wiesenfeld. 1982. "Nociceptors and Warm Receptors Innervated by C Fibres in Human Skin." *Journal of Neurology, Neurosurgery & Psychiatry* 45 (4): 313–19. <https://doi.org/10.1136/jnnp.45.4.313>.
- Harper, A A, and S N Lawson. 1985. "Conduction Velocity Is Related to Morphological Cell Type in Rat Dorsal Root Ganglion Neurones." *The Journal of Physiology* 359 (February): 31–46.
- Hayes, Dave J., and Georg Northoff. 2012. "Common Brain Activations for Painful and Non-Painful Aversive Stimuli." *BMC Neuroscience* 13 (June): 60. <https://doi.org/10.1186/1471-2202-13-60>.
- Hellon, R F, and N K Misra. 1973. "Neurones in the Ventrobasal Complex of the Rat Thalamus Responding to Scrotal Skin Temperature Changes." *The Journal of Physiology* 232 (2): 389–99. <https://doi.org/10.1113/jphysiol.1973.sp010276>.
- Hellon, R. F., and David C. M. Taylor. 1982. "An Analysis of a Thermal Afferent Pathway in the Rat." *The Journal of Physiology* 326 (1): 319–28. <https://doi.org/10.1113/jphysiol.1982.sp014195>.
- Hensel, H., and K. Schafer. 1984. "Thermoreception and Temperature Regulation in Man." In *Recent Advances in Medical Thermology*, edited by E. Francis J. Ring and Barbara Phillips, 51–64. Boston, MA: Springer New York. https://doi.org/10.1007/978-1-4684-7697-2_8.
- Hodge, C. J., and A. V. Apkarian. 1990. "The Spinothalamic Tract." *Critical Reviews in Neurobiology* 5 (4): 363–97.
- Hong, Y. Kate, Clay O. Lacefield, Chris C. Rodgers, and Randy M. Bruno. 2018. "Sensation, Movement and Learning in the Absence of Barrel Cortex." *Nature* 561 (7724): 542–46. <https://doi.org/10.1038/s41586-018-0527-y>.
- Huh, Yeowool, and Jeiwon Cho. 2013. "Urethane Anesthesia Depresses Activities of Thalamocortical Neurons and Alters Its Response to Nociception in Terms of Dual Firing Modes." *Frontiers in Behavioral Neuroscience* 7. <https://doi.org/10.3389/fnbeh.2013.00141>.
- Hylden, J.L.K., F. Anton, and R.L. Nahin. 1989. "Spinal Lamina I Projection Neurons in the Rat: Collateral Innervation of Parabrachial Area and Thalamus." *Neuroscience* 28 (1): 27–37. [https://doi.org/10.1016/0306-4522\(89\)90229-7](https://doi.org/10.1016/0306-4522(89)90229-7).
- Jahns, R. 1975. "Types of Neuronal Responses in the Rat Thalamus to Peripheral Temperature Changes." *Experimental Brain Research* 23 (2). <https://doi.org/10.1007/BF00235458>.
- Jones, E. G. 1981. "Functional Subdivision and Synaptic Organization of the Mammalian Thalamus." *International Review of Physiology* 25: 173–245.
- Jones, Edward G., ed. 1985. *The Thalamus*. Boston, MA: Springer US. <https://doi.org/10.1007/978-1-4615-1749-8>.

- Jun, James J., Nicholas A. Steinmetz, Joshua H. Siegle, Daniel J. Denman, Marius Bauza, Brian Barbarits, Albert K. Lee, et al. 2017. "Fully Integrated Silicon Probes for High-Density Recording of Neural Activity." *Nature* 551 (7679): 232–36. <https://doi.org/10.1038/nature24636>.
- Kandel, Eric R., John Koester, Sarah Mack, and Steven Siegelbaum, eds. 2021. *Principles of Neural Science*. Sixth edition. New York: McGraw Hill.
- Kanosue, Kazuyuki, Teruo Nakayama, Youzou Ishikawa, Takayoshi Hosono, Tatsuro Kaminaga, and Akira Shosaku. 1985. "Responses of Thalamic and Hypothalamic Neurons to Scrotal Warming in Rats: Non-Specific Responses?" *Brain Research* 328 (2): 207–13. [https://doi.org/10.1016/0006-8993\(85\)91031-5](https://doi.org/10.1016/0006-8993(85)91031-5).
- Karashima, Yuji, Karel Talavera, Wouter Everaerts, Annelies Janssens, Kelvin Y. Kwan, Rudi Vennekens, Bernd Nilius, and Thomas Voets. 2009. "TRPA1 Acts as a Cold Sensor in Vitro and in Vivo." *Proceedings of the National Academy of Sciences of the United States of America* 106 (4): 1273–78. <https://doi.org/10.1073/pnas.0808487106>.
- Katanosaka, Kimiaki, Satomi Takatsu, Kazue Mizumura, Keiji Naruse, and Yuki Katanosaka. 2018. "TRPV2 Is Required for Mechanical Nociception and the Stretch-Evoked Response of Primary Sensory Neurons." *Scientific Reports* 8 (November): 16782. <https://doi.org/10.1038/s41598-018-35049-4>.
- Kenshalo, D. R., and R. Duclaux. 1977. "Response Characteristics of Cutaneous Cold Receptors in the Monkey." *Journal of Neurophysiology* 40 (2): 319–32. <https://doi.org/10.1152/jn.1977.40.2.319>.
- Kenshalo, D. R., G. J. Giesler, R. B. Leonard, and W. D. Willis. 1980. "Responses of Neurons in Primate Ventral Posterior Lateral Nucleus to Noxious Stimuli." *Journal of Neurophysiology* 43 (6): 1594–1614. <https://doi.org/10.1152/jn.1980.43.6.1594>.
- Kimura, A., H. Imbe, and T. Donishi. 2010. "Efferent Connections of an Auditory Area in the Caudal Insular Cortex of the Rat: Anatomical Nodes for Cortical Streams of Auditory Processing and Cross-Modal Sensory Interactions." *Neuroscience* 166 (4): 1140–57. <https://doi.org/10.1016/j.neuroscience.2010.01.032>.
- Knowlton, Wendy M., Amber Fisher, Diana M. Bautista, and David D. McKemy. 2010. "TRPM8, but Not TRPA1, Is Required for Neural and Behavioral Responses to Acute Noxious Cold Temperatures and Cold-Mimetics in Vivo." *Pain* 150 (2): 340–50. <https://doi.org/10.1016/j.pain.2010.05.021>.
- Kobayashi, Shigeo. 2015. "Temperature Receptors in Cutaneous Nerve Endings Are Thermostat Molecules That Induce Thermoregulatory Behaviors against Thermal Load." *Temperature: Multidisciplinary Biomedical Journal* 2 (3): 346–51. <https://doi.org/10.1080/23328940.2015.1039190>.
- Kumazawa, T., and E. R. Perl. 1978. "Excitation of Marginal and Substantia Gelatinosa Neurons in the Primate Spinal Cord: Indications of Their Place in Dorsal Horn Functional Organization." *The Journal of Comparative Neurology* 177 (3): 417–34. <https://doi.org/10.1002/cne.901770305>.
- Kumazawa, T., E. R. Perl, P. R. Burgess, and D. Whitehorn. 1975. "Ascending Projections from Marginal Zone (Lamina I) Neurons of the Spinal Dorsal Horn." *The Journal of Comparative Neurology* 162 (1): 1–11. <https://doi.org/10.1002/cne.901620102>.
- Lamas, J. Antonio, Lola Rueda-Ruzafa, and Salvador Herrera-Pérez. 2019. "Ion Channels and Thermosensitivity: TRP, TREK, or Both?" *International Journal of Molecular Sciences* 20 (10): 2371. <https://doi.org/10.3390/ijms20102371>.

- Leem, J. W., W. D. Willis, and J. M. Chung. 1993. "Cutaneous Sensory Receptors in the Rat Foot." *Journal of Neurophysiology* 69 (5): 1684–99. <https://doi.org/10.1152/jn.1993.69.5.1684>.
- Lerner, Talia N., Carrie Shilyansky, Thomas J. Davidson, Kathryn E. Evans, Kevin T. Beier, Kelly A. Zalocusky, Ailey K. Crow, et al. 2015. "Intact-Brain Analyses Reveal Distinct Information Carried by SNC Dopamine Subcircuits." *Cell* 162 (3): 635–47. <https://doi.org/10.1016/j.cell.2015.07.014>.
- Li, Jinlian, Kanghui Xiong, Youwang Pang, Yulin Dong, Takeshi Kaneko, and Noboru Mizuno. 2006. "Medullary Dorsal Horn Neurons Providing Axons to Both the Parabrachial Nucleus and Thalamus." *The Journal of Comparative Neurology* 498 (4): 539–51. <https://doi.org/10.1002/cne.21068>.
- Liao, Chia-Chi, and Chen-Tung Yen. 2008. "Functional Connectivity of the Secondary Somatosensory Cortex of the Rat." *Anatomical Record (Hoboken, N.J.: 2007)* 291 (8): 960–73. <https://doi.org/10.1002/ar.20696>.
- Light, A. R., and E. R. Perl. 1979. "Spinal Termination of Functionally Identified Primary Afferent Neurons with Slowly Conducting Myelinated Fibers." *The Journal of Comparative Neurology* 186 (2): 133–50. <https://doi.org/10.1002/cne.901860203>.
- Lipshetz, Brett, Sergey G. Khasabov, Hai Truong, Theoden I. Netoff, Donald A. Simone, and Glenn J. Giesler. 2018. "Responses of Thalamic Neurons to Itch- and Pain-Producing Stimuli in Rats." *Journal of Neurophysiology* 120 (3): 1119–34. <https://doi.org/10.1152/jn.00264.2018>.
- Lomber, Stephen G. 1999. "The Advantages and Limitations of Permanent or Reversible Deactivation Techniques in the Assessment of Neural Function." *Journal of Neuroscience Methods* 86 (2): 109–17. [https://doi.org/10.1016/S0165-0270\(98\)00160-5](https://doi.org/10.1016/S0165-0270(98)00160-5).
- Luo, Maohui, Zhe Wang, Hui Zhang, Edward Arens, Davide Filingeri, Ling Jin, Ali Ghahramani, Wenhua Chen, Yingdong He, and Binghui Si. 2020. "High-Density Thermal Sensitivity Maps of the Human Body." *Building and Environment* 167 (January): 106435. <https://doi.org/10.1016/j.buildenv.2019.106435>.
- Ma, Qiufu. 2010. "Labeled Lines Meet and Talk: Population Coding of Somatic Sensations." *The Journal of Clinical Investigation* 120 (11): 3773–78. <https://doi.org/10.1172/JCI43426>.
- Maksymchuk, Natalia, Akira Sakurai, Daniel N. Cox, and Gennady Cymbalyuk. 2022. "Transient and Steady-State Properties of Drosophila Sensory Neurons Coding Noxious Cold Temperature." *Frontiers in Cellular Neuroscience* 16. <https://www.frontiersin.org/articles/10.3389/fncel.2022.831803>.
- Mantyh, Patrick W. 1983. "The Terminations of the Spinothalamic Tract in the Cat." *Neuroscience Letters* 38 (2): 119–24. [https://doi.org/10.1016/0304-3940\(83\)90027-7](https://doi.org/10.1016/0304-3940(83)90027-7).
- Marics, Irène, Pascale Malapert, Ana Reynders, Stéphane Gaillard, and Aziz Moqrich. 2014. "Acute Heat-Evoked Temperature Sensation Is Impaired but Not Abolished in Mice Lacking TRPV1 and TRPV3 Channels." *PLoS ONE* 9 (6): e99828. <https://doi.org/10.1371/journal.pone.0099828>.
- Márquez-Legorreta, Emmanuel, José de Ancheta C. Horta-Júnior, Albert S. Berrebi, and Enrique Saldaña. 2016. "Organization of the Zone of Transition between the Pretectum and the Thalamus, with Emphasis on the Prepectothalamic Lamina." *Frontiers in Neuroanatomy* 10. <https://www.frontiersin.org/articles/10.3389/fnana.2016.00082>.

- Martin, Henry F, and John W Manning. 1971. "Thalamic 'Warming' and 'Cooling' Units Responding to Cutaneous Stimulation." *Brain Research* 27 (2): 377–81. [https://doi.org/10.1016/0006-8993\(71\)90265-4](https://doi.org/10.1016/0006-8993(71)90265-4).
- McAllister, J. P., and J. Wells. 1981. "The Structural Organization of the Ventral Posterolateral Nucleus in the Rat." *The Journal of Comparative Neurology* 197 (2): 271–301. <https://doi.org/10.1002/cne.901970208>.
- Mease, Rebecca A., and Antonio J. Gonzalez. 2021. "Corticothalamic Pathways From Layer 5: Emerging Roles in Computation and Pathology." *Frontiers in Neural Circuits* 15 (September): 730211. <https://doi.org/10.3389/fncir.2021.730211>.
- Meyers, D. E., and P. J. Snow. 1986. "Distribution of Activity in the Spinal Terminations of Single Hair Follicle Afferent Fibers to Somatotopically Identified Regions of the Cat Spinal Cord." *Journal of Neurophysiology* 56 (4): 1022–38. <https://doi.org/10.1152/jn.1986.56.4.1022>.
- Milenkovic, Nevena, Wen-Jie Zhao, Jan Walcher, Tobias Albert, Jan Siemens, Gary R Lewin, and James F A Poulet. 2014. "A Somatosensory Circuit for Cooling Perception in Mice." *Nature Neuroscience* 17 (11): 1560–66. <https://doi.org/10.1038/nn.3828>.
- Miyashita, Toshio, and Daniel E. Feldman. 2013. "Behavioral Detection of Passive Whisker Stimuli Requires Somatosensory Cortex." *Cerebral Cortex* 23 (7): 1655–62. <https://doi.org/10.1093/cercor/bhs155>.
- Mo, Christina, Iraklis Petrof, Angela N. Viaene, and S. Murray Sherman. 2017. "Synaptic Properties of the Lemniscal and Paralemniscal Pathways to the Mouse Somatosensory Thalamus." *Proceedings of the National Academy of Sciences* 114 (30): E6212–21. <https://doi.org/10.1073/pnas.1703222114>.
- Moqrich, Aziz, Sun Wook Hwang, Taryn J. Earley, Matt J. Petrus, Amber N. Murray, Kathryn S. R. Spencer, Mary Andahazy, Gina M. Story, and Ardem Patapoutian. 2005. "Impaired Thermosensation in Mice Lacking TRPV3, a Heat and Camphor Sensor in the Skin." *Science (New York, N.Y.)* 307 (5714): 1468–72. <https://doi.org/10.1126/science.1108609>.
- Muniak, Michael A., Supratim Ray, Steven S. Hsiao, J. Frank Dammann, and Sliman J. Bensmaia. 2007. "The Neural Coding of Stimulus Intensity: Linking the Population Response of Mechanoreceptive Afferents with Psychophysical Behavior." *The Journal of Neuroscience* 27 (43): 11687–99. <https://doi.org/10.1523/JNEUROSCI.1486-07.2007>.
- Nakamura, Kazuhiro, and Shaun F Morrison. 2008. "A Thermosensory Pathway That Controls Body Temperature." *Nature Neuroscience* 11 (1): 62–71. <https://doi.org/10.1038/nn2027>.
- Nakamura, Kazuhiro, and Shaun F. Morrison. 2010. "A Thermosensory Pathway Mediating Heat-Defense Responses." *Proceedings of the National Academy of Sciences* 107 (19): 8848–53. <https://doi.org/10.1073/pnas.0913358107>.
- Necker, R., and C. C. Meinecke. 1984. "Conduction Velocities and Fiber Diameters in a Cutaneous Nerve of the Pigeon." *Journal of Comparative Physiology A* 154 (6): 817–24. <https://doi.org/10.1007/BF00610682>.
- Neugebauer, Volker, and Weidong Li. 2002. "Processing of Nociceptive Mechanical and Thermal Information in Central Amygdala Neurons With Knee-Joint Input." *Journal of Neurophysiology* 87 (1): 103–12. <https://doi.org/10.1152/jn.00264.2001>.
- Norrsell, U., and A. D. Craig. 1999. "Behavioral Thermosensitivity After Lesions of Thalamic Target Areas of a Thermosensory Spinothalamic Pathway in the Cat." *Journal of Neurophysiology* 82 (2): 611–25. <https://doi.org/10.1152/jn.1999.82.2.611>.

- Ocobock, Cara. 2016. "Human Energy Expenditure, Allocation, and Interactions in Natural Temperate, Hot, and Cold Environments." *American Journal of Physical Anthropology* 161 (4): 667–75. <https://doi.org/10.1002/ajpa.23071>.
- Otchy, Timothy M., Steffen B. E. Wolff, Juliana Y. Rhee, Cengiz Pehlevan, Risa Kawai, Alexandre Kempf, Sharon M. H. Gobes, and Bence P. Ölveczky. 2015. "Acute Off-Target Effects of Neural Circuit Manipulations." *Nature* 528 (7582): 358–63. <https://doi.org/10.1038/nature16442>.
- Pachitariu, Marius, Shashwat Sridhar, and Carsen Stringer. 2023. "Solving the Spike Sorting Problem with Kilosort." Preprint. Neuroscience. <https://doi.org/10.1101/2023.01.07.523036>.
- Pack, Andrea R., Max D. Murphy, Scott Barbay, Randolph J. Nudo, and David J. Guggenmos. 2020. "Task Related Neural Activity Following Primary Motor Cortical Ischemic Injury in Rats." Preprint. Neuroscience. <https://doi.org/10.1101/2020.06.11.146266>.
- Paricio-Montesinos, Ricardo. n.d. "The Sensory Coding of Warm Perception."
- Paricio-Montesinos, Ricardo, Frederick Schwaller, Annapoorani Udhayachandran, Florian Rau, Jan Walcher, Roberta Evangelista, Joris Vriens, Thomas Voets, James F.A. Poulet, and Gary R. Lewin. 2020. "The Sensory Coding of Warm Perception." *Neuron* 106 (5): 830–841.e3. <https://doi.org/10.1016/j.neuron.2020.02.035>.
- Park, Una, Nisha Vastani, Yun Guan, Srinivasa N. Raja, Martin Koltzenburg, and Michael J. Caterina. 2011. "TRP Vanilloid 2 Knock-Out Mice Are Susceptible to Perinatal Lethality But Display Normal Thermal and Mechanical Nociception." *The Journal of Neuroscience* 31 (32): 11425–36. <https://doi.org/10.1523/JNEUROSCI.1384-09.2011>.
- PENFIELD, WILDER, and EDWIN BOLDREY. 1937. "SOMATIC MOTOR AND SENSORY REPRESENTATION IN THE CEREBRAL CORTEX OF MAN AS STUDIED BY ELECTRICAL STIMULATION1." *Brain* 60 (4): 389–443. <https://doi.org/10.1093/brain/60.4.389>.
- Ploner, M., H.-J. Freund, and A. Schnitzler. 1999. "Pain Affect without Pain Sensation in a Patient with a Postcentral Lesion." *Pain* 81 (1): 211–14. [https://doi.org/10.1016/S0304-3959\(99\)00012-3](https://doi.org/10.1016/S0304-3959(99)00012-3).
- Prescott, Steven A., Qiufu Ma, and Yves De Koninck. 2014. "Normal and Abnormal Coding of Somatosensory Stimuli Causing Pain." *Nature Neuroscience* 17 (2): 183–91. <https://doi.org/10.1038/nn.3629>.
- Raithel, Stephen J., Matthew R. Sapiro, Michael J. Iadarola, and Andrew J. Mannes. 2018. "Thermal A-δ Nociceptors, Identified by Transcriptomics, Express Higher Levels of Anesthesia-Sensitive Receptors Than Thermal C-Fibers and Are More Suppressible by Low-Dose Isoflurane." *Anesthesia & Analgesia* 127 (1): 263–66. <https://doi.org/10.1213/ANE.0000000000002505>.
- Ralston, H. J., and D. D. Ralston. 1994. "Medial Lemniscal and Spinal Projections to the Macaque Thalamus: An Electron Microscopic Study of Differing GABAergic Circuitry Serving Thalamic Somatosensory Mechanisms." *The Journal of Neuroscience: The Official Journal of the Society for Neuroscience* 14 (5 Pt 1): 2485–2502. <https://doi.org/10.1523/JNEUROSCI.14-05-02485.1994>.
- Ramsey, I. Scott, Markus Delling, and David E. Clapham. 2006. "AN INTRODUCTION TO TRP CHANNELS." *Annual Review of Physiology* 68 (1): 619–47. <https://doi.org/10.1146/annurev.physiol.68.040204.100431>.
- Ran, Chen, Mark A Hoon, and Xiaoke Chen. 2016a. "The Coding of Cutaneous Temperature in the Spinal Cord." *Nature Neuroscience* 19 (9): 1201–9. <https://doi.org/10.1038/nn.4350>.

- Reimann, Henning Matthias, Jan Hentschel, Jaroslav Marek, Till Huelnhagen, Mihail Todiras, Stefanie Kox, Sonia Waiczies, et al. 2016. "Normothermic Mouse Functional MRI of Acute Focal Thermostimulation for Probing Nociception." *Scientific Reports* 6 (1): 17230. <https://doi.org/10.1038/srep17230>.
- Rikhye, Rajeev V., Ralf D. Wimmer, and Michael M. Halassa. 2018. "Toward an Integrative Theory of Thalamic Function." *Annual Review of Neuroscience* 41 (1): 163–83. <https://doi.org/10.1146/annurev-neuro-080317-062144>.
- Rodríguez de Rivera, Pedro Jesús, Miriam Rodríguez de Rivera, Fabiola Socorro, and Manuel Rodríguez de Rivera. 2022. "Heat Flow Measurement of Human Skin Using a Calorimetric Sensor with a Programmable Thermostat. An Alternative to Climate Chambers." *Measurement* 201 (September): 111693. <https://doi.org/10.1016/j.measurement.2022.111693>.
- Rodriguez-Moreno, Javier, Astrid Rollenhagen, Jaime Arlandis, Andrea Santuy, Angel Merchán-Pérez, Javier DeFelipe, Joachim H R Lübke, and Francisco Clasca. 2018. "Quantitative 3D Ultrastructure of Thalamocortical Synapses from the 'Lemniscal' Ventral Posteromedial Nucleus in Mouse Barrel Cortex." *Cerebral Cortex* 28 (9): 3159–75. <https://doi.org/10.1093/cercor/bhx187>.
- Roy, Dheeraj S., Ying Zhang, Michael M. Halassa, and Guoping Feng. 2022. "Thalamic Subnetworks as Units of Function." *Nature Neuroscience* 25 (2): 140–53. <https://doi.org/10.1038/s41593-021-00996-1>.
- Sakata, Y., A. Morimoto, and N. Murakami. 1989. "Responses of Thalamic Neurons in Rats to Skin Cooling and Hypothalamic Temperature." *American Journal of Physiology-Regulatory, Integrative and Comparative Physiology* 256 (6): R1293–98. <https://doi.org/10.1152/ajpregu.1989.256.6.R1293>.
- Sampathkumar, Vandana, Andrew Miller-Hansen, S. Murray Sherman, and Narayanan Kasthuri. 2021. "Integration of Signals from Different Cortical Areas in Higher Order Thalamic Neurons." *Proceedings of the National Academy of Sciences* 118 (30): e2104137118. <https://doi.org/10.1073/pnas.2104137118>.
- Sanganahalli, Basavaraju G., Garth J. Thompson, Maxime Parent, Justus V. Verhagen, Hal Blumenfeld, Peter Herman, and Fahmeed Hyder. 2022. "Thalamic Activations in Rat Brain by fMRI during Tactile (Forepaw, Whisker) and Non-Tactile (Visual, Olfactory) Sensory Stimulations." Edited by Yen-Yu Ian Shih. *PLOS ONE* 17 (5): e0267916. <https://doi.org/10.1371/journal.pone.0267916>.
- Saper, Clifford B. 1995. "The Spinoparabrachial Pathway: Shedding New Light on an Old Path." *The Journal of Comparative Neurology* 353 (4): 477–79. <https://doi.org/10.1002/cne.903530402>.
- Sawatari, Hiroyuki, Yoshihide Tanaka, Makoto Takemoto, Masataka Nishimura, Kayoko Hasegawa, Kazuya Saitoh, and Wen-Jie Song. 2011. "Identification and Characterization of an Insular Auditory Field in Mice: Insular Auditory Field in Mice." *European Journal of Neuroscience* 34 (12): 1944–52. <https://doi.org/10.1111/j.1460-9568.2011.07926.x>.
- Schingnitz, G, and J Werner. 1980. "Thalamic Burst Firing — a Neuronal Code for Temperature Information?" *Brain Research* 195 (2): 467–70. [https://doi.org/10.1016/0006-8993\(80\)90081-5](https://doi.org/10.1016/0006-8993(80)90081-5).
- Schingnitz, Günter, and Jürgen Werner. 1980a. "Responses of Thalamic Neurons to Thermal Stimulation of the Limbs, Scrotum and Tongue in the Rat." *Journal of Thermal Biology* 5 (1): 53–61. [https://doi.org/10.1016/0306-4565\(80\)90040-6](https://doi.org/10.1016/0306-4565(80)90040-6).

- Schröder, Hannsjörg, Natasha Moser, and Stefan Huggenberger. 2020. *Neuroanatomy of the Mouse: An Introduction*. Cham: Springer.
- Shamash, Philip, Matteo Carandini, Kenneth D Harris, and Nicholas A Steinmetz. 2018. "A Tool for Analyzing Electrode Tracks from Slice Histology." Preprint. Neuroscience. <https://doi.org/10.1101/447995>.
- Sherman, S. Murray. 2005. "Thalamic Relays and Cortical Functioning." *Progress in Brain Research* 149: 107–26. [https://doi.org/10.1016/S0079-6123\(05\)49009-3](https://doi.org/10.1016/S0079-6123(05)49009-3).
- Sherman, S Murray. 2016. "Thalamus Plays a Central Role in Ongoing Cortical Functioning." *Nature Neuroscience* 19 (4): 533–41. <https://doi.org/10.1038/nn.4269>.
- Sherman, S. Murray, and R. W. Guillery. 2001. *Exploring the Thalamus*. San Diego: Academic Press.
- Sherman, Stephen E, Lei Luo, and Jonathan O Dostrovsky. 1997. "Altered Receptive Fields and Sensory Modalities of Rat VPL Thalamic Neurons During Spinal Strychnine-Induced Allodynia." *Journal of Neurophysiology* 78 (5): 2296–2308. <https://doi.org/10.1152/jn.1997.78.5.2296>.
- Siegle, Joshua H, Xiaoxuan Jia, Séverine Durand, Sam Gale, Corbett Bennett, Nile Graddis, Greggory Heller, et al. 2019. "A Survey of Spiking Activity Reveals a Functional Hierarchy of Mouse Corticothalamic Visual Areas." *bioRxiv*, 805010. <https://doi.org/10.1101/805010>.
- Silverman, Harold A., Adrian Chen, Nigel L. Kravatz, Sangeeta S. Chavan, and Eric H. Chang. 2020. "Involvement of Neural Transient Receptor Potential Channels in Peripheral Inflammation." *Frontiers in Immunology* 11 (October): 590261. <https://doi.org/10.3389/fimmu.2020.590261>.
- Slonina, Zuzanna A., Katarina C. Poole, and Jennifer K. Bizley. 2022. "What Can We Learn from Inactivation Studies? Lessons from Auditory Cortex." *Trends in Neurosciences* 45 (1): 64–77. <https://doi.org/10.1016/j.tins.2021.10.005>.
- Song, K., H. Wang, G. B. Kamm, J. Pohle, F. D. C. Reis, P. Heppenstall, H. Wende, and J. Siemens. 2016. "The TRPM2 Channel Is a Hypothalamic Heat Sensor That Limits Fever and Can Drive Hypothermia." *Science* 353 (6306): 1393–98. <https://doi.org/10.1126/science.aaf7537>.
- Staiger, Jochen F., and Carl C. H. Petersen. 2021. "Neuronal Circuits in Barrel Cortex for Whisker Sensory Perception." *Physiological Reviews* 101 (1): 353–415. <https://doi.org/10.1152/physrev.00019.2019>.
- Starr, Christopher J., Lumy Sawaki, George F. Wittenberg, Jonathan H. Burdette, Yoshitetsu Oshiro, Alexandre S. Quevedo, and Robert C. Coghill. 2009. "Roles of the Insular Cortex in the Modulation of Pain: Insights from Brain Lesions." *The Journal of Neuroscience* 29 (9): 2684–94. <https://doi.org/10.1523/JNEUROSCI.5173-08.2009>.
- Suzuki, Makoto, Atsuko Mizuno, Kunihiko Kodaira, and Masashi Imai. 2003. "Impaired Pressure Sensation in Mice Lacking TRPV4." *The Journal of Biological Chemistry* 278 (25): 22664–68. <https://doi.org/10.1074/jbc.M302561200>.
- Svoboda, Karel, and Ryohei Yasuda. 2006. "Principles of Two-Photon Excitation Microscopy and Its Applications to Neuroscience." *Neuron* 50 (6): 823–39. <https://doi.org/10.1016/j.neuron.2006.05.019>.
- Swadlow, Harvey A. 2003. "Fast-Spike Interneurons and Feedforward Inhibition in Awake Sensory Neocortex." *Cerebral Cortex (New York, N.Y.: 1991)* 13 (1): 25–32. <https://doi.org/10.1093/cercor/13.1.25>.

- Swadlow, Harvey A . 2002. "Thalamocortical Control of Feed–Forward Inhibition in Awake Somatosensory ‘Barrel’ Cortex." Edited by P. Adams, R. W. Guillory, S. M. Sherman, and A. M. Sillito. *Philosophical Transactions of the Royal Society of London. Series B: Biological Sciences* 357 (1428): 1717–27. <https://doi.org/10.1098/rstb.2002.1156>.
- Takasaki, Kevin, Reza Abbasi-Asl, and Jack Waters. 2020. "Superficial Bound of the Depth Limit of Two-Photon Imaging in Mouse Brain." *Eneuro* 7 (1): ENEURO.0255-19.2019. <https://doi.org/10.1523/ENEURO.0255-19.2019>.
- Talwar, Sanjiv K., Pawel G. Musial, and George L. Gerstein. 2001. "Role of Mammalian Auditory Cortex in the Perception of Elementary Sound Properties." *Journal of Neurophysiology* 85 (6): 2350–58. <https://doi.org/10.1152/jn.2001.85.6.2350>.
- Tan, Chun-Hsiang, and Peter A. McNaughton. 2016. "The TRPM2 Ion Channel Is Required for Sensitivity to Warmth." *Nature* 536 (7617): 460–63. <https://doi.org/10.1038/nature19074>.
- Togashi, Kazuya, Yuji Hara, Tomoko Tominaga, Tomohiro Higashi, Yasunobu Konishi, Yasuo Mori, and Makoto Tominaga. 2006. "TRPM2 Activation by Cyclic ADP-Ribose at Body Temperature Is Involved in Insulin Secretion." *The EMBO Journal* 25 (9): 1804–15. <https://doi.org/10.1038/sj.emboj.7601083>.
- Turecek, Josef, Brendan P. Lehnert, and David D. Ginty. 2022. "The Encoding of Touch by Somatotopically Aligned Dorsal Column Subdivisions." *Nature* 612 (7939): 310–15. <https://doi.org/10.1038/s41586-022-05470-x>.
- Van Duuren, E., G. Van Der Plasse, R. Van Der Blom, R. N. J. M. A. Joosten, A. B. Mulder, C. M. A. Pennartz, and M. G. P. Feenstra. 2007. "Pharmacological Manipulation of Neuronal Ensemble Activity by Reverse Microdialysis in Freely Moving Rats: A Comparative Study of the Effects of Tetrodotoxin, Lidocaine, and Muscimol." *Journal of Pharmacology and Experimental Therapeutics* 323 (1): 61–69. <https://doi.org/10.1124/jpet.107.124784>.
- Vandewauw, Ine, Katrien De Clercq, Marie Mulier, Katharina Held, Silvia Pinto, Nele Van Ranst, Andrei Segal, et al. 2018. "A TRP Channel Trio Mediates Acute Noxious Heat Sensing." *Nature* 555 (7698): 662–66. <https://doi.org/10.1038/nature26137>.
- Veldhuijzen, D.S., J.D. Greenspan, J.H. Kim, and F.A. Lenz. 2010. "Altered Pain and Thermal Sensation in Subjects with Isolated Parietal and Insular Cortical Lesions." *European Journal of Pain* 14 (5): 535.e1-535.e11. <https://doi.org/10.1016/j.ejpain.2009.10.002>.
- Venkatachalam, Kartik, and Craig Montell. 2007. "TRP Channels." *Annual Review of Biochemistry* 76 (1): 387–417. <https://doi.org/10.1146/annurev.biochem.75.103004.142819>.
- Vestergaard, M., M. Carta, G. Güney, and J. F. A. Poulet. 2023. "The Cellular Coding of Temperature in the Mammalian Cortex." *Nature* 614 (7949): 725–31. <https://doi.org/10.1038/s41586-023-05705-5>.
- Vierock, Johannes, Enrico Peter, Christiane Grimm, Andrey Rozenberg, I-Wen Chen, Linda Tillert, Alejandro G. Castro Scalise, et al. 2022. "WiChR, a Highly Potassium-Selective Channelrhodopsin for Low-Light One- and Two-Photon Inhibition of Excitable Cells." *Science Advances* 8 (49): eadd7729. <https://doi.org/10.1126/sciadv.add7729>.
- Voets, Thomas, Guy Droogmans, Ulrich Wissenbach, Annelies Janssens, Veit Flockerzi, and Bernd Nilius. 2004a. "The Principle of Temperature-Dependent Gating in Cold- and Heat-Sensitive TRP Channels." *Nature* 430 (7001): 748–54. <https://doi.org/10.1038/nature02732>.
- Wang, Feng, Erik Bélanger, Sylvain L. Côté, Patrick Desrosiers, Steven A. Prescott, Daniel C. Côté, and Yves De Koninck. 2018a. "Sensory Afferents Use Different Coding Strategies

- for Heat and Cold." *Cell Reports* 23 (7): 2001–13. <https://doi.org/10.1016/j.celrep.2018.04.065>.
- Wang, Hong, and Jan Siemens. 2015. "TRP Ion Channels in Thermosensation, Thermoregulation and Metabolism." *Temperature* 2 (2): 178–87. <https://doi.org/10.1080/23328940.2015.1040604>.
- Willis, W. D., and K. N. Westlund. 1997. "Neuroanatomy of the Pain System and of the Pathways That Modulate Pain." *Journal of Clinical Neurophysiology: Official Publication of the American Electroencephalographic Society* 14 (1): 2–31. <https://doi.org/10.1097/00004691-199701000-00002>.
- Willis, W. D., X. Zhang, C. N. Honda, and G. J. Giesler. 2001. "Projections from the Marginal Zone and Deep Dorsal Horn to the Ventrobasal Nuclei of the Primate Thalamus." *Pain* 92 (1): 267–76. [https://doi.org/10.1016/S0304-3959\(01\)00268-8](https://doi.org/10.1016/S0304-3959(01)00268-8).
- Willis, William D, Xijing Zhang, Christopher N Honda, and Glenn J Giesler. 2002. "A Critical Review of the Role of the Proposed VMpo Nucleus in Pain." *The Journal of Pain* 3 (2): 79–94. <https://doi.org/10.1054/jpai.2002.122949>.
- Winter, Ian M., Donald Robertson, and Graeme K. Yates. 1990. "Diversity of Characteristic Frequency Rate-Intensity Functions in Guinea Pig Auditory Nerve Fibres." *Hearing Research* 45 (3): 191–202. [https://doi.org/10.1016/0378-5955\(90\)90120-E](https://doi.org/10.1016/0378-5955(90)90120-E).
- Woodbury, C. Jeffery, Melissa Zwick, Shuying Wang, Jeffrey J. Lawson, Michael J. Caterina, Martin Koltzenburg, Kathryn M. Albers, H. Richard Koerber, and Brian M. Davis. 2004. "Nociceptors Lacking TRPV1 and TRPV2 Have Normal Heat Responses." *The Journal of Neuroscience* 24 (28): 6410–15. <https://doi.org/10.1523/JNEUROSCI.1421-04.2004>.
- Xue, Yawen, Yonglu Yang, Yu Tang, Mengping Ye, Jianhui Xu, Yixin Zeng, and Jie Zhang. 2016. "In Vitro Thermosensitivity of Rat Lateral Parabrachial Neurons." *Neuroscience Letters* 619 (April): 15–20. <https://doi.org/10.1016/j.neulet.2016.02.058>.
- Yahiro, Takaki, Naoya Kataoka, Yoshiko Nakamura, and Kazuhiro Nakamura. 2017. "The Lateral Parabrachial Nucleus, but Not the Thalamus, Mediates Thermosensory Pathways for Behavioural Thermoregulation." *Scientific Reports* 7 (1): 5031. <https://doi.org/10.1038/s41598-017-05327-8>.
- Yamawaki, Naoki, Martinna G Raineri Tapias, Austin Stults, Gregory A Smith, and Gordon MG Shepherd. 2021. "Circuit Organization of the Excitatory Sensorimotor Loop through Hand/Forelimb S1 and M1." Edited by Solange P Brown, Ronald L Calabrese, Barry Connors, and Yutaka Yoshida. *eLife* 10 (April): e66836. <https://doi.org/10.7554/eLife.66836>.
- Yang, Wen Z., Xiaosa Du, Wen Zhang, Cuicui Gao, Hengchang Xie, Yan Xiao, Xiaoning Jia, et al. 2020. "Parabrachial Neuron Types Categorically Encode Thermoregulation Variables during Heat Defense." *Science Advances* 6 (36): eabb9414. <https://doi.org/10.1126/sciadv.abb9414>.
- Yarmolinsky, David A., Yueqing Peng, Leah A. Pogorzala, Michael Rutlin, Mark A. Hoon, and Charles S. Zuker. 2016a. "Coding and Plasticity in the Mammalian Thermosensory System." *Neuron* 92 (5): 1079–92. <https://doi.org/10.1016/j.neuron.2016.10.021>.
- Yates, B. J., F. J. Thompson, and J. P. Mickle. 1988. "Responses of Spinal Cord Neurons Following Stimulation of A Beta Femoral-Saphenous Venous Afferent Fibers." *Brain Research* 451 (1–2): 285–94. [https://doi.org/10.1016/0006-8993\(88\)90773-1](https://doi.org/10.1016/0006-8993(88)90773-1).
- Yu, Linhui, and Kartikeya Murari. 2021. "Functional Monitoring and Imaging in Deep Brain Structures." In *Handbook of Neuroengineering*, edited by Nitish V. Thakor, 1–32. Singapore: Springer Singapore. https://doi.org/10.1007/978-981-15-2848-4_135-1.

- Zhang, Xijing, Steve Davidson, and Glenn J. Giesler. 2006a. "Thermally Identified Subgroups of Marginal Zone Neurons Project to Distinct Regions of the Ventral Posterior Lateral Nucleus in Rats." *The Journal of Neuroscience* 26 (19): 5215–23. <https://doi.org/10.1523/JNEUROSCI.0701-06.2006>.
- Zhang, Xijing, and Glenn J. Giesler. 2005. "Response Characteristics of Spinothalamic Tract Neurons That Project to the Posterior Thalamus in Rats." *Journal of Neurophysiology* 93 (5): 2552–64. <https://doi.org/10.1152/jn.01237.2004>.
- Zhang, Yan, Márton Rózsa, Yajie Liang, Daniel Bushey, Ziqiang Wei, Jihong Zheng, Daniel Reep, et al. 2023. "Fast and Sensitive GCaMP Calcium Indicators for Imaging Neural Populations." *Nature* 615 (7954): 884–91. <https://doi.org/10.1038/s41586-023-05828-9>.
- Zhang, Zhi-Hua, and Stephen M. Oppenheimer. 2000. "Baroreceptive and Somatosensory Convergent Thalamic Neurons Project to the Posterior Insular Cortex in the Rat." *Brain Research* 861 (2): 241–56. [https://doi.org/10.1016/S0006-8993\(00\)01990-9](https://doi.org/10.1016/S0006-8993(00)01990-9).
- Zhao, Zheng-Dong, Wen Z. Yang, Cuicui Gao, Xin Fu, Wen Zhang, Qian Zhou, Wanpeng Chen, et al. 2017. "A Hypothalamic Circuit That Controls Body Temperature." *Proceedings of the National Academy of Sciences* 114 (8): 2042–47. <https://doi.org/10.1073/pnas.1616255114>.

7. Appendix

7.1 Publications

Phillip Bokinec, Clarissa J Whitmire, **Tobias M Leva**, James F A Poulet, Brain-wide connectivity map of mouse thermosensory cortices, *Cerebral Cortex*, Volume 33, Issue 8, 15 April 2023, Pages 4870–4885, <https://doi.org/10.1093/cercor/bhac386>

Tobias M Leva, Clarissa J Whitmire, Thermosensory thalamus: parallel processing across model organisms, *Front. Neurosci. Sec. Translational Neuroscience* Volume 17 – 2023, 13 October 2023, <https://doi.org/10.3389/fnins.2023.1210949>

7.2 Declaration of independence

I, Tobias Marc Leva, confirm that the work presented here is my own. Information or data derived from other sources is cited or acknowledged as such in the text. This dissertation has been composed by myself and any data generated in collaboration with others is specified in the Statement of Contributions.

The work for this thesis was carried out at the Neural Circuits and Behavior lab from the Max Delbrück Center for Molecular Medicine, under the supervision of Prof. Dr. James Poulet.

This dissertation has not been submitted for any other degree or qualification at any University or similar institution.

7.3 Statement of contribution

Because of the interdisciplinary nature of this project, some of the data presented here was obtained by collaborators, to whom I am very grateful. All experiments and analysis performed by other people are:

- Experiments of Chapter 3.1 were performed by Dr. Phillip Wisinski-Bokiniec, analysis was done by Tobias Leva, Dr. Clarissa Whitmire and Dr. Phillip Wisinski-Bokiniec under the supervision of Prof. Dr. James Poulet
- Experiments of Chapter 3.2 were performed by Bibiana Horn, Charlene Memler and Tobias Leva, analysis was done by Tobias Leva under the supervision of Prof. Dr. James Poulet
- The analysis of paw movement recording that resulted in Figure 2.4.6-1 was done by Dr. Clarissa Whitmire and Tobias Leva

All experiments in this thesis were conceived and designed by my PhD supervisor, **Prof. Dr. James Poulet**, and myself, with additional input from the other investigators for the experiments they contributed to.

7.4 Abbreviations

AAV	Adeno-associated virus
AP	anterior-posterior coordinates relative to Bregma
aPO	anterior PO
aVPL	anterior VPL
CCFv3	Allen Institute Common Coordinate Framework - version 3
CI	confidence interval
CTB	Cholera Toxin Subunit B
DI	Duration Index
DMH	dorsomedial hypothalamus
DV	dorsal-ventral coordinates relative to Bregma
Eth	Ethmoid nucleus of the thalamus
fMRI	functional magnetic resonance imaging
FNR	false negative rate
GABA	γ -Aminobutyric acid
IQR	inter quartile range
ISI	Inter spike interval
KDE	Kernel density estimation
LDA	Linear discriminant analysis
LFP	Low frequency power
LP	Lateral posterior nucleus of the thalamus
LPN	lateral parabrachial nucleus
MGB/ MG	medial geniculate body
ML	medial-lateral coordinates relative to Bregma
MUA	multi-unit activity
PF	parafascicular nucleus
pIC	posterior Insular Cortex
PO	Posterior complex
POA	preoptic area
POL	posterior limiting nucleus
Pom	medial segment of Posterior complex
PoT	Posterior triangular nucleus

pPO	posterior PO
PSTH	Peri stimulus time histogram
pVPL	posterior VPL
RE	Nucleus of reuniens
RT	Reticular nucleus of the thalamus
S1	primary Somatosensory Cortex
S2	secondary Somatosensory Cortex
SGN	suprageniculate nucleus
SNR	Signal-to-noise ratio
TI	Tuning index
TRP	Transient Receptor Potential (ion channel)
TRPA	Transient Receptor Potential Ankyrin
TRPM	Transient Receptor Potential Melastatin
TRPV	Transient Receptor Potential Vanilloid
TTL	Transistor-Transistor logic
VAL	ventral anterolateral nucleus
VM	ventral medial nucleus
VPL	Ventral posterolateral nucleus
VPM	Ventral posteromedial nucleus
ZI	Zona incerta

7.5 Index of figures

Figure 1.1.1-1 TRP receptor family with activation temperature (bottom) and agonists (top)	14
Figure 1.2-1 Input from sensory afferents to spinal cord	18
Figure 1.2-2 Overview of ascending spinal cord pathways	19
Figure 1.3-1 Anatomical location of VPL, PO and PoT	23
Figure 1.6.1-1 Schematics of potential thalamocortical connectivity motifs	32
Figure 1.6.2-1 Influence of thalamic inactivation on thermal perception	33
Figure 1.6.3-1 Different models of thermal encoding in the thalamus	35
Figure 2.4.6-1: Thermosensory Stimulation-Induced Paw Movements and Their Thalamic Correlates (Analysis by Dr. Clarissa Whitmire and Tobias Leva, Visualization of results by Dr. Clarissa Whitmire and Tobias Leva)	43
Figure 2.8.5-1 Quality metrics employed in the categorization of units	53
Figure 2.9.1-1 Anatomical reconstruction of Neuropixel probe trajectories	55
Figure 3.1.1-1 Dual Injections in functionally targeted thermal representations of S1 and pIC	66
Figure 3.1.2-1 Whole-brain ipsilateral inputs to S1 and pIC	68
Figure 3.1.3-1: Whole-brain ipsilateral outputs from S1 and pIC	70
Figure 3.2.1-1 Stimulus detection task and pharmacological inactivation of somatosensory thalamus	73
Figure 3.2.2-1 Relationship of inactivation site and strength of behavioral impairment	76
Figure 3.3.1-1 Acute extracellular electrophysiology in awake, head-fixed mice	79
Figure 3.3.2-1 Characterization of response-types in thermally responsive thalamic cell population	82
Figure 3.3.3-1 Spatial representation of cooling and warming evoked sensory response	85
Figure 3.3.4-1 Subregion-specific thermal representations	88
Figure 3.3.5-1 Thermal stimulation elicits suppressed sensory response as well as warming-specific offset responses	90
Figure 3.3.6-1 Characterization of the neural representations of temperature and touch	94
Figure 3.4.1-1 Thalamic thermal encoding is tuned to stimulus intensity not stimulus specificity	98
Figure 3.4.2-1 Temperature evoked tuning curves show distinct encoding profiles	100
Figure 3.4.3-1 Saturation Profiles and Tuning Curves in Thalamic Neurons	104
Figure 3.4.4-1 Sensitivity of Thalamic Nuclei and Response-types to Cooling and Warming Stimulation	108

Figure 3.5.1-1 Characterization of cooling and warming evoked temporal dynamics	111
Figure 3.5.2-1 Characterization of sensory response dynamics across thalamic region	115
Figure 3.5.3-1 Characterization and spatial distribution of temporal response profiles across thalamus	121
Figure 3.5.4-1 Non-homogenous temporal dynamics in “Sustained” group	123
Figure 3.5.5-1 Characterization of tactile evoked response dynamics across thalamic regions	125
Figure 3.5.6-1 Characterization and spatial distribution of temporal dynamics type across thalamus	128
Figure 4.5.1-1 The diagrams schematically illustrate temperature activation profiles of warm/hot-sensitive ion channels (upper panel) and cold-sensitive channels (lower panel) inherent to primary afferent neurons specialized in temperature perception. Edited from H. Wang and Siemens 2015	147